DIPLOMARBEIT

Titel der Diplomarbeit

Statische Korrekturen in der Seismik bei komplexen Topographien

Fallbeispiel: Oichtental

angestrebter akademischer Grad

Magistra der Naturwissenschaften (Mag. rer. nat)

Verfasserin:	Karoline Alten
Matrikel-Nummer:	0347252
Studienrichtung:	A 416 Geophysik
Betreuer:	Univ. Prof. E. Brückl, Technische Universität Wien

Wien, Februar 2009

Zusammenfassung

Ein wichtiger Bestandteil jedes seismischen Datenprocessings ist die statische Korrektur. Sie dient zur Bereinigung von topographischen Unebenheiten, sowie Geschwindigkeitsstörungen die durch oberflächennahe Anomalien oder durch die Verwitterungsschicht hervorgerufen werden. Dabei wird die gesamte seismische Auslage nach unten gerechnet, um ein neues, tiefergelegenes Bezugsniveau zu erreichen.

Die Zeitkorrektur an den seismischen Daten bewirkt dadurch einen Effekt, als hätten die aufgenommenen Signalen nie diese oberflächennahen Schichten durchlaufen. Um diese obersten 10er bzw. 100er Meter wegrechnen zu können, muss ein Geschwindigkeitsmodell vorhanden sein. Umso hochauflösender und genauer dieses bekannt ist, desto besser kann die Rechnung der Sources & Receivers auf die statische Bezugsebene erfolgen und dadurch die Störeffekte der seichten, meist unregelmäßigen Schichtung eliminiert werden.

Bei dieser Diplomarbeit werden zwei verschiedene Methoden zur Erstellung eines solchen Geschwindigkeitsmodells getestet und mit einem bereits in der Produktion verwendeten Modell verglichen. Beim ersten Modell handelt es sich um eine 3D Tauchwellen-Tomographie, beim zweiten um eine 1D Inversion. Man versucht eine Möglichkeit zu finden, das Problem eines starken lateralen Geschwindigkeitskontrasts, welcher durch ein aufgefülltes Gletschertal geboten wird, zu bewältigen.

Im Auftrag von Rohöl Aufsuchungs Gesellschaft (RAG)

Static Corrections in Seismic Surveys over Complex Topographies

Case Study: Oichtental

An investigation conducted on behalf of Rohöl Aufsuchungs Gesellschaft (RAG)

Vienna, February 2009

Abstract

An essential step in the processing of seismic data is the application of static corrections. They account for time shifts caused by topographic undulations, velocity anomalies in the near-surface and delayed travel times of the signal through the weathered layer. The entire seismic layout is treated as if the survey had taken place below the unconsolidated layers, by projecting sources and receivers vertically downwards onto a reference datum.

The time shift applied to the seismic makes the traces appear as if they had never travelled through the weathered layer. In order to eliminate the effect of the shallow tens or hundreds of metres, a velocity model must be acquired. The quality and resolution of the model determines how accurately the sources and receivers can be projected down onto the statics datum and thus how well the delays and incoherent signals can be corrected.

The presented thesis investigates two different methods employed in the calculation of such a velocity model and compares them to a previously computed model used in production seismic. One method deals with a 3D diving wave tomography, while the other looks at a 1D inversion of travel time curves. Both aim to solve the difficulties encountered in complex topographies, such as an overdeep glacial in-fill valley with strong lateral velocity contrasts.

2

1 Introduction

Ever since the first experimental seismic surveys by petroleum companies in the 1920s, the industry has witnessed immense advances in regard to methodological and technological approaches. Before the days of seismic surveys, hydrocarbon fields were either encountered in the form of natural surface seeps or simply through exploration drills in previously unexplored territory. Surface seepages can still be found today in several places around the world, such as the Gulf of Mexico or the La Brea tar pits in California. Early exploratory drilling dates as far back as the 1860s in areas of today's Azerbaijan and Pennsylvania, where discovered seepages were the impelling force behind the search for subsurface oil and gas accumulations[1].

The first successful seismic surveys took place in the 1960s. They constituted small-scale 2D layouts over the prospective areas and whereas previously, data processing had to be performed by hand, which was very labour-intensive and rudimentary, the introduction of computer technology saw a drastic change in the possibilities of processing and thus came a leap forward in data quality. Geoscientists were now able to deal with the seismic data on a digital basis, permitting more computationally intensive processes to be performed in a shorter space of time, and laying the foundations for new mathematical approaches to improve data quality further. Digital data recording also brought an increase in the amount of data produced during a seismic survey. As well as an increase in the number of receiver and shot points, the lengths of the profiles increased to several kilometres, as more sensitive receivers were able to record waves over greater distances. Nowadays, it has become standard in the petroleum industry to record surveys – both land and marine – on a 3D basis to provide better resolution of underground structures and therefore facilitate interpretation.

Figure 1 shows a standard processing flow applied to raw seismic data before it can be sensibly used for interpretation. Essentially, the aim of any processing sequence is to maximise the signal-to-noise ratio such that the underground structures are clearly discernible. The exact sequence will depend on the type of data dealt with, for example,

---

[1] URL: http://www.npagroup.com/oilandmineral/offshore/oil_exploration/index.htm

marine data demands additional steps to remove water-bottom multiples and computing the correct arrival times to compensate for the boat speed during the survey. Land data, on the other hand, puts more emphasis on static corrections, seeing as topographic effects and associated rock type variations weigh quite heavily on the recorded data.
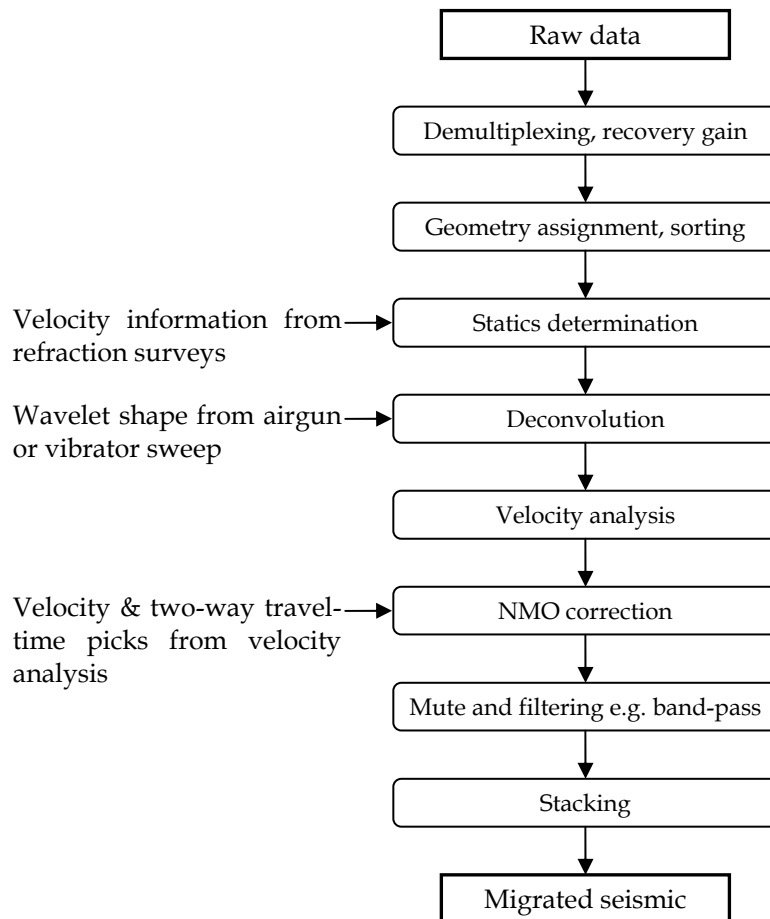
```
                          ┌──────────────────────┐
                          │      Raw data        │
                          └──────────────────────┘
                                     │
                          ┌──────────────────────────┐
                          │ Demultiplexing, recovery gain │
                          └──────────────────────────┘
                                     │
                          ┌──────────────────────────┐
                          │ Geometry assignment, sorting │
                          └──────────────────────────┘
                                     │
Velocity information from ──────────►┌──────────────────────┐
refraction surveys                   │ Statics determination │
                                     └──────────────────────┘
                                     │
Wavelet shape from airgun ──────────►┌──────────────────────┐
or vibrator sweep                    │    Deconvolution      │
                                     └──────────────────────┘
                                     │
                          ┌──────────────────────┐
                          │  Velocity analysis   │
                          └──────────────────────┘
                                     │
Velocity & two-way travel- ─────────►┌──────────────────────┐
time picks from velocity             │    NMO correction     │
analysis                             └──────────────────────┘
                                     │
                          ┌────────────────────────────┐
                          │ Mute and filtering e.g. band-pass │
                          └────────────────────────────┘
                                     │
                          ┌──────────────────────┐
                          │      Stacking        │
                          └──────────────────────┘
                                     │
                          ┌──────────────────────┐
                          │   Migrated seismic   │
                          └──────────────────────┘
```

Figure 1 A standard seismic processing flow chart, applicable to 2D/3D or land/marine data

This thesis concentrates on the static corrections required in the processing of 3D land seismic and investigates ways to obtain optimum static corrections for data in geologically complex terrain. Why statics are such a work-intensive and indispensable processing step is detailed in Chapter 2, explaining the necessity to handle data from a mutual reference datum in order to produce focussed stacks which are not subject to cycle skips or blurring as a result of incoherency. Chapter 3 outlines the case study used in this investigation, while chapter 4 deals with the two implemented methods used for computing a velocity model and describes their theory, as well as the parameter testing. Interpolation of discrete velocity values onto a 3D cube and the subsequent comparison

of the two results is also carried out in Chapter 4, along with the actual statics computation. Chapter 5 examines the calculated static correction and their application to the seismic. Conclusively, Chapter 6 summarises the results and reflects upon the methodology of the study, putting forward possible recommendations and improvements, and pointing out any shortfalls of the employed procedures.

2 Static Corrections

Static corrections are, as the name suggests, a "static" shift which applies a constant time shift to an entire seismic trace, as opposed to a dynamic shift, whose size is time-variant. The most commonly used definition of statics in geophysics can be found in Sheriff's Encyclopedic Dictionary of Exploration Geophysics,

> *Corrections applied to seismic data to compensate for the effects of variations in elevation, weathering thickness, weathering velocity, or reference to a datum. The objective is to determine the reflection arrival times which would have been observed if all measurements had been made on a (usually) flat reference plane with no weathering or low-velocity material present.*

In very rudimentary terms, this means that the uppermost layers, which delay the received signal, need to be eliminated in order to produce an image of better focus at target depth. The result is a scenario in which we treat the data as though they were recorded by placing the sources and receivers below this shallow layer on an arbitrarily defined reference datum. In the early days of seismic, this used to be done by the field crew in situ, using data from refraction surveys or uphole shots and was therefore referred to as field statics. The first reference to time corrections associated with near-surface layers can be found in the 1920s according to Karcher (1987)[2], where scientists were aware of the problems arising due to weathering layers during experimental surveys.

Sleep and Fujita[3] compared the datum static corrections to the Bouguer corrections in gravity, as both aim to remove the effects of near-surface structures to gain better insight into what lies below.

Nowadays, statics are mostly carried out in processing centres in a series of more complicated steps, requiring control data and further information to ensure best possible results. The most prevalent methods will be described in the following

---

[2] Karcher, J.C., 1987. The reflection seismograph: its invention and use in the discovery of oil and gas fields: The Leading Edge, 6, No. 11, 10-19.

[3] Sleep, N.H., Fujita, K., 1997. Principles of geophysics, 362

subchapters, but prior to that, the aforementioned definition by Sheriff will be looked at in more detail.

2.1 The Weathered/Unconsolidated Layer

The term "weathering" in its geological sense refers to the decomposition of a material when exposed to wind and water, but also due to other natural phenomena such as living organisms. The break-down of rock into smaller fragments caused by, for example, freeze-thaw, dissolving by acids, corrosion, abrasion by wind, as well as the destruction caused by organisms such as digging animals and roots of growing plants, is a process that is generally confined to the shallow layers. The rock becomes unconsolidated and loosened compared to deeper layers, which tend to stay compact because of the weight of the overburden and by being cut off from any weathering processes. The weathered layer has the same effect as a low-pass filter, as it shows a high rate of energy absorption which mostly affects high frequencies. Due to its loose and highly variable structure, it may not just delay the seismic energy, but also scatter it.

The weathered layer in terms of seismic usually encompasses more than just this very shallow area below the surface. It refers to the whole unconsolidated layer in which the pore spaces are filled with air rather than water[4], leading to a notable reduction in seismic velocity compared to waterlogged earth. Depending on the geological setting, however, the weathering thickness may vary from a few centimetres to several hundred metres and the way this is handled during processing depends on the target depth or objective of the survey. In most petroleum exploration surveys on land, where targets may lie at a couple of kilometres depth, the uppermost few hundred metres are dealt with in statics while any deeper structures are regarded as velocity anomalies and treated during velocity analysis. This is also due to the fact that the near-surface is often characterised by spatially high-frequent rock type alterations, leading to high frequency velocity variations in both horizontal and vertical direction. Deeper structures, on the other hand, often show greater spatial extents and more gradual rock

---

[4] Sheriff, R.E., 1991. Encyclopedic dictionary of exploration geophysics

type transitions. These produce long-wavelength anomalies that can be more easily handled during velocity analysis.

The weathering layer which is to be removed by static correction encompasses the whole low-velocity area of the shallow subsurface. Only removing the geologically weathered layer directly at the surface will not suffice, as the sub-weathered layer might also have air-filled pores and show a significantly lower velocity than the underlying consolidated rock. The base of the weathered layer can have varying definitions, but generally tends to be either where there is a markedly higher velocity in the layer below, or where the velocity gradient appears to become constant, both of which often coincides with the depth of the water table.

Some studies may take seasonal-variations of the weathered layer into account. Its thickness can depend on the time of year, for example, if carried out in winter in regions where permafrost might be an issue, or whenever temperatures and precipitation influence the height of the water table. These effects are only important if dealing with repeated (4D) surveys and will therefore not be relevant in this study.

2.2   Effects of Topography

Variations in height along the surface where a seismic survey is carried out are the most outwardly apparent source of static delays in the recorded signal. In areas of great elevation differences, the seismic waves would have to travel through varying thicknesses of low-velocity layer before the reflection reaches the receivers, giving incoherent signals and hence producing poor quality stacks, as the data would stack deconstructively if out of phase.

Yet even in perfectly flat terrain, we cannot neglect statics because rapid horizontal variations in rock type can still occur. These circumstances are known as mature topography[5], where the surface profile provides no information on the subsurface profile in terms of bedrock depths or lateral near-surface variations. In contrast to youthful topography, where vertical erosion is still active, mature topography is a case of old erosion channels being infilled with recent sediments. The case study presented in Chapter 3 falls under this classification, as it deals with a deep

---

[5] Cox, M.J.G., 1999. Static corrections for seismic reflection surveys

glacial valley from the last ice age that has been infilled with sediments since the retreat of the glacier and thus forms a body of loose, low-velocity material embedded in a high-velocity crystalline basement.

In order to come up with static corrections, we require the weathering thickness and weathering velocity. The first step is to obtain an elevation model of the area from which the thickness down to the reference datum can be calculated. Topographic effects call for static corrections, no matter if the base of the low-velocity layer runs parallel to the surface or whether it forms a flat layer underneath the undulating surface.

2.3 Seismic Velocity of the Weathered/Unconsolidated Layer

The propagation of seismic waves in the ground is based on the assumption that the earth behaves as an elastic body. Materials which are seen as elastic deform reversibly when a force is applied on their surface, as Hooke's Law states that the strain on a material (relative deformation of the body) is linearly proportional to the stress (force per unit area) applied. Deformation will only be permanent if the elastic limit of a material is exceeded, otherwise the body will return to its original shape when the stress is removed. Seismic P- or S-waves propagate according to the Wave Equation, which is a partial differential equation. By integrating it we can predict the wavefield at any point and time from the initial solution, providing the medium is isotropic and homogeneous. The velocity with which P-waves (longitudinal) propagate through the ground, v_p, is associated with the density and elasticity of the rocks concerned, as shown in Equation [1]:

$$v_p = \sqrt{\frac{\lambda + 2\mu}{\rho}} \qquad [1]$$

The shear modulus $\mu(\rho)$ and the elastic modulus $\lambda(\rho)$ are the Lamé constants, both being a function of density, ρ, hence the inverse relationship between velocity and density displayed by the equation at first glance does not apply. The Lamé constants are material properties related to Young's modulus and Poisson's ratio.

Anisotropy, in other words, velocity being a function of the direction of travel through a material, would have to be dealt with during special processing. As the earth is hardly ever homogeneous and tends to show variations in density and compressibility, a simplifying premise is made, splitting a heterogeneous layer into

several sub-layers within which the material properties are assumed to be homogeneous.

Besides density and incompressibility, there are several other factors contributing to the velocity of rock layers. In extreme cases, for instance, a type of rock with water-filled pores can have a velocity of a factor 10 greater than its dry equivalent. Likewise, cold regions which experience temperatures below 0^{oC} for long periods of time can show higher velocities due to frozen pore water. Regions with permafrost can thus prove challenging during data processing, as the usual situation where the weathered layer is above a slightly faster-velocity subweathered layer is inverted.

The following table (Figure 2, based on Cox (1999)) presents typical velocity ranges for compressional waves in various rocks. It can be seen that velocities in consolidated rock are on the whole higher than in unconsolidated sediments and, similarly, how saturated rock tends to be faster than its dry equivalent.

Material	Vp compressional velocity [ms^{-1}]
Consolidated	
Gneiss (metamorphic)	3500-7500
Dolomite (sedimentary)	3500-6900
Chalk (sedimentary)	2100-4200
Limestone (sedimentary)	1700-7000
Sandstone	1400-4300
Sandstone-shale	2100-4500
Unconsolidated	
Clay	1100-2500
Alluvium	500-2000
Glacial sand and gravel (unsaturated)	380-500
Glacial sand and gravel (saturated)	1670
Glacial till (unsaturated)	430-1040
Glacial till (saturated)	1730
Sand loose	200-2000
Sand loose above water table	1000
Sand loose below water table	1800
Water	1400-1500
Air	330

Figure 2 Table showing seismic P-wave velocities in different types of rock[6]

The values quoted above mostly refer to rocks at greater depth. They are therefore slightly higher than in the near surface layers and not strictly applicable in the

[6] Press, F., 1966. Seismic velocities, in Handbook of geophysical constants (ed. Sydney P. Clark)

shallow. Given the broad range of these values, it is not sensible to rely on tabulated values for static corrections, even if the regional geological setting is known, as the subsurface is still unique with regard to other influences, such as saturation and small-scale variations in rock composition.

Complications may arise if the subsurface shows anisotropy. This manifests itself in the form of the propagation velocity being a function of the direction of travel through a material because the relationship of stress and strain does not hold equally in all azimuths[7]. Looking at Hooke's Law,

$$\sigma_{ij} = \sum_{kl} c_{ijkl} \cdot \epsilon_{kl} \qquad [2]$$

where σ_{ij} is the stress tensor, ϵ_{kl} the strain tensor and c_{ijkl} a fourth order tensor containing 81 elastic coefficients, we can see that in isotropic materials the stress and strain tensors would be symmetrical and due to linear combinations, only 2 of the elastic coefficients are independent. In anisotropic materials, where strain is not independent of the direction in space, the elastic coefficient tensor would contain 81 independent elements.

Generally, rocks contain numerous different minerals, each of which may be anisotropic on a crystalline level, but in the overall amassment they are placed at random and anisotropic properties cancel out. Even though anisotropy is not normally taken into account in standard processing, static corrections might have to consider it if it transpires that there is a significant difference between the velocity parallel and the velocity perpendicular to the bedding plane of the weathering layer. This is because of how the calculation of static corrections is performed (see section 2.4), which chiefly involves a vertical downward projection of sources and receivers, but depending on whether the velocity field used was obtained from refraction seismics or uphole shots, the velocity value would be in the parallel or the perpendicular direction to the bedding plane, respectively.

---

[7] Lowrie, W., 1997. Fundamentals of geophysics

2.4 The Reference Datum and Principles of Datum Static Corrections

The idea behind static corrections is to remove the near surface layers, which obscure the target depth due to delays they impose on the seismic signal as a result of their low velocity. This is most relevant in land seismic and surveys in transition zones, where complex geological environments give rise to high-frequency spatial changes in velocity, both horizontally and vertically. In marine seismic, this is not so big an issue, as the water layer tends to be regarded as a homogeneous constant velocity area where no static corrections in the classic sense are required, unless there are strong variations in the water bottom topography or when working in an area of rapid deposition, such as deltas. The problem is not always *how* to deal with such settings, but how to deal with them in an economical fashion that is adequate for large-scale 3D surveys, where each processing step for the client is a question of time and money. There are plenty of simplifications that enable models to be created very crudely and quickly, but their quality obviously falls short of the desired standard. Furthermore, limiting the accuracy of the static model can have drawbacks during subsequent processing steps which rely on coherent signals, such as stacking. The more intricate a near-surface model becomes, the more time-intensive the processing, so a compromise between effort and effectiveness has to be found.

To better explain the underlying theory of statics, it helps to take a look at the definition of the reference datum involved in the correction; according to Sheriff[8], a seismic datum is "an arbitrary reference surface, reduction to which minimises local topographic and near-surface effects". Reduction to this datum means, a trace undergoes a constant time shift to produce the seismic signal that would have been recorded if the relevant source and receiver had been positioned on this reference datum. By applying static correction time shifts to all traces, the entire survey is shifted vertically downwards from the surface onto this arbitrary plane, accounting for any low-velocity layers and other near-surface irregularities that are found in between. The choice of reference datum is therefore critical in calculating statics, and there are several possible approaches which to take.

---

[8] Sheriff, R.E., 1991. Encyclopedic dictionary of exploration geophysics

Figure 3 demonstrates the basic concept of how static corrections, often called datum static corrections, are performed. On condition that the necessary information on weathering velocity, subweathering velocity, weathering thickness and elevation is known, we can calculate the vertical time shift to project source S1 and receiver G1 onto the base of the weathering layer (Fig. 3a). By convention, the time shift applied to the seismic trace when projecting its source-receiver pair onto the base of the weathering layer is negative (as the reflection time would be reduced i.e. the reflected signal would arrive at an earlier time if the receiver were closer to the reflecting horizon). This is known as the weathering correction.
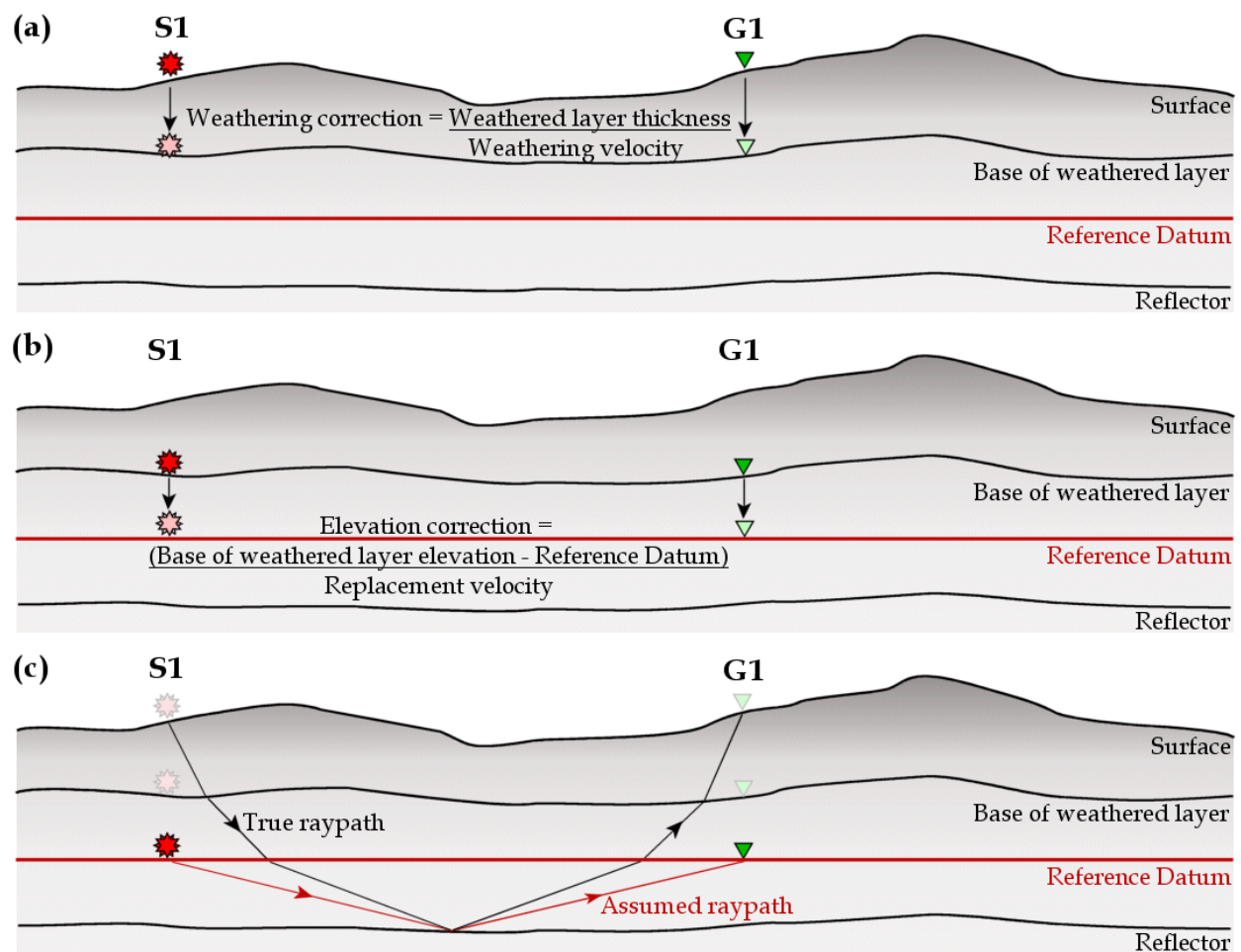
Figure 3 (a) Vertical shift of source (S1) and receiver (G1) onto base of weathered layer; time adjustment corresponds to weathering correction (b) Projection onto flat reference datum; elevation correction can be positive or negative, depending on datum's position relative to base of weathered layer (c) Incorrect inherent assumption of static corrections which leads to departure of presumed raypath from true raypath

The next step is to project S1 and G1 onto the desired reference datum (Fig. 3b), relative to which all subsequent processing will take place. The velocity used for this second time adjustment is called the replacement velocity. If the reference datum lies deeper than the base of the weathered layer, the value used can be obtained from the known velocity depth profile at this location. Should the reference datum lie above the base of the weathered layer though, the replacement velocity would have a value from near the base of the weathered layer and act as an infill up to the desired datum.

This second time shift is the elevation correction and – depending on the position of the base of the weathered layer with respect to the reference datum – it has a positive or negative sign – as the convention is negative for downward projection, the elevation correction would be positive if the base of the weathered layer were below the final reference datum and the trace would need a time adjustment to increase the reflection times. The sum of the weathering correction plus the elevation correction gives the total datum static correction. Static corrections are thus not simply the time shift between the surface and the reference datum, as often incorrectly assumed. This is only the case if the weathered layer is negligible and the static correction essentially just contains the elevation correction, as Thralls and Mossman (1952)[9] already stated, "The arbitrary application of any set type of near-surface corrections to seismic data can lead to erroneous results. The determination of the type of correction to be used must be based, in part, on the type of formations present in the near-surface."

Figure 3c shows the inherent problem of datum static corrections, which is the fact that the new source and receiver position, vertically below their original surface location, would not yield the same raypath as the recorded signal. With increasing offset (distance between source and receiver), there is a hyperbolic relationship in the reflection times from a point in the subsurface. This hyperbolic relationship would no longer hold perfectly true if the sources and receivers were calculated onto a new plane below where the actual recording took place. The issue can be neglected if the raypaths down to the reference datum are almost vertical, or if the datum static corrections are small relative to the reflection times. Reducing the error of this inherent assumption is

---

[9] Thralls, H.M., Mossman, R.W., 1952. Relation of seismic corrections to surface geology, Geophysics 17, 218

directly linked to the choice of reference datum. In his book on static corrections, Cox[10] mentioned the vital criteria that play a part in the datum choice:

If the near-surface irregularities are adequately accounted for by datum statics, one should see a decent similarity between the time and the depth section of a seismic line. In this way, there should be a slow spatial change in the time-to-depth relationship, while any irregularities below the reference datum are treated as velocity anomalies during NMO analysis (dealt with in dynamic corrections). In order to accommodate the velocity variations in the shallow as part of datum static corrections, the reference datum must be deep enough, which might mean several hundred metres below the surface in areas of geological complexity. The drawback of a deep reference datum is the aforementioned problem of projecting the survey a longer distance vertically downwards, which would increase the difference between the true raypath and the virtual one at the datum level, causing the hyperbolic relationship of reflections to break down.

Incomplete or imprecise knowledge of the replacement velocity is clearly a hindrance in ensuring accurate datum statics. It is therefore helpful to choose a reference datum close to the base of the weathered layer, so that the effect of an incorrect replacement velocity is minimised. In areas with pronounced weathered layer undulations, this could pose a challenge when using a flat reference datum. Advanced solutions might be to use a sloping datum (though this would provide a distorted time section, as a flat event in reality would appear as a sloping event in the seismogram) or a contoured datum. The most reliable, yet complicated, method would be an intermediate or floating datum. Whereas normally, complete datum static corrections are followed by velocity analysis and NMO corrections, the use of a floating datum sees only part of the static corrections applied as a first step. Stacking velocities are then picked in respect to this intermediate datum, which is often fairly close to the surface to reduce the effect of non-hyperbolic moveout creating wrong velocity picks. The remaining part of the static corrections down to the desired final datum is only applied post-NMO correction.

---

[10] Cox, M.J.G., 1999. Static corrections for seismic reflection surveys

2.5 Methods to Obtain a Near-Surface Model

It should be noted that up to now, the terms static corrections and datum static corrections were used interchangeably. Strictly speaking, datum static corrections are the time adjustments from the surface to the reference datum, whereas static corrections as a whole include datum statics and residual statics. This, however, will be explained in more depth in the later chapters; it is worth mentioning here that residuals constitute the short-wavelength component of static corrections (affecting the quality of CMP stacks, as they are in the order of magnitude of ¼ wavelength of the seismic waves), while datum statics typically handle longer wavelength components (impacting structural times)[11].

What information is needed to compute datum static corrections was already brought up in the preceding section:

- Elevation model of the surface
- Weathering thicknesses
- Weathering velocity
- Subweathering velocity (replacement velocity)

Values for these parameters tend to only be available at discrete locations, rather than continuously over a whole survey area. The elevation model is usually the most complete data set, as most petroleum explorations today involve an aerial scan of the topography on a standard basis, possibly even at quite a high resolution. Even if such advanced technology is not available to small-scale investigations, heights above sea level are still the easiest of the parameters to determine e.g. using GPS. The more the altitude within a survey area fluctuates, the more samples are required in order to have a sufficiently sampled data set. Undersampling any of the above parameters will ultimately lead to problems during interpolation, as short-wavelength anomalies can only be resolved if a dense enough grid of data is provided. Data in the spatial domain falls under the same sampling theorem (or Nyquist theorem) as temporal data, meaning that the higher the number of data points per unit distance, the greater the frequency of spatial anomalies which can be resolved.

$$k_{Ny} = \frac{\pi}{\Delta x} \tag{3}$$

---

[11] Cox, M.J.G., 1999. Static corrections for seismic reflection surveys

Equation [3] shows that the Nyquist wavenumber k_{Ny}, in other words, the maximum spatial frequency that can be reconstructed from a data set, is inversely proportional to the sampling interval Δx. This theory applies to the time domain in terms of sampling interval during acquisition, as well as to the spatial domain in regards to receiver spacing to record as many wavelengths per unit distance as possible.

As the obtainment of surface elevations presents the smallest problem from a practical point of view, we will now look at ways to gather the other parameters for the near-surface model. The most common approach is to carry out refraction surveys alongside the main exploration. Data from these is typically supported by uphole shots, but other geophysical methods can also be used as control, like shallow reflection surveys, GPR (ground penetrating radar) or even electrical methods. Only if the geological environment is very simple, might data from only one of these sources suffice to produce a surface model. On the whole, lateral and vertical variations tend to be more complicated and therefore demand a combination of methods to support each other and to increase the number of data points available for interpolation. Also, while some methods might only yield data about the weathering layer thickness, others would give the missing information on the weathering velocity.

2.6 Refraction Surveys

Refraction is a concept from the field of optics, the Physics concerned with the properties of light. It can be analogously applied to seismic waves and is best explained using some of the basic laws from optics. The first of these is Huygens's Principle, which according to Tipler and Mosca[12] states that

> *Each point on a primary wavefront serves as the source of spherical*
> *secondary wavelets that advance with a speed and frequency equal to those*
> *of the primary wave. The primary wavefront at some later time is the*
> *envelope of these wavelets.*

Waves in the backward direction that would be generated if each point along the wavefront were a source of spherical waves were shown by Kirchhoff to be non-

---

[12] Tipler, P.A., Mosca, G., 2003. Physics for scientists and engineers, 1010

existent, because the intensity of the new wavelets has an angel dependency (zero at 180º).

Refraction can be described as the change of direction a raypath undergoes at a boundary, when it experiences a change of velocity on passing from the first medium into the second. If the velocity increases when going from the first medium into the second, the raypath will bend away from the normal and vice versa. If the incident raypath is perpendicular to the boundary, no change in direction can be observed. The law required to fully explain this phenomenon is Snell's law (Equ. [4]), where v_1 and v_2 are the respective velocities in media 1 and 2 and θ_1 and θ_2 the angles between the rays and the normal to the interface (assuming that $v_2 \geqslant v_1$):

$$\frac{\sin \theta_1}{v_1} = \frac{\sin \theta_2}{v_2}$$

[4]

It is generally known that the angle of incidence equals the angle of reflection (Law of Reflection). When a light ray passes from, for example, air into glass, it is partially reflected and partially transmitted, with the angle of refraction depending on the initial angle of incidence and the relative velocity within the two media. The same can be said about seismic waves. Note that seismic reflection, though, is a matter of contrasting acoustic impedances (density times velocity) and refraction a consequence of contrasting velocities. Usually, these scenarios are concurrent, as a change in velocity causing refraction is unlikely to be accompanied by such a change in density, as to not produce a change in acoustic impedance.

Seismic refraction surveys are only interested in a special case of refraction, that is to say, the one where the refracted ray runs along the boundary between the layers. Explaining this in terms of equation [4], the angle of refraction θ_2 should be 90º, giving a ray perpendicular to the normal, or parallel to the boundary. The angle of incidence now becomes $\sin \theta_1 = \frac{v_1}{v_2}$ and is known as the critical angle, $\theta_1 = \theta_c$. To demonstrate this more clearly, Figure 4 illustrates a case where an incident wavefront approaches the interface at the critical angle. Incident rays at an angle to the normal smaller than θ_c experience refraction down into layer 2 (besides some partial reflection), while rays incident at $\theta_2 > \theta_c$ will only experience reflection.
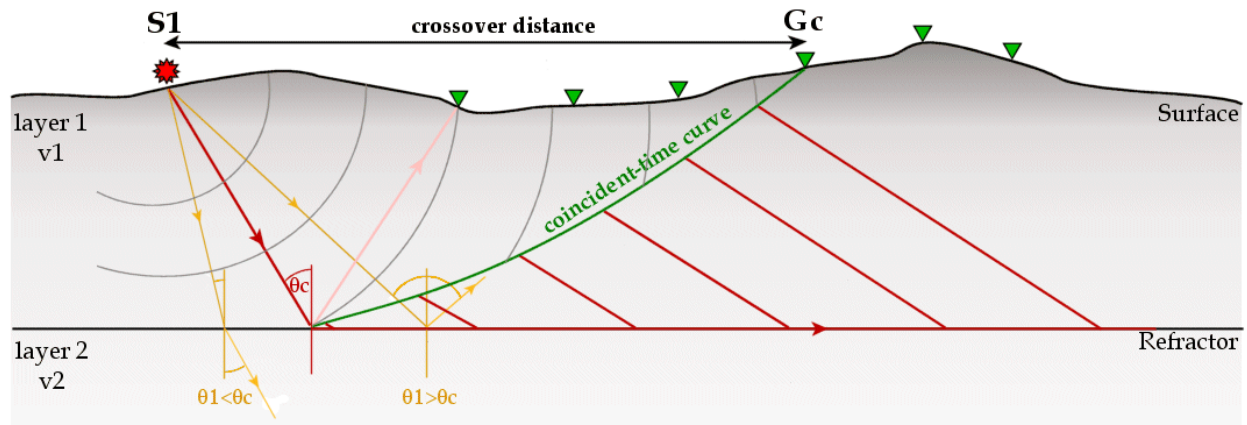
Figure 4 Illustration of refracted wave arrivals: red lines indicate refracted wavefronts emerging back into medium 1; grey spherical wavefield shows direct wave; bold green line corresponds to so-called coincident-time curve, where direct and refracted waves have the same travel-time, thus at receiver Gc, refracted waves will overtake direct arrivals

As the refracted wave propagates along the layer boundary, it is subjected to Huygens's principle and all particles along its wavefront act as secondary sources. These emit secondary wavelets at the critical angle, which return to the receivers through medium 1. It can be seen from Snell's law that the refracted ray, which is assumed to travel along the interface, travels at the velocity of layer 2, v_2. Secondary wavefronts emerging from the interface are therefore generated along the boundary, but the wavefronts themselves travel at the slower velocity v_1 through layer 1 up to the receivers.

At stations near the shot point, the first signal recorded will be the direct wave. After a certain offset, the effect of travelling at the faster velocity v_2 along the boundary will outweigh the fact that the refracted raypaths had to cover a greater distance, and the refracted rays will overtake the direct waves and be the first to arrive at the receivers. At this point, the offset between shot S_1 and receiver G_c, where the refracted wave is the first arrival, is called the crossover distance; hence the refracted wave is known as the head wave.

Refraction surveys usually accompany reflection surveys, but rely on their own setup of shots and receivers. Even though refractions are the first arrivals on reflection survey data too, the recording criteria are normally different and not ideal for refraction interpretation (some of the most common techniques are detailed below). The group spacing used in reflection surveys is too large to allow accurate resolution of thin refractors, which normally requires distances of around 5-20m between geophones and,

additionally, very short offsets are desirable to record the direct arrival. Despite the large offsets available from reflection surveys, which allow deep refractors to be evaluated, the data from reflection surveys is not extremely useful when it comes to picking first arrivals for refraction interpretation. This is due to the processing applied to it, as refraction surveys preferably produce unfiltered and broadband data to ensure optimum first breaks. As refractions are the first energy to arrive at the receivers, there is no need for filtering to increase the signal-to-noise ratio, as any coherent noise such as ground roll would arrive later anyway. Further incompatibilities arise from the need to deconvolute reflection data when the sweep signal generated by vibro-trucks is removed from the data. The first arrivals would not consist of the same kind of causal wavelet as from a dynamite source, commonly used during refraction surveys, because remnants of the autocorrelation of the sweep would be found in it.

2.6.1   Intercept-time Method

To understand how refraction techniques acquire information for the near-surface model, it is best to look at a hypothetical time-distance curve in Figure 5. This example deals with plane, horizontal interfaces of constant velocity, representing a 1D scenario where only one shot would be necessary to attain all the information, as there are no dipping surfaces. Above the time-distance curve in Fig. 5, there is a simplified model of the spread layout. It shows that the boundary between the two parallel layers is at depth z and the emergent point of the first refracted wave on the interface is called A. We have seen above that in close proximity to the shot point, the first arrival is the direct wave and it is apparent that the slope of the time-distance curve in this area is a direct measure of the velocity in the first layer, v_1. The refracted rays may be visible in the form of second arrivals. Rays emergent at point B arrive simultaneously with the direct arrivals, so the two travel-time curves intersect (the crossover distance is the offset at the surface, not along the refractor). At distances beyond B, refracted arrivals reach the receivers ahead of the direct wave and produce a slope with gradient $\frac{1}{v_2}$ on the time-distance plot.
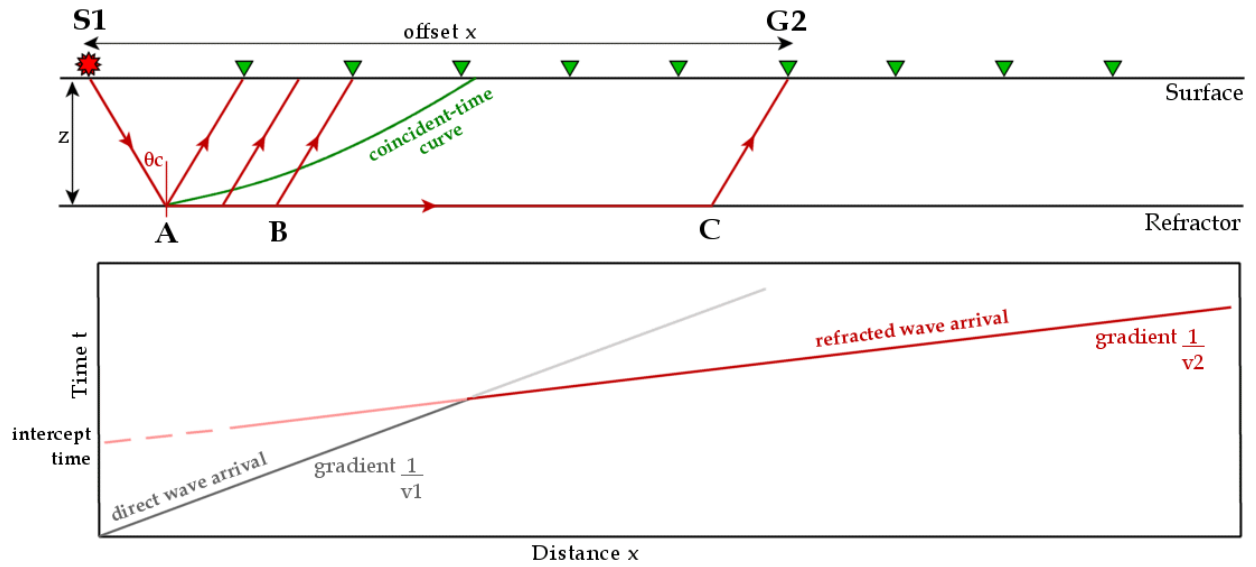
Figure 5 Time-distance plot for horizontal two-layer case, showing first arrivals from direct and refracted wave and extrapolation to read off the intercept time

To prove that the velocity of the second layer can be directly deduced from these recordings, we can set up the following equations:

If the time taken to travel from S_1 to G_2 (via A and C) is $t = \frac{S_1A}{v_1} + \frac{AC}{v_2} + \frac{CG_2}{v_1}$ and we know the line S_1A hits the interface at the critical angle θ_c at depth z, we can rewrite the equation to give $t = \frac{z}{v_1 \cos \theta_c} + \frac{x - 2z \tan \theta_c}{v_2} + \frac{z}{v_1 \cos \theta_c}$. Using Snell's law, this is equivalent to

$$t = \frac{x}{v_2} + \frac{2z \cos \theta_c}{v_1} \qquad [5]$$

which has the form of a straight line equation, $\frac{1}{v_2}$ being the gradient. In order to be able to solve this equation with three unknowns (z, v_1, v_2), we determine v_1 from the slope of the direct arrival, v_2 from the slope of the refracted arrival and z is worked out by assuming the offset x to be zero and reading the intercept time off the extrapolated time-distance plot to obtain a value for the term $\frac{2z \cos \theta_c}{v_1}$, in which the refractor depth is now the only unknown.

The crucial point to note here is that this method is limited to a simple case of parallel bedding. The velocity is presumed to be constant within the two media and the structures are horizontal. None of these preconditions is usually fulfilled in real terrain. One has to consider multi-layered geologies and the possibility of dipping refractors, as well as a gradual velocity increase with depth. Figure 5 shows that a correct determination of near-surface information demands a recording of the head wave over

many receivers, so that a precise gradient can be read off the time-distance plot. Shortening the distance over which the measurable slope is available is likely to result in errors of judgement on the interpreter's behalf, giving inadequate results for v_2 and z. This problem becomes even more recognisable in multi-layer cases featured below, where the number of refractors that can be mapped is bound by structural factors and spread layouts; note that this is still a 1D situation with no dips.
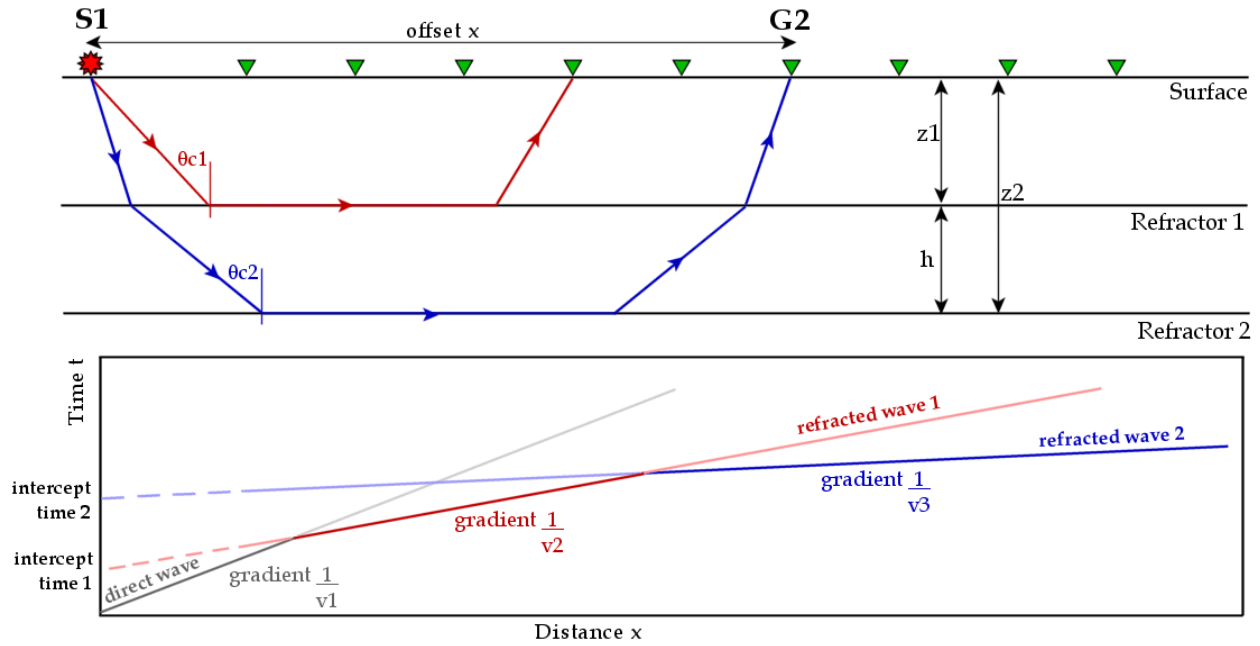
Figure 6 Time-distance plot for horizontal three-layer case, where two bends in the first arrival curve at the crossover distances mark increases in velocity

Figure 6 shows the time-distance curve of first arrivals in a three-layer case. The equations for the two top layers are the same as in a simple two-layer case, and the third layer can be computed by applying the same concept with a few modifications. The slope of the third refractor is equivalent to $\frac{1}{v_3}$, providing we assume parallel horizontal layering. In order to calculate the depth of this layer (z_2), we apply the same theory as above, working with the depth of the refractor relative to the layer above (h) and using its intercept time (intercept time 2). Whereas the depth of the shallow refractor is equal to its thickness, the depth of the deeper refractor is the sum of its thickness and the depth of the layer above.

Theoretically, this method could be extended indefinitely to any number of layers, building up the equation system to satisfy ever more refractors. Practical limitations, however, such as the need for very long offsets to record first arrivals from

22

deep refractors and the problem of differentiating clearly between the layers, particularly if the velocity changes are small, reduce the standard model to a maximum of 2 to 3 layers. The geology of the survey area greatly affects the resolution of the model. The bend in the travel-time curves marks the onset of a new layer and indicates where the crossover distance along the surface is found i.e. where the refracted wave overtakes the direct wave, or in multi-layer cases, where the waves from a deeper refractor overtake those from the shallower refractor. A reasonably strong velocity contrast between two layers manifests itself as a clear bend and hence an easier velocity determination. Too strong a contrast between thin layers, however, might result in hidden layers, as they are not obviously separate refractors on the time-distance plots and lead to erroneous depths. Layers of very small thickness compared to the surrounding ones might only appear as a second arrival and not as a first, which makes them impractical for refraction analysis. Another situation which can give rise to hidden layers are velocity inversions. These, common in permafrost regions, cause seismic waves to be refracted towards the normal when they hit the interface between the fast layer and the underlying slower layer. Incident waves will not strike the lower layer at the critical angle in order to produce the refracted wave that runs along the interface and eventually produces the measurable head wave.

This shows that the concept of refraction surveys to provide near-surface information is only valid if the velocity increases with depth. This is true even when dealing with non-horizontal layering, leading to 2D/3D scenarios i.e. where one shot does not suffice to acquire subsurface information. Dipping refractors, whether that is just one or multiple dipping interfaces, can be resolved adequately as long as reciprocal shots are employed. Reciprocal shots require shot-receiver locations to be interchangeable to give a forward and reverse shot for the same underground profile. That way, an up-dip and down-dip velocity, along with an up-dip and down-dip thickness can be determined, from which the true values can be deduced. The reciprocity of this method refers to the travel-time of the wave, which should be the same if the shot and the receiver station are reversed.

If the stratigraphy consists of very thin layers, the resolution (governed by the geophone spacing of the refraction profile) might not be sufficient to distinguish them as individual layers and, instead, the curved travel-time plots appear to give a velocity

gradient. Gradual velocity changes with depth, as opposed to discrete homogeneous layering, will be considered further in Chapter 4, regarding diving wave tomography.

2.6.2   Delay Time Method

The delay time method is basically a continuation of the two-layer intercept method. Equation [5] for the travel-time t at any offset x was said to be $t = \frac{x}{v_2} + \frac{2z\cos\theta_c}{v_1}$, which can be rewritten as an expression of the intercept time t_0 (where x = 0) to give depth z as $z = \frac{t_0}{2}\frac{v_1}{\cos\theta_c}$. When rewriting this once again to get rid of θ_c, we get

$$z = \frac{t_0}{2}\frac{v_1 v_2}{(v_2^2 - v_1^2)^{\frac{1}{2}}} \qquad [6]$$

The delay time concept now splits this intercept time t_0 into a shot and receiver component and argues that, if the true refractor velocity is known, the intercept time at offset x corresponds to the time difference between the actual arrival time t and the time travelled along the interface vertically below shot and receiver, $t_0 = t - \frac{x}{v_{refractor}}$.

The raypaths in Figure 7 show which travel paths and travel times this concept corresponds to. The delay time as defined by Gardner [13](1939) is composed of the receiver delay time $t_{R|delay}$ at one end of the profile and the source delay time $t_{S|delay}$ at the other, so that in the special case of horizontal parallel layers, these two delay times are equal. If this is the case, each delay time is half the intercept time and Equation [6] can be rewritten as $z_R = t_{R|delay}\frac{v_1 v_2}{(v_2^2 - v_1^2)^{\frac{1}{2}}}$ or $z_S = t_{S|delay}\frac{v_1 v_2}{(v_2^2 - v_1^2)^{\frac{1}{2}}}$, giving the refractor depths at receiver and shot station, respectively.

---

[13] Gardner, L.W., 1939. An areal plan of mapping subsurface structure by refraction shooting: Geophysics, v.4, p. 247-259
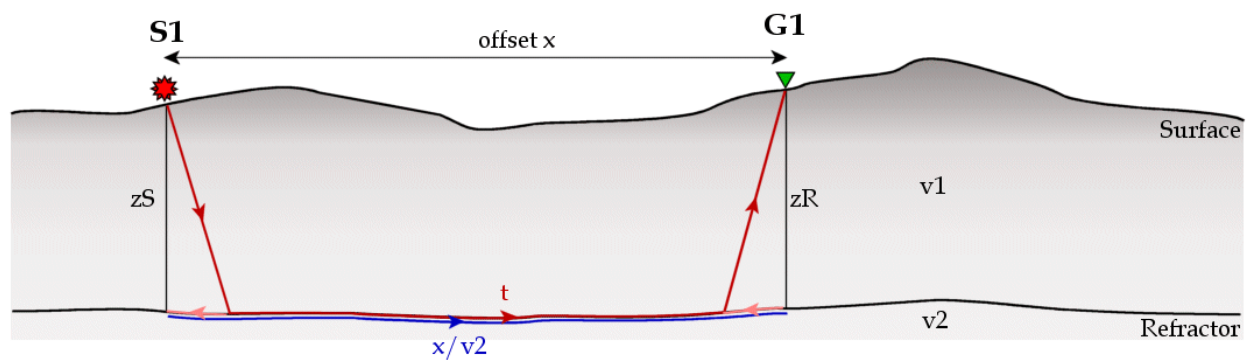
Figure 7 Blue raypath corresponds to distance between vertical downward projection of S1 and G1, waves taking time $\frac{x}{v_2}$; red raypath corresponds to actual travel time t; delay time is the difference between the two and can be decomposed to give depths z_S and z_R at either end of the profile

Further use of the delay time concept is sometimes made directly in datum statics, where the delay times are taken to be weathering corrections when the layering is sufficiently flat or only has limited dip, and the critical angle is small enough to assume the incident rays to be close to vertical.

2.6.3 Other Refraction Interpretation Techniques

There are numerous ways how to interpret refraction surveys, many being based on similar principles to the ones already mentioned, others taking wholly different approaches, such as wavefront methods. One important method which should not go unmentioned is the Plus-Minus method by Hagedoorn[14]. It requires a reversed refraction profile with receivers at common surface locations for a forward and reverse shot. The so-called plus time – the sum of the two travel times from the sources to the common surface location, minus the reciprocal time between the two sources – gives information about the travel time from the surface to the refractor and is thus a measure of the delay time. The minus time leads to a straight line equation with a gradient corresponding to the refractor velocity.

A generalisation of this approach is Palmer's idea of the generalised reciprocal method[15] (GRM), which can be applied to common surface, as well as common subsurface locations. Likewise, it relies on reciprocal times on a reversed refraction

---

[14] Hagedoorn, J.G., 1959. The plus-minus method of interpreting seismic refraction sections: Geophysical Prospecting, 7, 159-182

[15] Palmer, D., 1980. The generalized reciprocal method of seismic refraction: SEG

profile, but while the Plus-Minus approach works on parallel horizontal layering, the GRM is insensitive to dips up to 20° and can handle velocity gradients. The drawback of Plus-Minus and GRM approaches is that they are limited to inline applications, or 2D layouts, while the Delay Time method can be extended to a 3D configuration. More about these techniques can be found in Cox's book on static corrections in seismic[16].

2.7   Uphole Surveys

A vital part of the near-surface information we come to know prior to a production survey stems from uphole surveys. They are used to support data from refraction surveys, or vice versa, in order to produce a denser grid for interpolation and extrapolation of a near-surface model within the investigated area. The locations where these are carried out are chosen on a basis of how irregular the shallow geology is and where further sample locations are needed to ensure stable interpolation. It makes sense to choose sites where there is an intersection of lines during the production survey, since the acquired information would be directly applicable to two lines or more.

Typically, on an average production area covering some hundred square kilometres, there is one refraction survey per square kilometre, along with however many uphole shots are deemed necessary, as is later shown to be applicable to the case study at hand. The procedure of an uphole survey is to drill a borehole to a depth below the weathered layer, into the deeper refractor, in order to determine the subweathering velocity too. The depth is uniquely determined by the geological setting, but average values range from a couple of hundred metres up to 500m in extreme cases[17]. A series of dynamite charges is lowered into the hole at regular spatial intervals, where the detonations will be set off and recorded at the surface using uphole geophones. It is standard to do it this way round, as opposed to lowering hydrophones into the drill fluid and shooting at the surface, because a drawback is that the receivers are unusable if the hole caves in during the survey, whereas the charges can still be detonated.

Besides deciding on an areal sampling interval for the uphole shots, it is just as important, if not even more so, to choose an appropriate depth interval for the shots.

---

[16] Cox, M.J.G., 1999. Static corrections for seismic reflection surveys

[17] Cox, M.J.G., 1999. Static corrections for seismic reflection surveys

There should be a compromise between efficiency and resolution, as uphole studies are a costly factor that cannot be carried out at an unlimited number of locations. The same applies to shot intervals within the borehole: the closer the shots are spaced, the greater the resolution of rock layers can be attained, but it is uneconomical if the objective of the survey is not as precise.

Once the sources are in place, several geophones are placed around the borehole so that the signal is recorded from different azimuths. The receiver positions are not imminently next to the borehole, but a few metres away, because the wavefield might be distorted if it travels too parallel to the shaft, as the drilling process disturbed the ground. Surrounding the borehole, material will have been shattered and is therefore only an approximation of the actual underground. Drilling fluid would also have penetrated the pores of the loosened rock and created something called an invaded zone. Waves travelling through this would be delayed and not give valid velocity information.

The travel-time plots from these shots are then used for picking the first breaks. A small enough shot interval should give at least three picks per geological unit through which a straight line can be drawn to measure its slope, the velocity. However, this also paves the ground for a variety of possible interpretations: an average trend line through the picks, having a certain slope, could also be interpreted as two individual lines of different slopes, providing a sufficient number of picks is available to define them well enough. In the first case, one would interpret the picks as a single refractor of a certain velocity and thickness, while the latter case gives an alternative result in the form of two separate refractors. It is a matter of judgement how to go about such ambiguous displays, but any additional information about the geology, for example, as obtained from the drilling core, might narrow down the options. The pertinence of such interpretations is simply geological; concerning the static corrections, they become negligible because the static times need to provide adequate corrections for however many layers.

Good quality first breaks are produced if the signal is as broadband as possible. This starts when using an explosive source so that a short impulse, as opposed to a longer wavelet, is emitted, which encompasses all frequencies. Furthermore, no filtering should be applied, except the antialias filter during digitisation, which might reduce

certain frequency contents or cause delayed signals. An influential factor during picking is the gain of the signal. Increasing this may cause the onset of the signal to appear earlier than on no-gain data. Once the picks have been placed, they are corrected for any known delays in timing and triggering, in addition to the time shift to convert uphole times to vertical times. The underlying assumption of this geometrical correction is that the raypaths travel directly from the sources to the receivers without being refracted at interfaces. Thicknesses and velocities of the geological layers are now estimated using the travel-time plots on a similar principle as described in section 2.6 on refraction surveys.

3 Case Study – Oichtental

3.1 Geology

The research of this thesis concerns a special geological setting known as a deep glacial valley. Being set along the Northern Alpine Front in the province of Salzburg (see map in Figure 8), the Oichtental is an overdeepened valley attributed to fluvial erosion during the last glacial period of the current ice age, known as Würm period. Overdeepening is a phenomenon associated with regions which were once covered in ice; it occurs when glaciers erode valley beds down to depths that lie below the level of the valley floor further downstream.
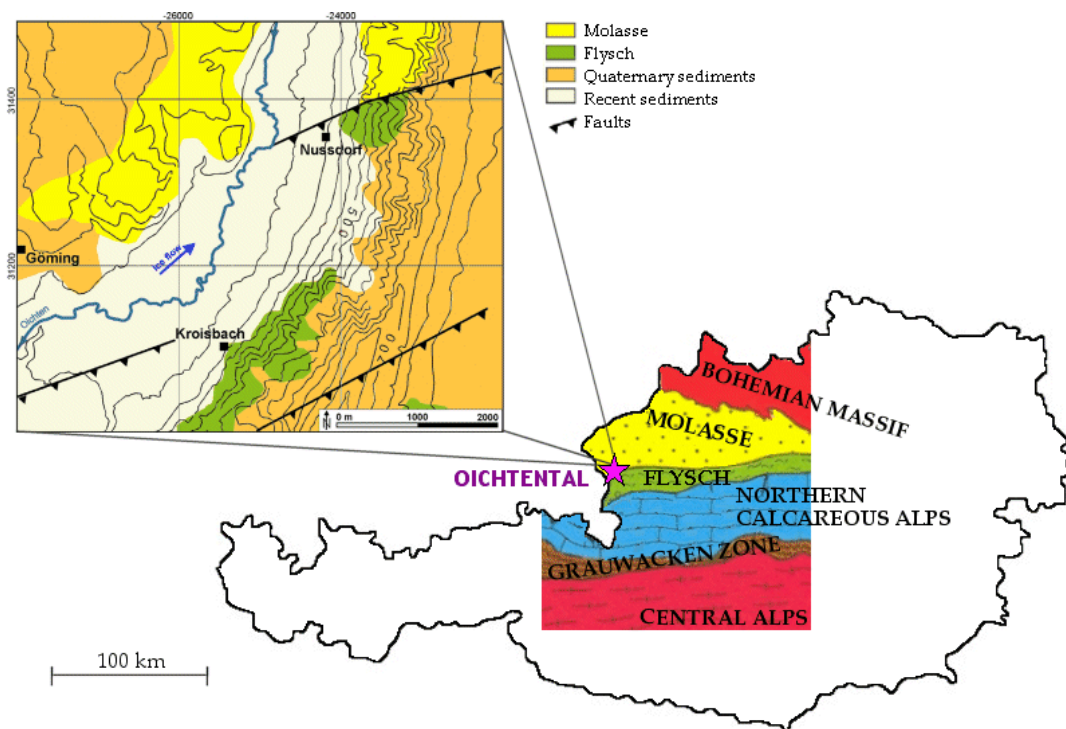
Figure 8 Location of the Oichtental valley with the overlain surface geology; close-up shows the detailed geology and faults in the area around Nussdorf

Deep glacial valleys are found in several places in the Alps, and are characterised by an erosion base which was covered by sediments once the glaciers had retreated at the end of the Würm period. Due to the recentness of this infill, the material in the valley tends to be unconsolidated compared to the surrounding flanks, which consequently leads to a slower seismic velocity than in the enclosing rock basement. This constitutes a sharp lateral velocity contrast that is difficult to delineate, yet

necessary in order to apply correct static corrections, hence the aim of this thesis is to accurately define a velocity model in such a complex subsurface.

The Oichtental is located in a compression zone where Flysch, a sedimentary rock stemming from deep marine facies in the foreland of developing orogens, overthrusts the Molasse of the Alpine foreland. The Molasse encompasses sediments that were deposited on top of the Flysch, once the Flysch sediments had filled in the deep marine environment of the foreland. The Molasse is therefore characterised by shallow marine or even terrestrial facies. Due to the northward movement of the Adriatic plate, the Flysch under the Alpine nappe is forced over the further-inland Molasse. A cross-section through the relevant area of the Alps can be seen in Figure 9.
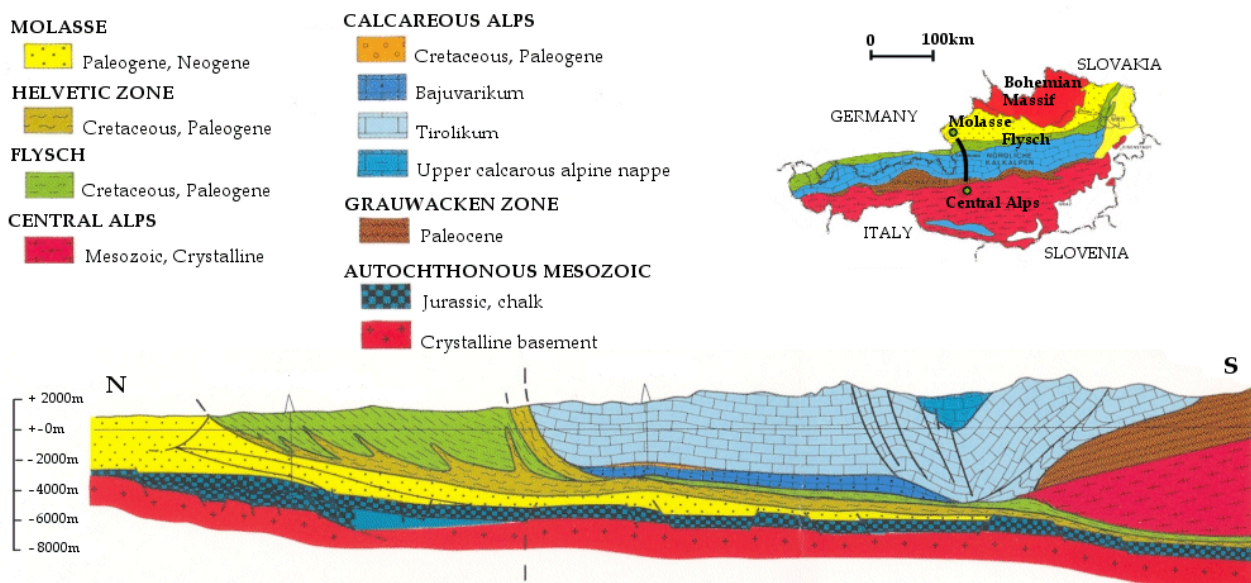
Figure 9 [18]Cross-section along a profile through the Eastern Alps near Salzburg; profile drawn as a black line between green end markers on small map insert

There is no single comprehensive explanation of why overdeepening in glacial valleys arises. Different ideas have been put forward, such as regions of confluence, where the ice masses of two or more glaciers need to fit into the same bed, thus carving the valley deeper. Overdeepening, though, was shown to be found even in areas where there is no confluence. Brückl et al. (2007)[19] proposed high water pressure on the glacial

---

[18] Brix, F., Schultz, O., 1993. Erdgas und Erdöl in Österreich, Enclosure 9

[19] Brückl, E., Brückl, J., Chwatal, W., Ullrich, Ch., 2007. Deep Alpine Valleys - examples of geophysical explorations in Austria

bed to be the cause of the deep Oichtental. This theory would also agree with the tendency of deep valleys not to appear in the typical U-shape associated with glacial erosion, but rather, showing a V-shape normally linked to river erosion; Brückl compared a set of three deep valleys in the Alps, showing that the deeper the erosion base, the more pronounced the V-shape.

According to Van Husen (1987)[20], the highest ice elevation in the Oichtental during the last glacial period was approximately 700m. Today's valley floor lies at around 400m (see topographic map of the region in Figure 10), and the maximum infill thickness found during seismic investigations leading up to Brückl et al.'s publication in 2007 was said to be around 350m, giving the old valley base an absolute elevation above mean sea level (AMSL) of around 50m.
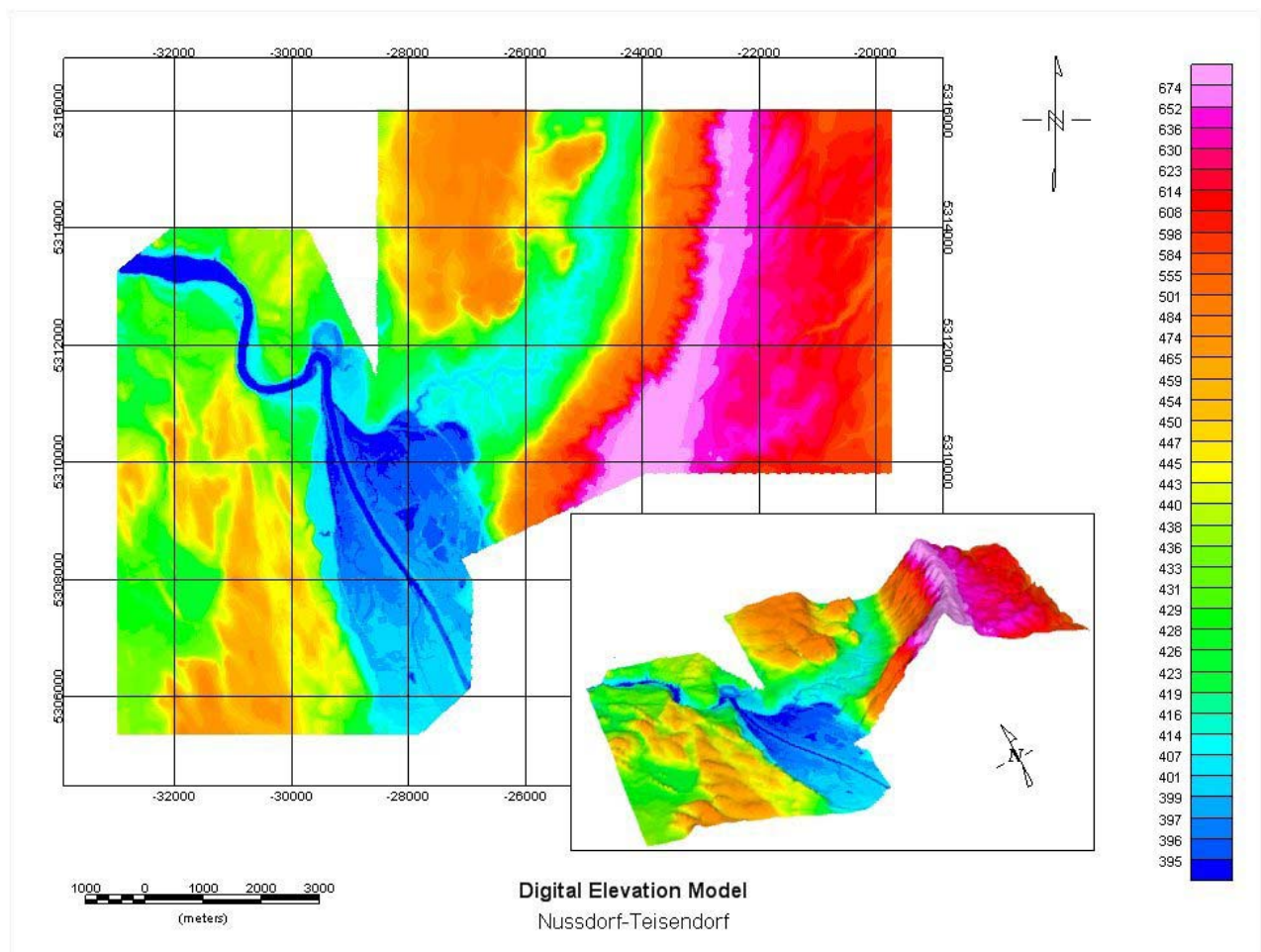
Figure 10 Digital terrain model in Upper Austrian coordinates of the investigated area; insert shows 3D display of topography, rotated to look in a North-East direction up the Oichtental valley

---

[20] Van Husen, D., 1987. Die Ostalpen in den Eiszeiten. Aus der geologischen Geschichte Österreichs. - Populärwiss. Veröff. Geol. B.-A.Wien, 24

In the seismic, the valley bed appeared as a flat, continuous reflector below a set of irregular reflections from the main infill body. This irregular infill was termed "old valley infill", while on top of it, one could find regular flat reflectors again. Their undisturbed and high frequency character is a strong indicator for unconsolidated lacustrine deposits, which is confirmed when looking at the borehole lithology from wells operated by Rohöl Aufsuchungs Aktiengesellschaft (RAG) in the vicinity, shown in Figure 11.

OICHT 5		OICHT 7	
depth [m]	Lithology	depth [m]	Lithology
14.5	marsh	14	detrital clay
100	lacustrine clay	176	lacustrine clay
105 (end depth)	gravel	201 (end depth)	gravel

OICHT 8		OICHT 9	
depth [m]	Lithology	depth [m]	Lithology
6	gravel	3	clay
213	lacustrine clay	214	lacustrine clay
214 (end depth)	gravel	243 (end depth)	gravel
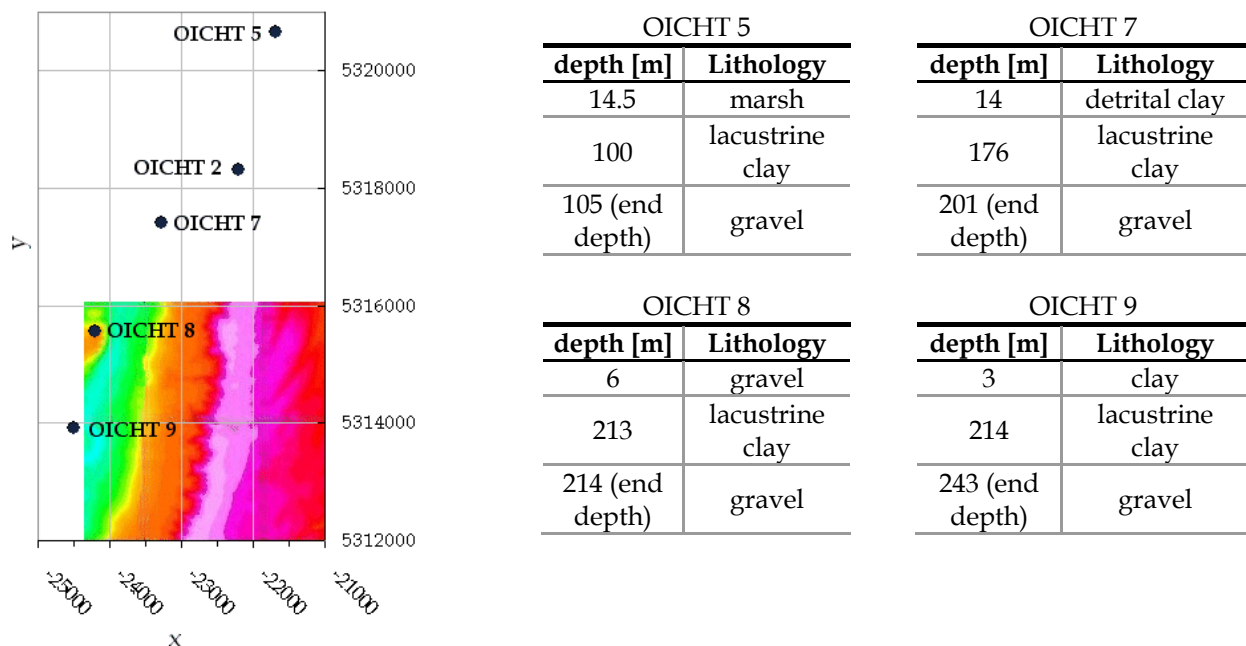
Figure 11 Map gives locations of boreholes in the Oichten valley (OICHT), mostly located outside the range of the digital elevation model; tables show where base of lacustrine clays was encountered

As the glacier would have retreated during the temperature increase at the end of the glacial, the end moraine would act as a natural barrier, trapping melt water in the trough behind it. This environment would provide undisturbed conditions for sediments to be deposited after glacio-fluvial transportation, resulting in layers of fine lacustrine clay. The sediments are typical examples of Quaternary rocks, which are characteristically not consolidated and found in depositional environments such as glacial landscapes, originating 1.8million years ago to present. The flow direction of the glacier is presumed to have been north-eastwards, as this would represent a flow direction away from the Alps into the foreland and coincides with the flow direction of the river Salzach, which is the largest river within this drainage system. Despite this, the

current Oichtenbach stream actually flows south-westwards. Figure 12 shows a detailed map of glacial landscape features found around Nussdorf in the Oichtental and the nearby surroundings.
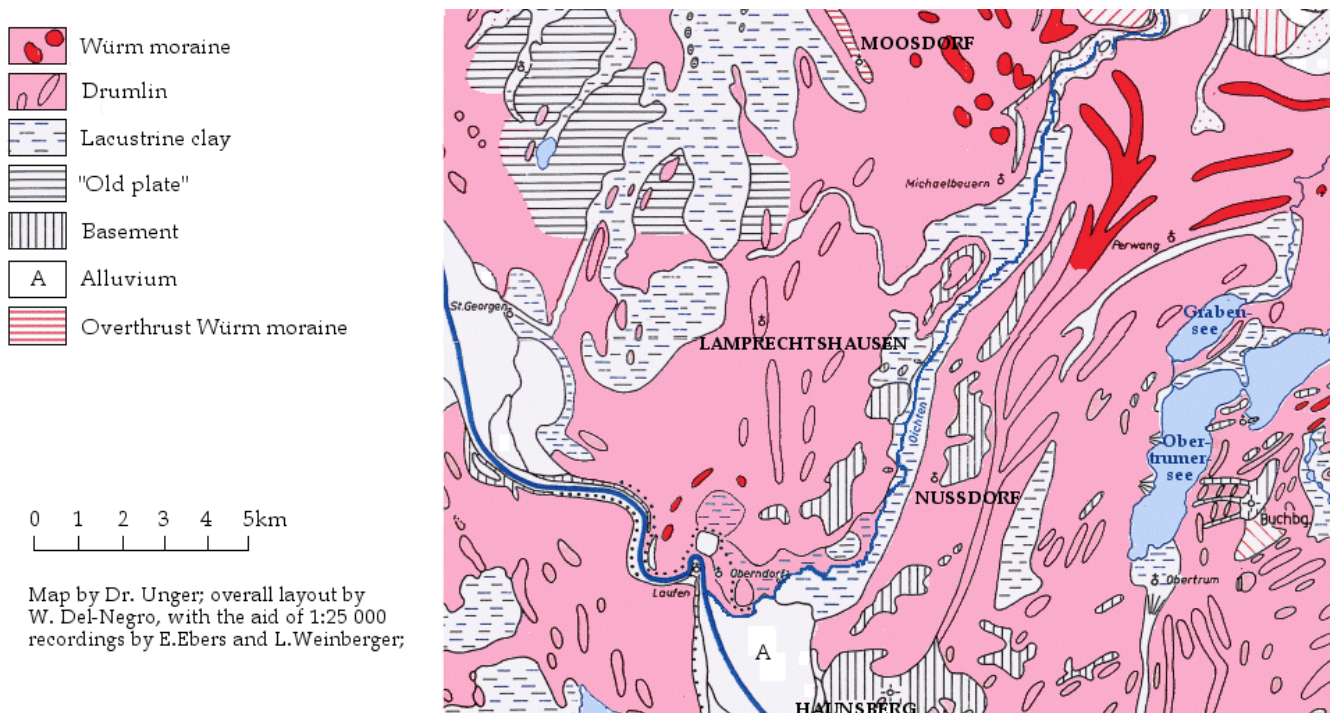
Figure 12 Glacial landscape features in and around the Oichtental as a result of the Salzach foreland glacier during the Würm ice age

3.2 Seismic Survey

The Oichtental falls within the area of the Nussdorf production survey near Salzburg, conducted on behalf of RAG during summer 2001. The data was processed by the in-house office of WesternGeco in 2002, and following further data acquisition for a survey near Teisendorf (Bavaria, Germany) in 2003, which overlapped the edge of the exploration area in Austria, the data was collectively reprocessed in an attempt to see if certain inconsistencies and difficulties with the near-surface model could be resolved.

The earlier of these two acquisitions, known as the Nussdorf survey, saw a requested processing flow which essentially involved surface consistent deconvolution, 3-layer datum static corrections, 3D DMO velocity analysis for 3D DMO stacking, and 3D post-stack time migration. Surface consistency, as in the case of deconvolution, is the idea of ascribing a value for a parameter to a certain surface location. In the case of statics, this would mean that the static correction time is specific to a station,

disregarding whether a source or receiver is placed there. In the case of deconvolution, the surface consistent parameter is the design window of the deconvolution filter.

Here is a list of the important acquisition parameters of the 58 km² Nussdorf survey, which was conducted in the form of five North-South oriented swaths:

Binsize:	12.5m x 12.5m
No. of processed shot records:	6812
Receiver station interval:	25m
Receiver line spacing:	250m, north-south oriented
Source line spacing:	375m, east-west oriented
Source station interval:	25m
Total no. of single traces:	9 620 389

The nomenclature of the layers and their respective velocities from now on shall be as follows:

1st layer: velocity v_0, thickness z_1 from surface to base of 1st layer

2nd layer (1st refractor): vel. v_1, thickness z_2 from base of 1st to top of 3rd layer

3rd layer (2nd refractor): vel. v_2, thickness z_3 from base of 2nd layer to ref. datum

Intercept time of first refracted wave:	ICT1
Intercept time of second refracted wave:	ICT2

Problems attributed to the Oichtental first emerged during surface consistent deconvolution. Due to the great elevation range in the area and the lateral change of velocity and thickness of the weathering layer in the Oichtental, there were irregularities in the constant offset travel times. As specified in the WesternGeco processing report, the travel time delays were produced by Oichtental's low velocity, which was said to be 1500-1700ms⁻¹. The thickness of the v_1 layer was also considerable and lay somewhere between 200m and 400m, while the topographic change from an average 400m AMSL within the Oichtental, up to 780m AMSL in the Haunsberg mountain range, was also not to be underestimated.

For the 2003 Teisendorf survey, 13 swaths were acquired over an area of 205km². The data were merged with two previously recorded adjacent surveys: Nussdorf (2001)

and Lamprechtshausen (1993); the area covered by these three surveys is displayed in Figure 13. The merged data extended over almost 370 km² and some of the important acquisition parameters are listed below:

Binsize:	25m x 25m
Inline orientation:	North-South
Data volume after merge:	591 828 bins
Total no. of traces after edits:	19 986 618
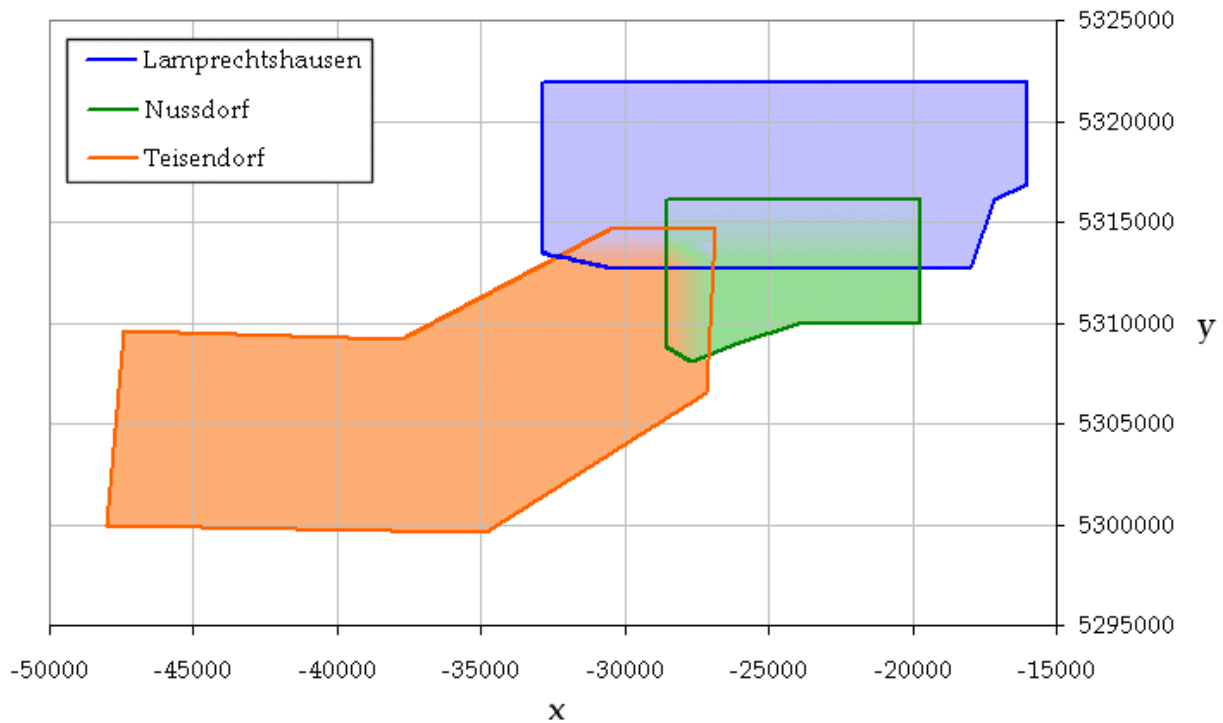
Figure 13 Three adjacent surveys (in Upper Austrian coordinates), Teisendorf (T), Lamprechtshausen (L) and Nussdorf (N), merged into one data set (TLN) preceding data processing

The merged Teisendorf-Lamprechtshausen-Nussdorf (TLN) data set was treated in the same sequence as the Nussdorf acquisition in 2001 (surface consistent deconvolution, 3-layer datum static corrections, 3D DMO velocity analysis for 3D DMO stack, and 3D post-stack time migration) with the addition of a 3D pre-stack Kirchhoff time migration at the end.

3.3 Previous Datum Static Corrections Calculated on the Nussdorf Survey by WesternGeco (2002)

Seeing as the Nussdorf processing was to be revised once the data was merged with the newly acquired Teisendorf seismic, I shall only give a brief outline of these first static corrections. The principle underlying the Nussdorf statics was a 3-layer model derived from a tomographic delay time approach, i.e. iteratively solving the delay time equations to find the exact source and receiver delay times down to the refractors. The seismic reference datum was set to 300m above mean sea level and the uppermost weathered layer was assumed to have a constant v_0 of 500ms^{-1}.

The starting model for the tomographic delay time method required values for v_1, v_2, ICT1 and ICT2. These were found through the intercept time method described in section 2.6.1 and involved automatically picked first arrivals on the production data. The challenge was therefore to design an appropriate pick window that would adequately find the first breaks at various offsets and surface locations. The gradient of this pick window is referred to as a variable, coordinate dependant pick-acceptance corridor velocity (VPAC). Once the picks were satisfactory, slopes (v_2) and intercept times (ICT2) were read off the plots, while v_1 and ICT1 were taken from short refraction profiles (SRF) acquired by Geophysik GGD over the survey area. From refraction profiles and borehole logs, the Oichtental was known to be a first refractor of relatively great thickness and low velocity compared to the much thinner refractor underneath, equating to the scenario of a hidden layer explained previously. The pick window was thus limited to offsets where any possible arrivals from the v_1 layer would be cut out.

The final model was checked against uphole shots available from wells in the Nussdorf area (called OICHT-8, OICHT-9 and Nuss-W-001), to see how the one-way travel time through the calculated model at the receiver nearest to the borehole compared to the recorded uphole times:

OICHT8: difference of -3ms to nearest receiver (station 441667, distance = 55m)

OICHT9: difference of -4ms to nearest receiver (station 451733, distance = 6m)

Nuss-W-001: difference of -18ms to nearest receiver (station 491732, distance = 97m)

3.4 Previous Datum Static Corrections Calculated on the TLN Survey (2003) by WesternGeco

The data merge brought a slight complication with it in terms of positioning, as the source and receiver locations for the Teisendorf data were in Bavarian coordinates, but the Lamprechtshausen and Nussdorf data in Upper Austrian coordinates. For means of comparison, all station coordinates were transformed into both systems, so that static corrections were computed for both grids. Again, a 3-layer model was used, but this time the reference datum was set to 450m AMSL.

Previously acquired short refraction profiles, along with new ones for the Nussdorf survey, were used to obtain attributes v_1, z_1 and ICT1. As with the previous Nussdorf processing, an elementary part was the first break picking on the production data. The software involved uses a combination of correlation techniques, such as the ratio of power (or amplitude) before and after each sample on a trace, correlated over neighbouring traces or stacked traces in order to increase the signal-to-noise ratio, which might be too low on a single trace. The maximum ratio would equate to maximum power increase and this represents the onset of the signal, i.e. the first break. The first break picking was known to be difficult in the area around the Oichtental from old processing of the Lamprechtshausen data, where 2D lines showed low signal-to-noise ratios due to the high absorption characteristic of lacustrine clays. The problem of the valley base lying below the seismic reference datum (300m at the time), and therefore not including the whole valley in the static corrections, was already recognised back in 1991, according to an internal RAG study. Incorrect static corrections were a cause of so-called cycle skips, where apparently continuous reflectors actually included peaks or troughs on certain traces that are half a wavelength shifted in relation to the other traces and their peaks and troughs.

In the 2002 processing, the v_0 layer was set to a constant 500ms^{-1}, whereas refraction surveys showed it had a variable velocity, ranging from 250ms^{-1} to 800ms^{-1}, with a thickness of 5-20m. According to WesternGeco's processing report, these values are not extremely reliable, but in view of the insignificant thickness of the first layer, any erroneous first-layer-statics contribute less severely to the overall statics. Values for the second layer are also found using SRF profiles, despite its occasional appearance as first arrivals on short-offset traces of the production seismic. But seeing as first breaks

from the second layer only ever spanned a few traces, they would have been too unreliable to pick. Thickness ranged from 20-350m and the velocity averaged around 2200ms^{-1} (note that the thickness and velocity of the Oichtental forms an exception to these average values for the main weathering layer). First breaks on the production seismic showed sharp bends where there was an onset of a linear refractor, suggesting there are distinct layers rather than velocity gradients that would cause diving waves. The third layer, apparent on medium offsets of the production seismic, had a slope of around 3000ms^{-1}.

As for the Nussdorf data, the static calculations were performed on a tomographic delay time basis. Information from SRF profiles was used to remove the first layer in time and depth, pretending the whole survey had taken place at the top of the first refractor. This method uses half the intercept time as the source and receiver delay time to project sources and receivers downwards, which is justified as long as the raypaths through the first layer are presumed to be almost vertical. The values for ICT2, v_1 and v_2 were the initial SRF input to the process, which solved the least square equations derived from the delay time equations. From these initial inputs, delay times at each station were computed by subtracting the linear moveout from the picked arrival time and taking half of the average remaining time (average, because supergathers were used). The results were iteratively calculated delay times (and hence z_2) for the first refractor and the velocity of the second refractor. The first layer is now added back on in time and depth to obtain the full near-surface model. That way, only ICT1 and z_1 are values used which directly relate to the first layer, and no assumptions about the velocity need to be made.

The Oichtental showed similar peculiarities in constant offset travel times as it had done during the previous 2002 processing. The findings were put down to its unusually low velocity, its relatively large thickness and great elevation changes over the survey area.

4   Producing a New Near-Surface Model

The task set for this thesis was to try two alternative approaches to the one taken by WesternGeco, by creating a new velocity model and see if any improvements to the datum static corrections could be achieved. The implemented methods are a 1D inversion of stacks, described by Behm et al. (2007)[21], and a 3D diving wave tomography using software by J.Hole[22]. For testing purposes, an 8.75km long (east to west) and 2km wide (north to south) swath was chosen from the Nussdorf seismic, which incorporated a transect over the Oichtental, as well as sufficient elevation changes on either side. The corner points in Bavarian coordinates [x, y] of the velocity model to be created are thus [4571000, 5312000], [4579750, 5312000], [4579750, 5314000] and [4571000, 5314000], see Figure 14.
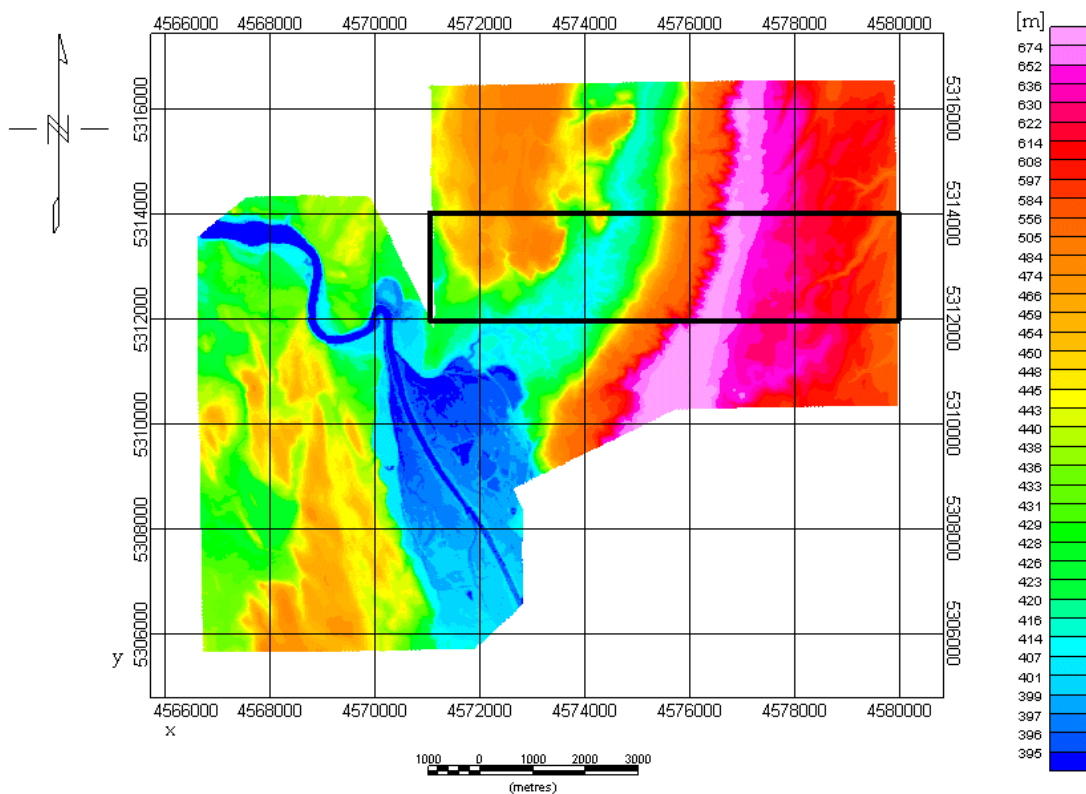
Figure 14 Elevation map, showing the testing area for this study surrounded by bold, black rectangle

---

[21] Behm, M., Brückl, E., Chwatal, W., Thybo, H., 2007. Application of stacking and inversion techniques to three-dimensional wide-angle reflection and refraction seismic data of the Eastern Alps, Geophys. J. Int.

[22] Hole, J.A., 1992. Nonlinear high-resolution three-dimensional seismic travel time tomography. J. Geophys. Res., 97, 6553-6562

4.1   1D Inversion of Stacked Data

4.1.1   Method

The idea of using stacked data to invert travel times and obtain a 1D velocity function within a cell tries to work around the problem of having a low signal-to-noise (S/N) ratio, which restricts adequate detection of the first arrivals. Picks on single-fold sections, as employed in travel time tomography, often suffer from poor data quality, particularly in complex near-surfaces where scattering introduces random noise. Stacking traces to increase the S/N ratio suppresses random noise and enhances coherent signals, suggesting that first arrivals on stacked sections could be detected more clearly.

The method described by Behm defines a regularly spaced grid over the survey area, where the grid points form the centre of the cells (see Figure 15). For this case study, the cell size was chosen to be 250m x 250m, giving a total of 35 cells in the west-east direction and 8 cells north-south, with the most south-westerly cell having its centre at [4571125, 5312125] and the most north-easterly at [4579625, 5313875]. The data are now sorted according to common midpoints (CMP); all traces with a common midpoint in one of the grid cells are collected in a CMP gather; note that this might involve traces that have either their receiver, their source, or both, outside the chosen 2km wide swath.
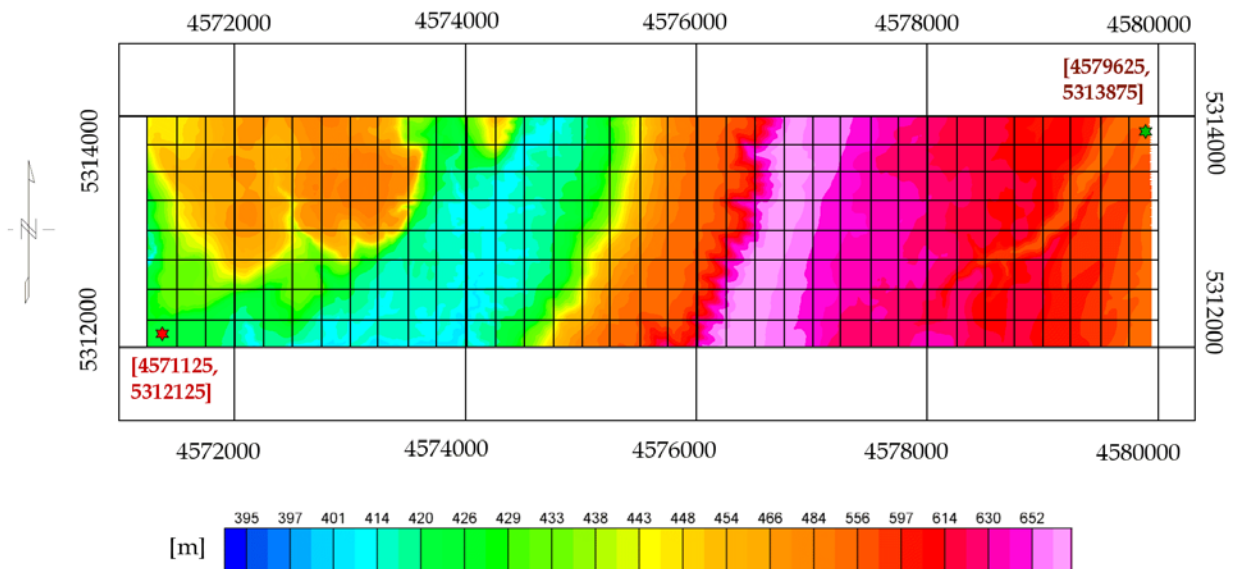
Figure 15 Test swath (8.75km x 2km) with overlain grid of 250m x 250m cells; central coordinates of the two outermost cells shown in brackets. Traces with CMP within a certain cell are collected into a gather

Conventional seismic reflection processing, according to Yilmaz[23], would call for a velocity analysis at this point in order to apply normal moveout correction to the data, prior to stacking CMP gathers. In our case, however, the absolute offset is specified as a secondary sort key to group all traces within a CMP gather that fall into the same offset range. The group size, also known as bin size because the traces are binned into these groups, was defined to be 25m. In other words, all traces within the CMP gather that had an absolute offset of 0 to 25m were grouped together, so were traces from 25-50m, 50-75m and so on. All traces within these offset bins were then stacked in order to pick the first breaks. Opposed to a conventional CMP stack, which yields only one trace per common midpoint, the offset bin stack (OFB) yields as many traces as there are offset bins within the CMP gather. A further difference is the fact that conventional CMP processing gathers and stacks traces within a relatively small area, like a 25m x 25m (or even 12.5m x 12.5m) bin, whereas the OFB stack contains traces with midpoints in a 250m x 250m large cell and simply groups them into offset gathers before stacking. Both, conventional CMP stacks and OFB stacks, have the inherent fault of smudging azimuths, but this is a far more severe issue in OFB stacking because the azimuths are smeared over a considerable geographical extent and traces at completely opposite ends of the cell could fall within the same offset bin, which is not helpful when trying to resolve short-wavelength lateral variations (Figure 16 is an illustration of CMP vs OFB). Nevertheless, the advantage here is that first arrivals can be picked to obtain a 1D travel time curve associated with a certain cell, which is inverted to derive the velocity-depth function.

---

[23] Yilmaz, Ö., 1987. Seismic data processing, Society of Exploration Geophysicists
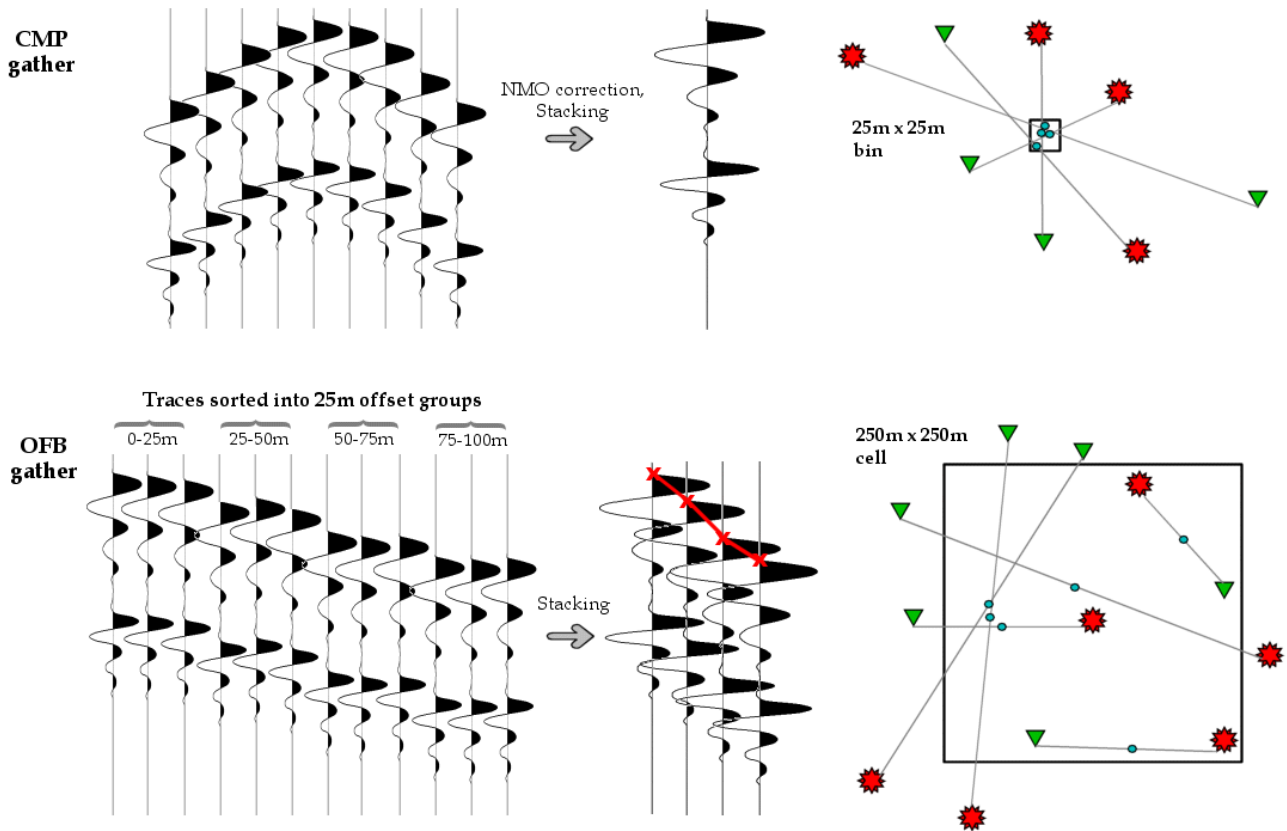
Figure 16 CMP vs OFB stack: a 1D travel time curve (red crosses marking first breaks) is obtainable on an OFB stack, but compromised by the fact that information is smudged over a much larger cell area compared to conventional CMP binning; blue dots mark common midpoints in the cells.

The OFB stacks for picking turned out to be most suitable when the traces were converted to their envelope prior to stacking. The envelope, or complex amplitude, is always a positive value and represents the reflection strength. An automatic picker was used to detect the first arrivals, choosing the maximum amplitude gradient as the pick criterion to detect the true onset, rather than going for maximum amplitude (i.e. peak). As the shape of the first arrival turned out to be too indistinct, however, we opted to pick all OFB stacks manually, which would not have been an efficient option for large-scale production seismic. The picking is quite a complicated issue for the inversion, as for example, very precisely picked travel time curves with fluctuating pick times are too detailed to resolve. Instead, the processor should pick a smooth line through the first arrivals, with a bend wherever one considers it necessary (see Figure 17a), making the procedure very subjective. Furthermore, the 1D algorithm is able to resolve inversions, yet these shadow zones should not be picked on the OFB stacks (Fig. 17b). Other un-

invertible travel time curves, such as in Figure 17c, should also be avoided when picking so as to allow a realistic velocity function inversion.
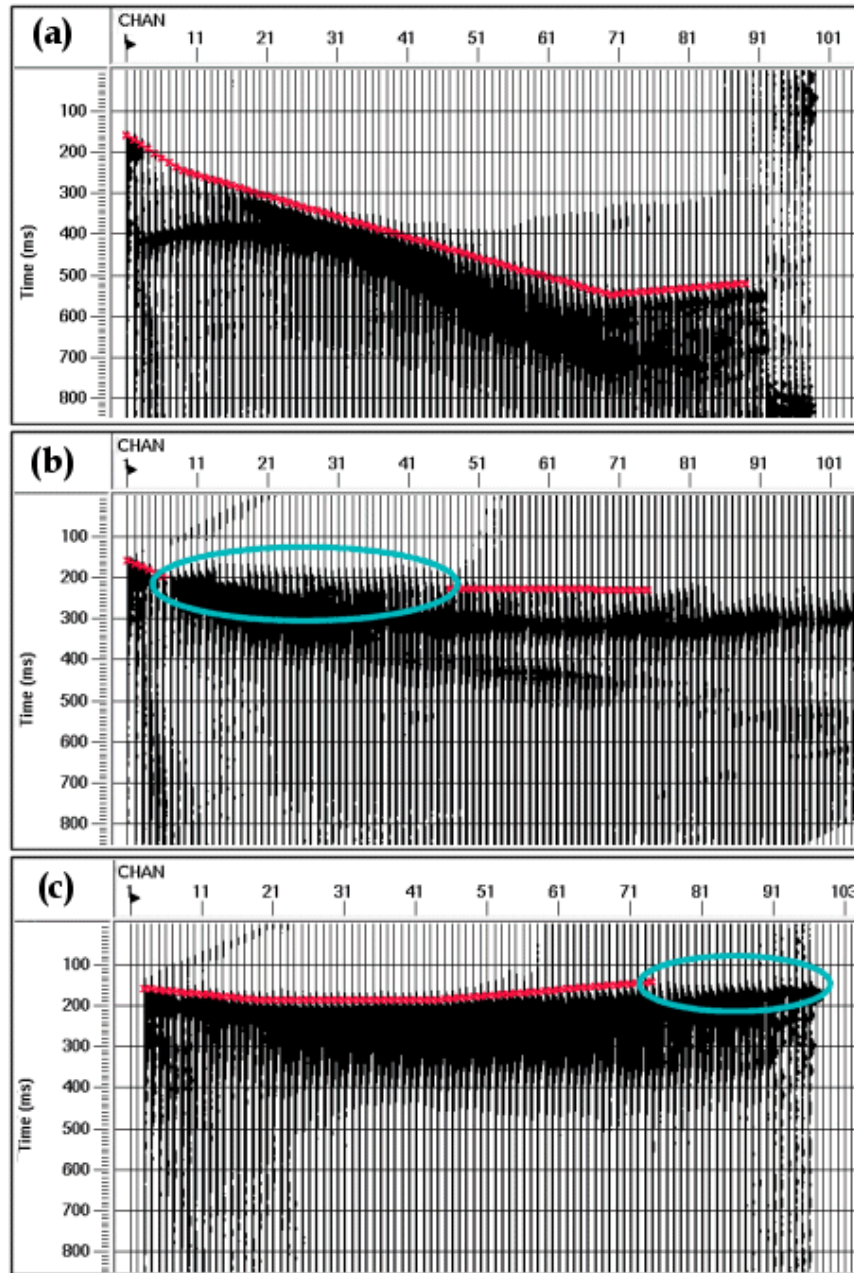
Figure 17 First breaks on OFB stacks, red crosses marking the picks: (a) optimally picked arrivals that contain no fluctuating picks, only easily invertible straight lines. (b) unrealistic arrivals which should not be picked (circled blue), and (c) a velocity inversion which should also be neglected

The quality of the OFB stacks was highly variable. Some were easy to pick, even on the long-offset bin traces, others had extremely blurred first arrivals that made picking difficult even at short- and medium-offsets. As a result, only a very limited velocity function could be inverted in those cells. The 1D inversion itself is a matrix inversion in form of a truncated singular value decomposition. The ray tracing

preceding the inversion works with the Eikonal equation (Equ. [7]) and applies a linear velocity gradient within each layer.

$$\left(\frac{\delta\tau}{\delta x}\right)^2 + \left(\frac{\delta\tau}{\delta y}\right)^2 = \frac{1}{v^2} \qquad [7]$$

Two further equations can be deduced from this, namely the definition of p_i, the ray parameter or slowness vector in a certain layer i.e. the inverse of velocity v (see Equ. [8]), as well as its gradient, where the ray parameter is differentiated by its path s (Equ. [9]). The dimension of τ is seconds, with its gradient representing the wavefront at a certain point in time.

$$\frac{\delta\tau}{\delta x_i} = p_i \qquad [8]$$

$$\frac{dp_i}{ds} = \frac{d}{ds}\frac{\delta\tau}{\delta x_i} = \frac{\delta}{\delta x_i}\left(\frac{1}{v}\right) \qquad [9]$$

v is given through the initial starting model, which is a file containing depth and velocity data pairs. The number of data pairs corresponds to the resolution of the final model, as the depths define where the tops and bottoms of the layers are. The 1D travel time curves are iteratively inverted, using the pick times and the starting model to define raypaths through a laterally invariant velocity model (the initial velocity model is transformed into an initial slowness model). Using the Eikonal equation, the algorithm aims to find the turning point of a ray and thus determine the velocity at that depth, inherently weighing those rays more which travel longer distances through a certain layer, implying that the model is better resolved at the turning point depth. This is confirmed in Behm's 2007 paper, where he claimed that synthetic tests produced well resolved velocities at maximum penetration depths.

The starting model is constantly updated, assuming lateral invariance within the layers, but introducing a constant gradient between the depth nodes. The ray geometry in a layer is therefore determined by the slowness on its upper and its lower boundary. The difference between the calculated arrival time and the picked arrival time at a certain absolute offset is used to adjust the model and minimise this difference. Changes in the raypath geometry between each iteration should be small in order not to make the inversion unstable, so a fairly accurate starting model is desirable.

4.1.2 Testing and Trials

The algorithm's matrix inversion is underdetermined, which means additional constraints need to be introduced to avoid ambiguous solutions. For this purpose,

several parameters of the programme were tested to produce results that appeared most reasonable. The paragraphs below explain what each of the tested parameters controls, followed by a table in Figure 18, showing samples from the investigated range of values, with the optimum value highlighted. The value to finally employ for each parameter during the calculation of the complete swath was decided on by analysing the visualisations of the computed velocity function. These graphs showed how the calculated function compared to the initial input, and the resulting travel time error for the picks relative to the offset. The initial velocity function itself was subject to trials, but the issues surrounding the chosen input function will be explained later.

Epsilon ϵ: The eigenvalues ϵ_i from the matrix inversions are sorted according to size and only those eigenvalues will be used which are larger than the specified ϵ, neglecting all eigenvalues ϵ_i, and the respective eigenvectors, smaller than epsilon. Similar to all underdetermined inversions, there is a compromise between smoothness and fitting the data to the pick times. A greater epsilon eliminates more eigenvalues, giving a smoother model but a worse fit to travel time curves, whereas too small an epsilon produced rougher models but a better fit.

Relaxation λ: This is a damping factor by which the slowness changes Δs are multiplied before being applied to the model, following each iteration. The coefficient prevents the slowness values from oscillating around the final result for too long,

$$s_{new} = s_{old} + \lambda \Delta s$$

Relative smoothness: A factor affecting the stability of the inversion – the greater the smoothing, the more stable each iteration.

Number of rays: A measure of how densely the rays should be shot through the model. Too few would lead to poor results, too many would be computationally intensive.

Default gradient: The gradient with which the velocity model is filled, down to the greatest depth stated in the initial input function, even when the inversion is not able to produce calculated values for such great a depth.

Maximum weight: When set to 1, all offsets are weighted equally. Using values greater than 1 introduces an inversely proportional weight function, such that smaller offsets, which tend to have better picks, are weighted more e.g. max. weight 3 means that all traces up to 1/3 of the maximum offset are weighted with a factor 3.

Every 250m x 250m cell had a unique 8-digit ID assigned to it, which was composed of the x and y coordinates of its cell centre. Digits 1 to 4 of the ID correspond to the last four digits of the x coordinate and digits 5 to 8 of the ID correspond to the last four digits of the y coordinate, such that, for example, the cell with its centre at coordinates [457**1125**, 531**2125**] would have the ID **1125**2125. All 35 cells within a row in the east-west direction thus share the same y coordinate as part of their ID. For the parameter tests, the first three cells in row 2125 were chosen (IDs 11252125, 13752125, 16252125).

Whenever the computation was faced with uninvertible inputs, it produced an error message for the relevant cells. The last but one column in Figure 18 refers to how many out of the three tested cells managed to have their velocity function inverted; obviously, any parameter choices which led to a failure in inverting all cells successfully had to be discarded as to ensure the inversion would work for the entire swath of 8 x 35 cells. The approximate order of magnitude of the parameters, such as how many decimal places to start with, was known from previous tests and other studies which employed the 1D inversion programme.

Starting velocity function (name)	Epsilon	Relaxation	Relative smoothness	No. of rays	No. of iterations	Default gradient [s^{-1}]	Max. weight	No .of cells worked (/3)	Comments
vel_01a	0.001	0.4	2	2000	50	5	2	3	
vel_02a	0.001	0.4	2	2000	50	5	2	3	
vel_03a	0.001	0.4	2	2000	50	5	2	3	
vel_01a	0.01	0.4	2	2000	50	5	2	2	
vel_02a	0.01	0.4	2	2000	50	5	2	2	
vel_03a	0.01	0.4	2	2000	50	5	2	1	
vel_01a	0.0001	0.4	2	2000	50	5	2	2	
vel_02a	0.0001	0.4	2	2000	50	5	2	3	
vel_03a	0.0001	0.4	2	2000	50	5	2	3	
vel_01a	0.0001	0.4	2	3000	50	5	2	2	slight
vel_02a	0.0001	0.4	2	3000	50	5	2	3	improvmt. comp.
vel_03a	0.0001	0.4	2	3000	50	5	2	3	to 2000 rays
vel_02a	0.0001	0.01	2	3000	50	5	2		
vel_03a	0.0001	0.01	2	3000	50	5	2	3	poor quality
vel_01a	0.0001	0.4	2	3000	50	1	2	2	
vel_02a	0.0001	0.4	2	3000	50	1	2	2	
vel_03a	0.0001	0.4	2	3000	50	1	2	2	
vel_linear	0.0001	0.4	2	3000	100	1	2	0	
vel_comp_a	0.0001	0.4	2	3000	100	1	2	3	_b better than
vel_comp_b	0.0001	0.4	2	3000	100	1	2	3	vel_comp_a
vel_comp_b	1e-06	0.4	2	3000	100	1	2	3	more relevance
vel_comp_b	1e-06	0.5	2	3000	100	1	2	0	to initial function
vel_comp_b	1e-06	0.05	2	3000	100	1	2	3	when ϵ 1e-06
vel_comp_b	1e-06	0.1	2	3000	100	1	2	3	large improvmt!
vel_comp_b	1e-06	0.1	2	3000	100	1	1.5	3	small diff. when
vel_comp_b	1e-06	0.1	2	3000	100	1	1.5	3	max. weight 1.5
vel_comp_b	1e-06	0.1	3	3000	100	1	1.5	3	compared to 2
vel_comp_b	1e-06	0.1	3	3000	100	0.5	1.5	3	
vel_comp_b	1e-06	0.1	3	3000	100	0.1	1.5	3	
vel_comp_b	1e-06	0.1	3	3000	150	0.1	1.5	3	
vel_comp	**1e-06**	**0.1**	**3**	**3000**	**150**	**0.1**	**1.5**		Optimum

Figure 18 Table showing the parameters and their tested values; yellow highlights contain the final values chosen to give the most acceptable results

The input to the 1D calculation consisted of a geometry file, a pick file and the initial velocity model. The geometry file contained information on the [x, y, z] coordinates of the cell centres, as well as the coordinates of the barycentre of each cell. This is the barycentre in terms of CMPs, calculated during the sorting of the traces, implying at what coordinates the 1D velocity function should theoretically be most applicable. The pick file contains the first arrival times on each trace of the common

offset bin stack; these are essentially just data pairs of time and offset, as [x, y] directions are no longer relevant when presuming a 1D function at the cell centre. Figure 19 shows the programme's interface where the pickfile from every cell can be combined with an individual velocity file; this combination served as one of the inputs to the actual 1D inversion, along with the specified parameters.
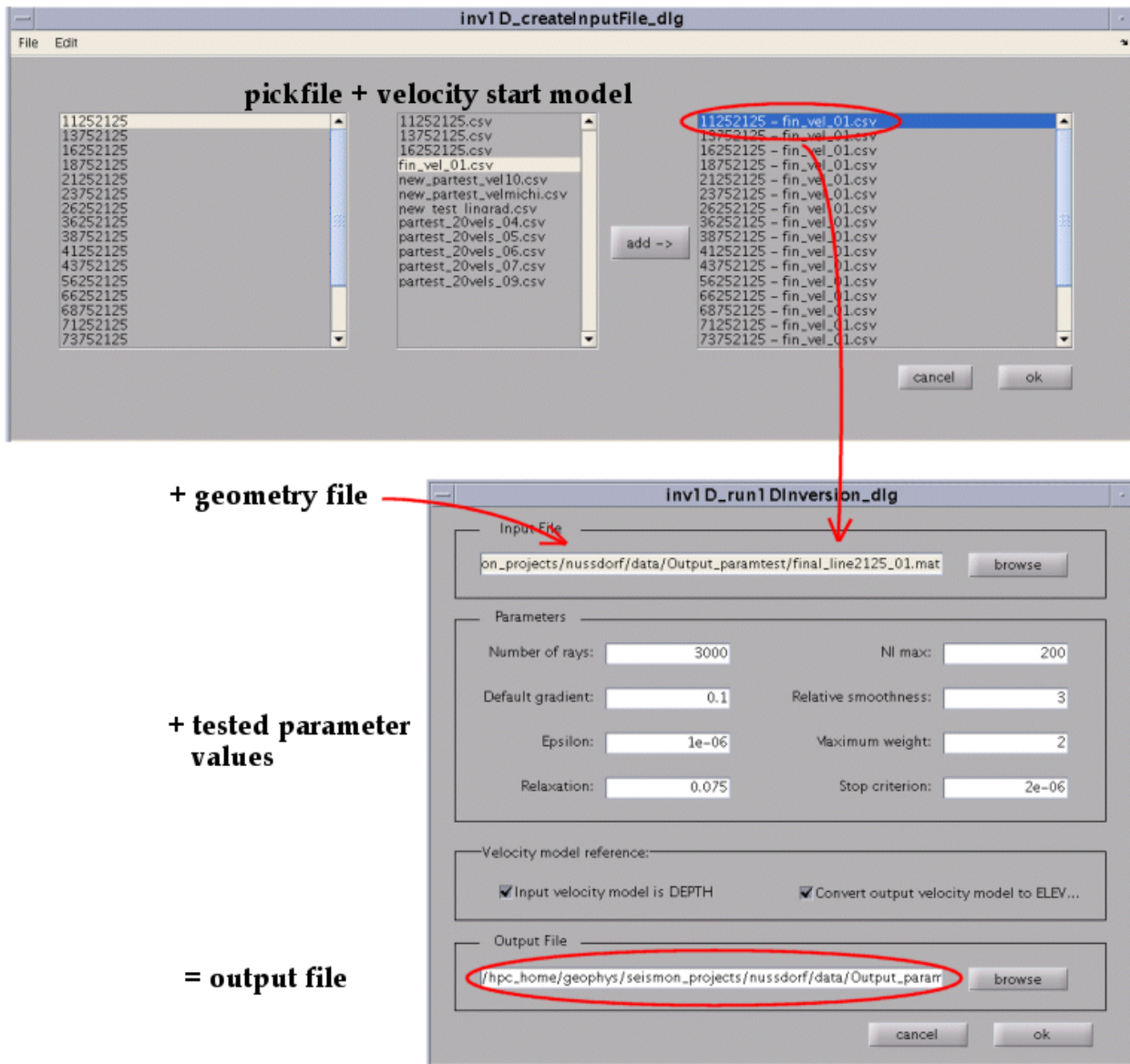
Figure 19 Programme's interfaces, showing how pick data are combined with start models, followed by the input of a geometry file and the selected parameter values

Originally, the idea was to input an as accurate as possible initial model, compiled from shallow velocity values known from short refraction surveys, old 2D lines and uphole shots. As already mentioned, short refraction profiles were carried out

every square kilometre of the Nussdorf survey. Old 2D seismic from the 80s was also available within the area, along with some uphole shots (see Figure 20 for locations).
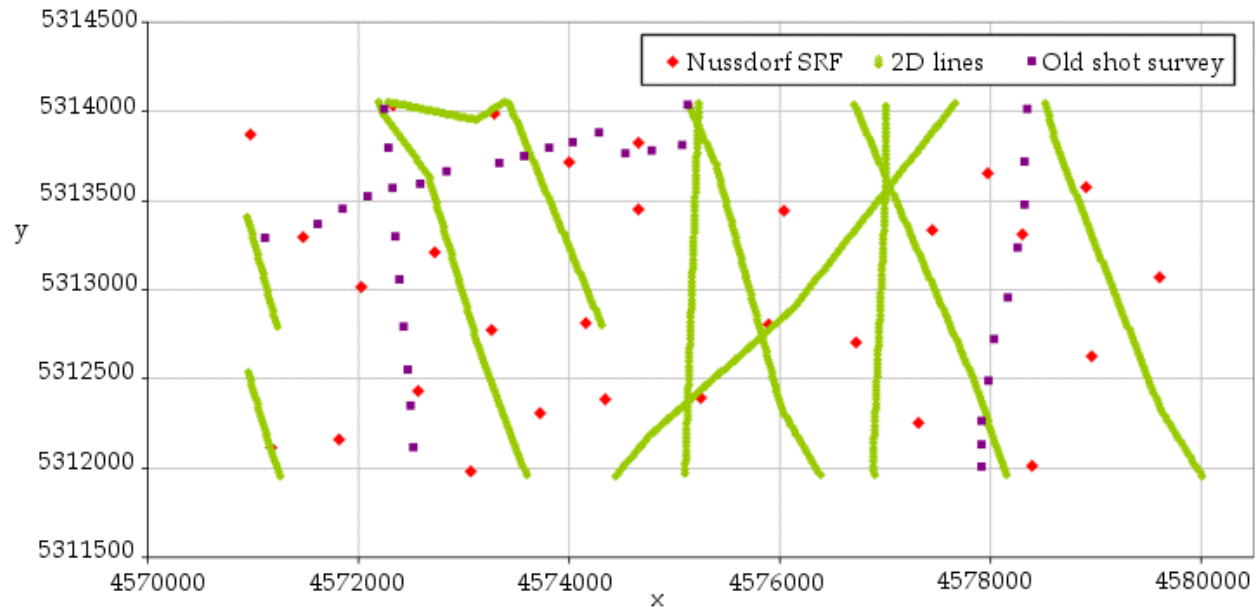
Figure 20 Basemap showing where near-surface velocity information was available from short refraction profiles, old 2D lines and uphole surveys

Values for v_0, v_1, v_2, z_1 and z_2 were taken from the data and interpolated onto a regular grid with nodes corresponding to the cell centres of the 1D inversion, supplying each cell with its own initial input. After preliminary tests using this interpolated function, it became apparent that the algorithm was unable to adequately invert these values. This might have been due to too much information in the shallow and too scarce a detail at greater depths, preventing long-offset rays from being inverted correctly. Clearly, finding each cell's invertible velocity function separately would be far too time-consuming and inefficient for production processing, so we opted to try three average functions (vel_01a, vel_02a and vel_03a) with additional pairs of values interpolated in between the reliable pairs known from the SRF information. With these three functions, as seen in the parameter table above, we faced the same problem again of not successfully inverting all tested cells. In addition to discarding the idea of supplying each cell with its own unique initial function, it was furthermore decided to stop adhering to any values known from SRF and instead, find one comprehensive overall function (vel_comp_a or vel_comp_b), containing more velocity-depth pairs and thus

being smoother, yet still realistic and reasonable for the survey area under investigation (see Figure 21).
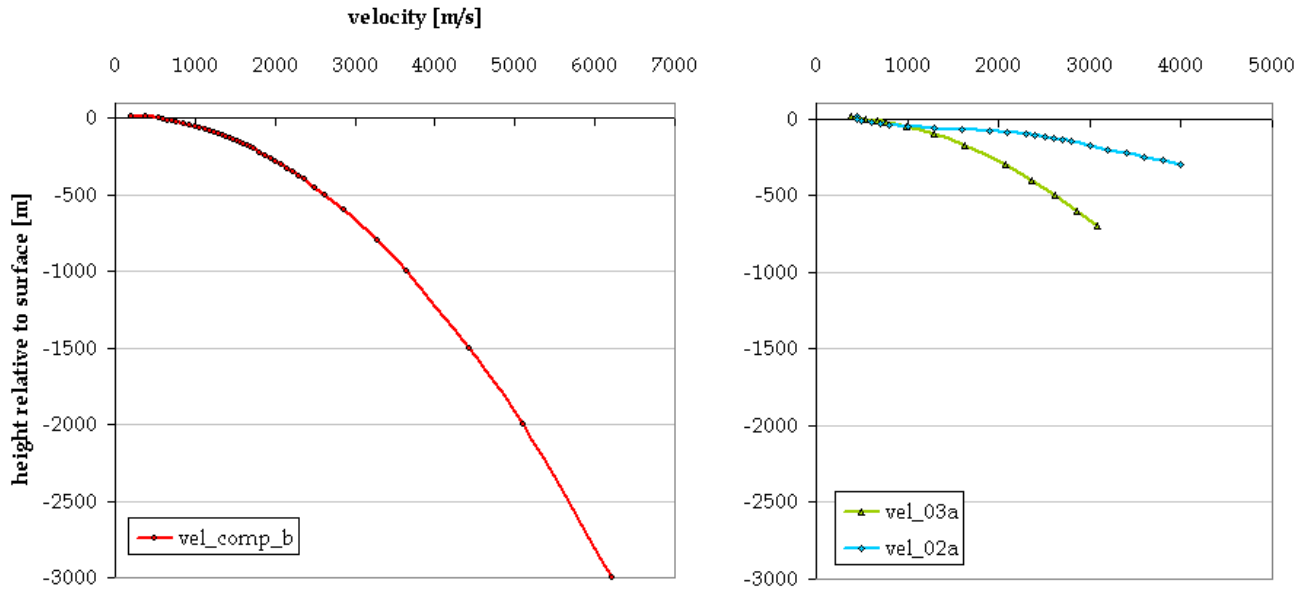
Figure 21 The smooth initial velocity function, left, which was decided to be applied to all cells, as opposed to velocity curves that are unique to each cell but contain fewer data pairs, such as the two examples on the right that represent average near-surface details available from SRF data

The final parameters used for the inversion can be seen in the last row of Figure 18. The choices were based on comparing the velocity output curves for each cell, whenever a parameter was adjusted, to see what changes yielded more realistic/better results.

4.1.3 Results

In an ideal case, the inversion would have produced velocity values at all those depths that were found in the input model. Yet as will be shown later, the inversion did not always penetrate down to the maximum depth of the input model.

The output .csv file contained the spatial coordinates along with the respective velocities and was read into a visualisation software (GOCAD). The velocity values were displayed for each of the eight processed lines, looking northwards at the cross-sections, see Figure 22. The lines themselves are sorted from north to south, hence the low-velocity area marked by red/orange squares (below 1000ms^{-1}) in the shallow, which represents the Oichtental, is further east on line 3875, but moves westwards with the direction of the valley when going from north to south.
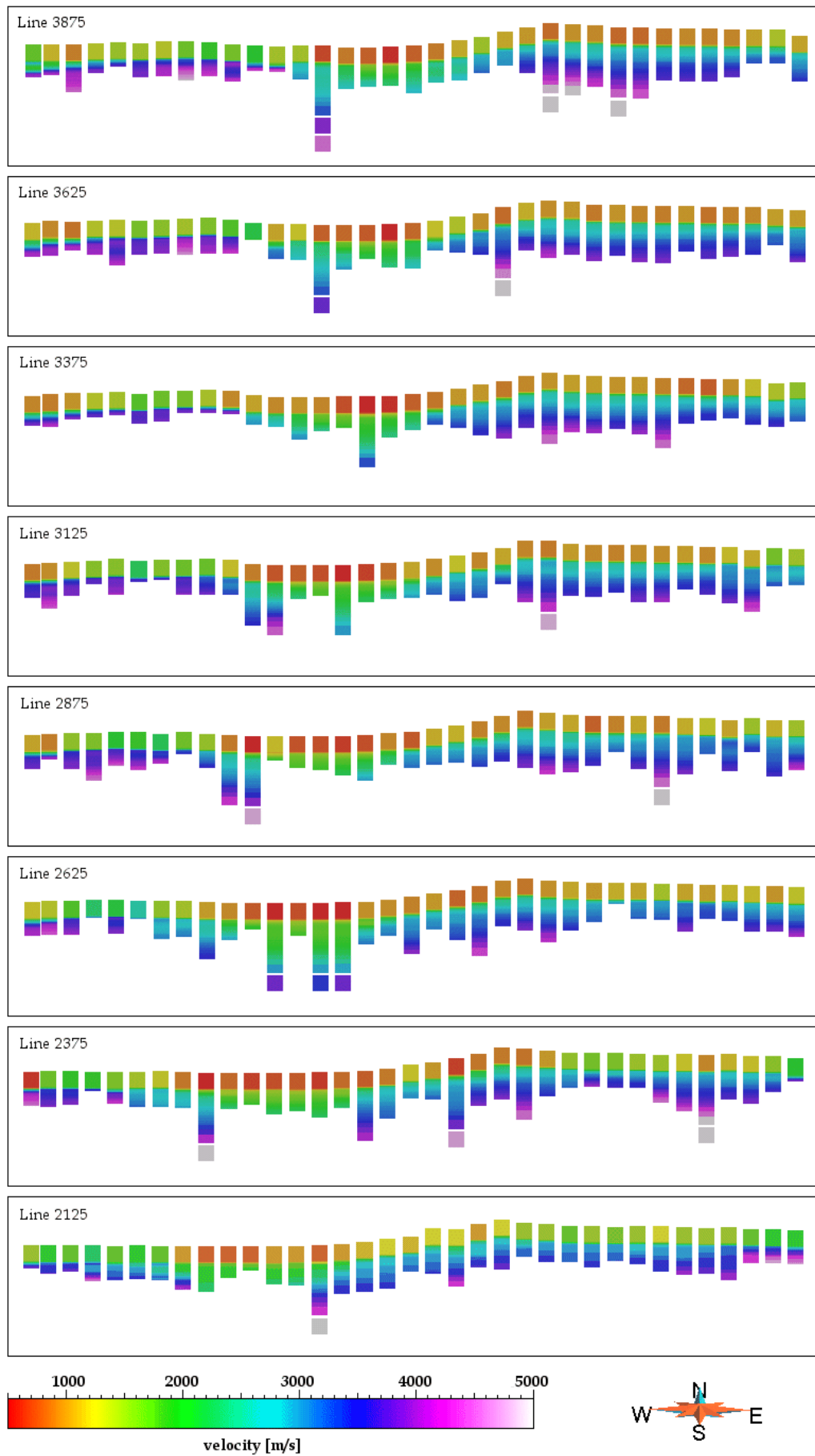
Figure 22 Velocities at every cell location for each of the eight lines constituting the test swath

The penetration depth of the inversion was highly variable, with some cells being assigned velocity functions almost 900m below surface, while other cells, notably on the western edge of the survey (see Figure 24), had a shallow resolution of only one to two hundred metres depth. The deepest functions in Figure 22, in the form of the shaded columns protruding down to greater depths, show a light purple/white colour suggesting velocities of up to 4500-5000ms^{-1}. The cross-sections also show that the velocity does increase with depth everywhere, but the Oichtental stands out as a region where this increase is less striking than in the surrounding rock. From the bird's-eye view of the swath, top Figure 23, a low-velocity area along the surface correlating to the location of the Oichtental is marked by dots of around 500ms^{-1}.

To show that the programme managed to resolve this low velocity of the valley infill all the way down to the deepest penetration point for each cell, the bird's eye view in Figure 23 was flipped to display the Oichtental from below. The conspicuous green region, representing a velocity of around 1800ms^{-1} to 2000ms^{-1}, clearly stands out compared to the surrounding blue/purple dots corresponding to approximately 3500-4500ms^{-1}.
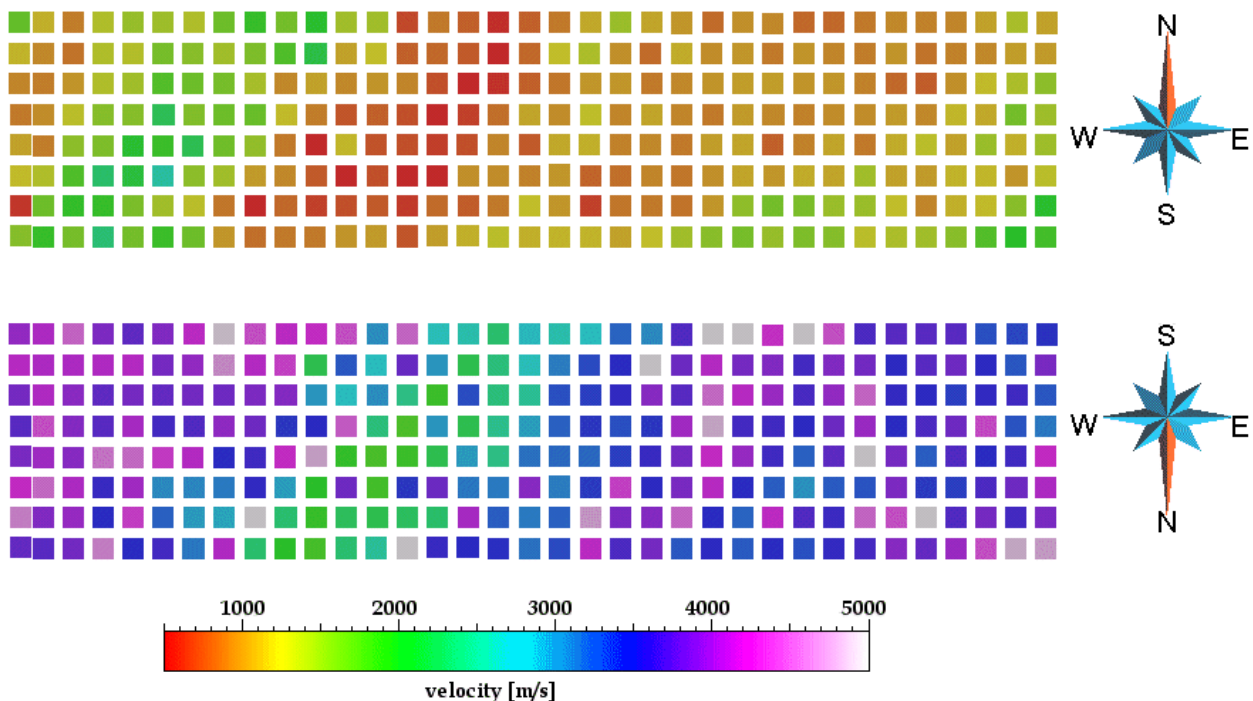
Figure 23 Top: Bird's eye view of all eight lines in the swath, red region marking the shallow velocities in the Oichtental; Bottom: Rotated plot such as to view low-velocity valley infill from below
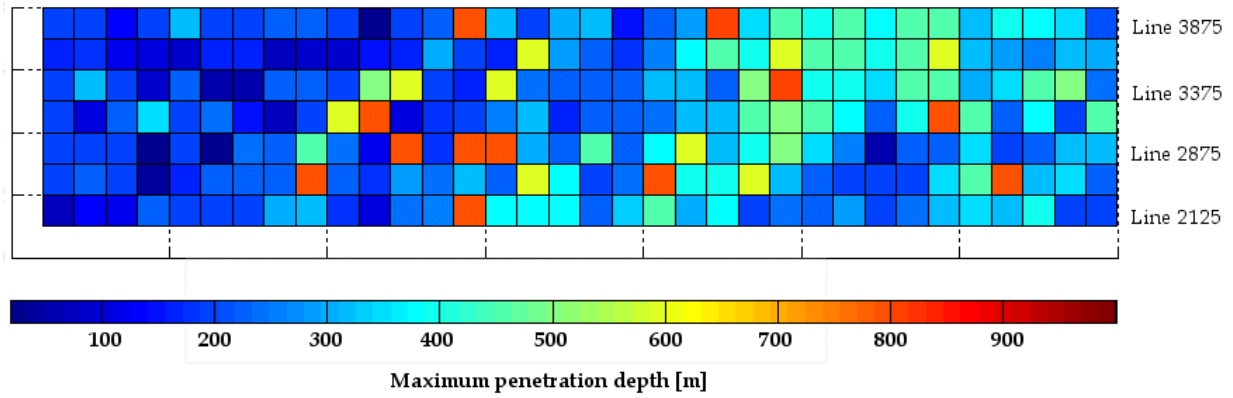
Figure 24 Penetration depths for cells across the swath

4.1.4   Validity of the Method

The blurring of azimuths inherent to conventional CMP processing is exacerbated in the common offset bin method, because the information is smeared over a much larger area than the standard bin size of 12.5m or 25m. Generalising the available first break information over an area as large as 250m by 250m, when the underlying aim is to obtain better lateral resolution, raises doubts in the method's suitability. One solution could be to decrease the cell size to e.g. 100m, followed by smaller offset bins. Smaller cells would not eliminate the drawback of smearing azimuths, but at least it shrinks the area over which information is blurred and increases the density of velocity functions, allowing more accurate resolution of horizontal gradients. As the seismic survey layout was designed to provide manifold coverage for 12.5m size bins, there should be no shortage of traces for smaller offset groups. This approach might only be slightly problematic at the edge of the survey where the number of traces available for stacking might be insufficient in certain offset groups.

To eradicate the aforementioned problem completely, anisotropy processing might have been appropriate. That way, smudging of azimuth-dependent velocities might have been avoided and velocities normal to the striking direction of the valley (i.e. rays going across Oichtental) would not have distorted the values within the structure (i.e. rays running parallel to the valley). A trace with its raypath across the valley would deliver too small a delay time and not correctly present the valley's true depth due to the curvature of the valley floor, while rays parallel to the valley would deliver longer delay times, yielding its true lower velocity.

Comparisons between the geographical cell centres and the average CMP locations within the cells (referred to as their barycentre) revealed good collocation, suggesting the CMPs are equally distributed within the cells, so that the velocity function, which is actually calculated at the barycentre, can be considered the same at the geographical centre.

Figure 25 shows another type of quality control in terms of the number of traces available for inversion in each cell. For most of the test swath, this lies in the range of 10000 – 14000 rays per cell, even going up to 17000 in the south-west. Except for the very western edge, where the ray number drops to below 1000 per cell, the quality of inversion should thus not suffer due to a shortage of traces.
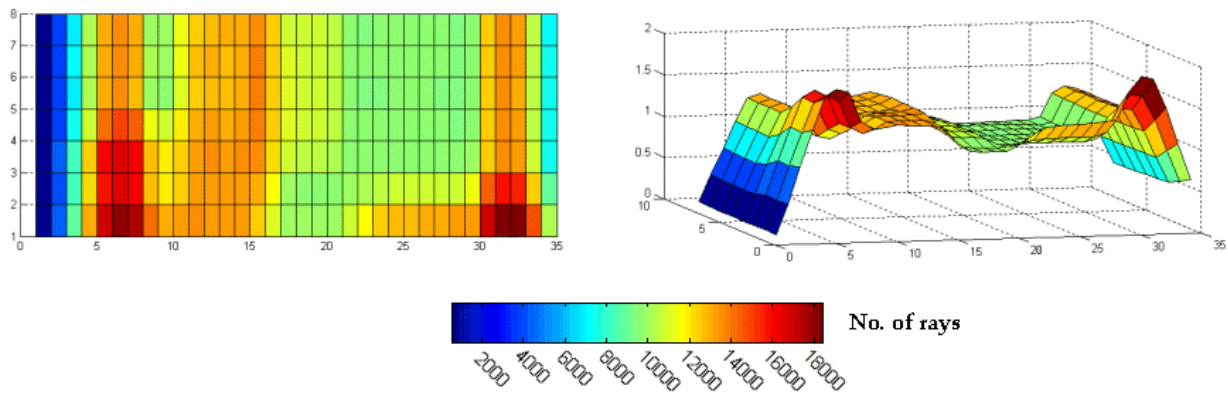
Figure 25 Number of rays involved in 1D inversion for each cell; left: bird's eye view, right: 3D view

4.2 3D Diving Wave Tomography

4.2.1 Method

Diving waves are an occurrence in areas where there is a velocity gradient in the subsurface, such that rays are not just refracted at discrete layer boundaries, but rather, refraction seems to be continuous along the raypath, giving a turning ray. Working with diving waves is relevant in areas of geological complexity, where simplified models of discrete layers without lateral or horizontal velocity variations no longer hold true.

The software used for this study is based on a travel time tomography by Hole (1992), which poses a robust and relatively computationally efficient tool in seismics. Essentially, all the information in a seismic trace is reduced to a single travel time pick, so that the input to the calculations consists of the first breaks times (and their

geometry) along with an initial velocity model. As with the 1D inversion, all traces which had their CMP in the test swath were filtered. It was decided to use picks from every second shot in the area, as the shots were spaced fairly closely and including every shot would have considerably extended the time spent on first break picking. The traces were organised into shot gathers and a linear moveout of 3000ms^{-1}, plus a bulk shift of 150ms, were applied prior to picking. Automatic picking was employed using a defined search gate and so-called power ratio stabilisation, which determined where the picks were placed in respect to the amplitude (power) increase that would indicate the onset of the signal (note that peaks, not zero-crossings were picked). As the data quality was highly variable, depending on where the shots and receivers were, the parameters defined for the automatic picker were never perfect. There were several shot gathers which had a low S/N ratio and thus incorrectly placed picks, or some shot gathers even had their first arrivals outside the defined pick window, but adjusting the window parameters to accommodate these exceptions would have made too big a difference on those gathers that had their picks placed accurately in the first place. All shot gathers were thus reviewed manually, and any picks on traces which showed no clear first break were removed, while wrongly placed picks were adjusted to what the observer considered the true peak. The pick times were stored in the header of the traces and later all the information was written into the survey database. From this database, an ASCII file was exported, containing the following ten parameters for all picked traces (s and SOU referring to source, and r and REC to receiver): SOU_ID, sx, sy, sz, REC_ID, rx, ry, rz, pick_time, abs_offset. Prior to exporting the file, the previously applied linear moveout was added back on and the pick times were shifted by -10ms, which corresponds to about ¼ of the time period of the first arrival, and thus placed the picks on the signal onset rather than the peak. The ASCII file served as one of the inputs to the tomography, besides the initial velocity model.

The Hole tomography relies on forward modelling in form of wavefront propagation. An initial velocity model consisting of three-dimensional cells uses an Eikonal solver to compute wavefronts according to Huygen's secondary sources. Wherever the wavefronts reach a geophone, the inversion unambiguously traces the raypath back to a source. Integrating along the normal of the wavefronts during the path reconstruction gives the ray's travel time t_{calc}, which is compared to its pick time

t_{pick}. The time difference Δt between these values needs to be minimised, which is done by adjusting the velocities along the raypath accordingly. In other words, the original velocity model needs to be altered such as to explain the observed pick times. As each cell of the model will be crossed by several rays in the course of the propagation calculation, with some rays giving a positive and others a negative Δt, the tomography shares out the difference amongst all the cells traversed by a ray in such a way as to adequately attribute it to all cells. Effectively, after every iteration the calculated travel times should converge towards the picked times so that the model represents the true subsurface situation. Any unrealistic scenarios, such as an updated cell having a much higher velocity than its imminently surrounding ones, are prevented by smoothing the model prior to the next iteration.

The starting model should be dimensioned quite liberally in order to avoid long raypaths going beyond its boundaries, if velocities do not confine the rays within the edges of the model. If the model is too shallow, not all raypaths can be traced back to their generating shot. Note that the inversion itself is linear, whereas the Eikonal solver works on the non-linear partial differential Eikonal equation.

4.2.2 Testing and Trials

A few problematic issues were encountered during the first couple of runs of the programme. For a start, it turned out during parameter tests for cell size, that the algorithm can only handle a certain number of cells in combination with however many raypaths transect them. The inference from this was that a cell size of 10m x 10m x 10m would not just be far too computationally intensive (with a probable duration of several weeks), but would also require the area to be split into far too many subplots as to be reasonable in production processing. Therefore, a cell size of 25m x 25m x 25m seemed more appropriate, as this would take considerably less time, yet still provide an adequate resolution for the problem on hand. The survey area still had to be divided into four parts, however, passing each one through the tomography separately in order not to crash the programme. This required four input velocity models and four input text files (containing the 10 parameters mentioned above), with the additional challenge of having to position each input section as closely as possible to the coordinate origin, as the Hole algorithm always starts the tomography of the model at [0, 0, 0]. Figure 26

shows how the seismic was divided and the values for the relative coordinate shifts. There was a 500m overlap between adjacent parts.
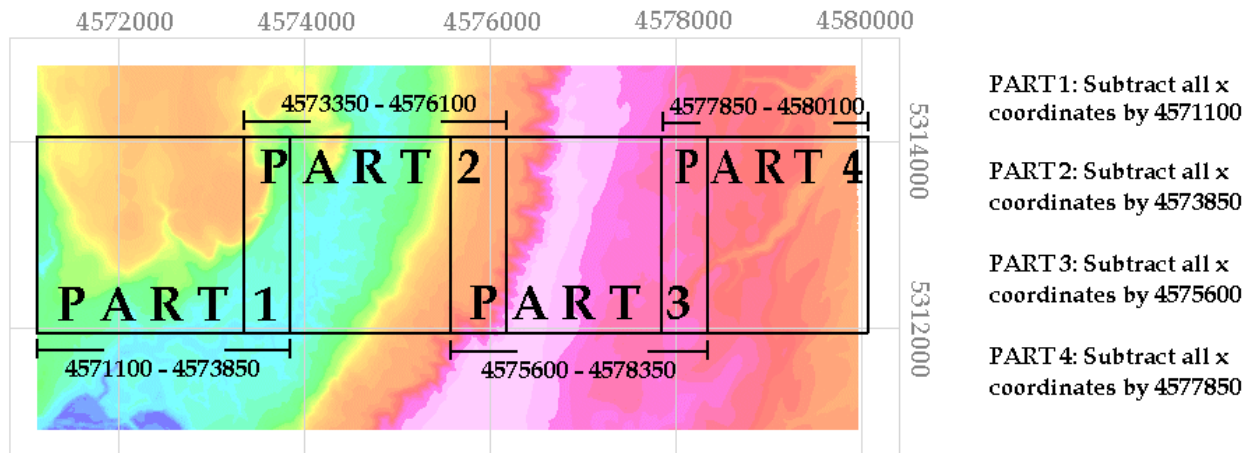
Figure 26 Investigated area split into four parts, each of roughly the same dimensions, requiring the coordinates of the sources and receivers in the input text file, as well as the initial velocity model, to be shifted towards the origin

The command line calling up the Hole tomography contains the input velocity model and an auxiliary file. This auxiliary file provides the geometry information for sources and receivers, the dimensions of the model in terms of node numbers and its cell size, as well as the number of iterations to perform. The iteration number is specified through a combination of offset limits and smoothing parameters; in our case, two offset limits (1.0km and 3.0km) and three smoothing values (20, 10 and 5) were specified, which means the tomography uses all picks up to an absolute offset of 1.0km for the computation of wavefront propagation, then smoothes the model across 20 cells prior to the next iteration, after which it smoothes across 10 cells, before it finally smoothes across 5 cells after the third iteration. Now all picks up to an offset of 3.0km are included and the smoothing procedure is repeated. That way, the tomography involved a total of 6 iterations. The number of cells across which to smooth after an iteration was the same in the x and y direction (20, 10 and 5), but smaller in the z direction (10, 6 and 2).

The input velocity file was the same for all four parts, containing the initial velocity model for the entire survey area. The only difference was the coordinate shift applied to the contents prior to the tomography, which positioned the model relative to the origin in such a way, as to exclude the irrelevant sections (i.e. place one end of the

input model below [0, 0 ,0], and have the other end extend beyond the x and y boundary specified by the number of nodes in the auxiliary file). As described in Figure 26, the velocity model for the calculation of Part 1 would have a shift of -4571100 applied in the x-direction, Part 2 -4573850 and so on.

The velocity start model was created using information from the short refraction profiles and the old 2D lines. The available values for v_0, v_1, v_2, z_1 and z_2 were loaded into MATLAB© and their coordinates transformed from the Upper Austrian system to Bavarian coordinates, to be in accordance with the seismic. A dense [x,y] grid with nodes every 125m was laid across the test swath, giving 73 nodes in the x direction and 35 in the y direction. The first x node was at 4571000 and the first y node at 5310700 – note that this latter value lies considerably below the lower edge of the swath (5312000), but the velocity model needs to extend far enough to include all source and receiver locations that resulted in a CMP within the swath. As the receiver lines were laid out North-South, the locations extend beyond the y boundaries of the test area. MATLAB provides four ways of interpolating data onto a 2D grid, called "nearest", "linear", "cubic" and "v4". The first one assigns the nearest neighbour value to a node, while the second one calculates a linearly interpolated value. These two were discarded for being too imprecise and providing non-smooth surfaces. Comparing cubic (triangle-based) and v4 (internal MATLAB method)[24] showed they both fit a smooth surface through the data, and there was hardly any difference between them, despite v4 being a more computationally intensive algorithm. It was therefore decided to use cubic interpolation of v_0, v_1, v_2, z_1 and z_2 onto the regularly spaced [x,y] nodes. Surface elevation, v_0, v_1 and z_1 were available from SRF *and* 2D data, while v_2 and z_2 were only available from the 2D lines, as SRF did not provide those values. Prior to any interpolation, data was filtered to omit any negative or zero values. The results were put into column vectors that were combined to give a matrix with columns x, y, z and v. There were three rows for every single [x,y] grid point, because the values for v_0, v_1, and v_2 were expressed separately at their respective absolute height z (elevation, z_1 and z_2). Figure 27 shows plots of the interpolated velocity values with their associated depths i.e. the velocity plots on the right are not depth slices, but the values are allocated to an undulating refractor surface whose height is illustrated in the left-side plots.

---

[24] URL: http://www.mathworks.com/access/helpdesk/help/techdoc/index.html
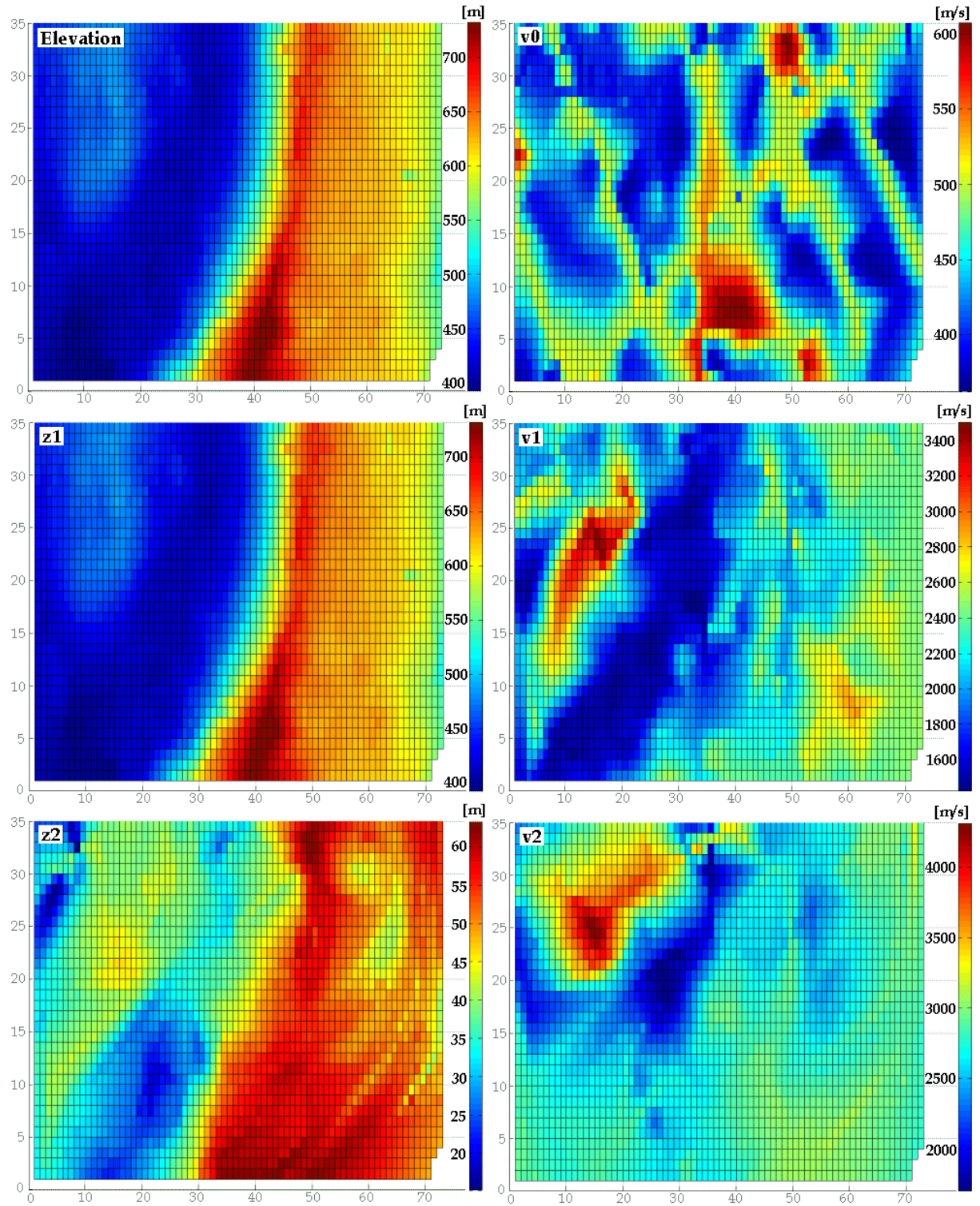
Figure 27 Plots on the left show absolute height (elevation minus refractor depth), with the associated velocity on the right. The data are paired up in the way shown here to give the three z-v pairs for every grid node in the matrix

After the first couple of tomography test runs, the log file showed that only very few rays were able to be traced correctly. The model updates were therefore unsuccessful and increasing the number of iterations did not change the situation. One

possible explanation was that the input model contained too much detail in the shallow, as the difference between the elevation z and the first refractor depth z_1 was only an average of 3m, while at the same time not extending down far enough to permit rays to be traced back to all shots. The solution was a compromise between using the available SRF and 2D information, and creating a resolvable model with greatly smoothed values. v_0 was set to a constant 1000ms^{-1} and paired up with the surface elevation values; v_1 remained unchanged, but instead of being paired up with z_1, the same values were placed at the absolute height of z_2; to ensure greater model depths than z_2, the third depth value for every node was set at an absolute height of surface elevation minus 1500m i.e. the model would be 1500m deep everywhere; the associated velocity value with this height was calculated from v_2 plus an additional gradient. Below is a summary table of what the matrix looked like previously, and how the values were altered to produce the final input model to the tomography; Figure 28 is a graphical illustration of these two models.

Original model structure				Modification after trial runs			
x	**y**	**z**	**v**	**x**	**y**	**z**	**v**
x_i	y_i	surface elevation	v_0	x_i	y_i	surface elevation	1000ms^{-1}
x_i	y_i	z_1	v_1	x_i	y_i	z_2	v_1
x_i	y_i	z_2	v_2	x_i	y_i	elev. -1500m	$v_2+(z_2-(\text{elev. -1500}))*0.1$
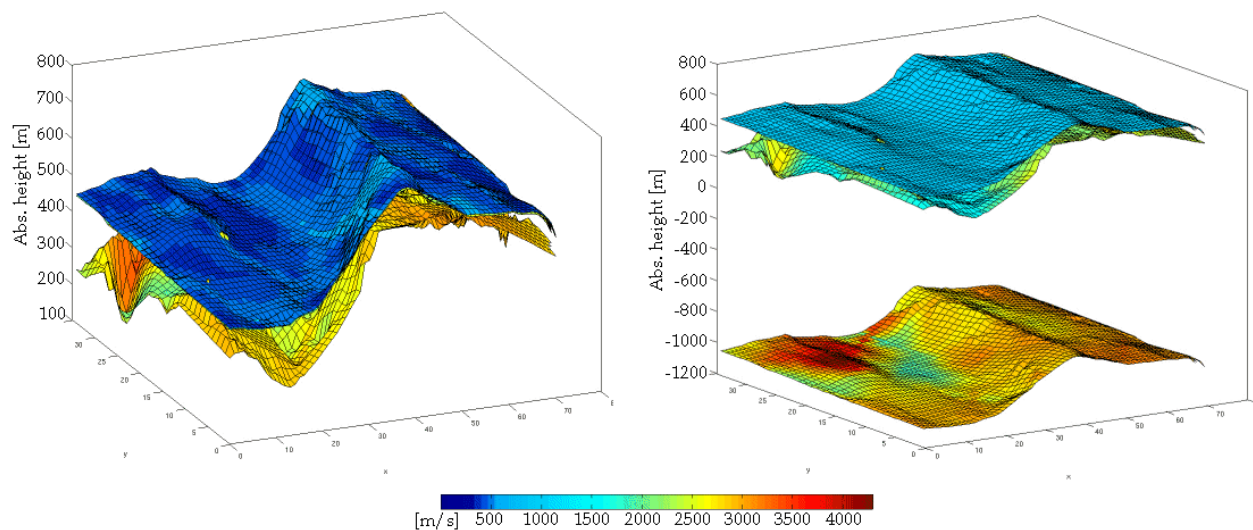
Figure 28 Comparing the three layers of the original model (left) to the modified ones (right), which served as the tomography start model; colour shading represents the velocity at the mapped heights

4.2.3 Results

The principal indication of the 3D tomography is the same as for the 1D inversion, namely, that a low velocity region can be distinctly resolved and attributed to the sedimentary valley in-fill of the Oichtental. It was clear from the outset that the diving wave tomography would yield a velocity field of much higher resolution, seeing as the cell size was a tenth of that for the 1D inversion. Consequently, much more detail can be seen in the GOCAD model of the visualised velocity file (see Figure 29). It is evident when looking at Figure 23 vs 29, that the 1D method was restricted solely to the swath boundary, whereas the tomography produced a velocity model with frayed edges, where some cells are outside the 2km wide test swath; this is because the input model had to extend far enough to include all source and receiver locations, which gave a CMP in the investigated area.
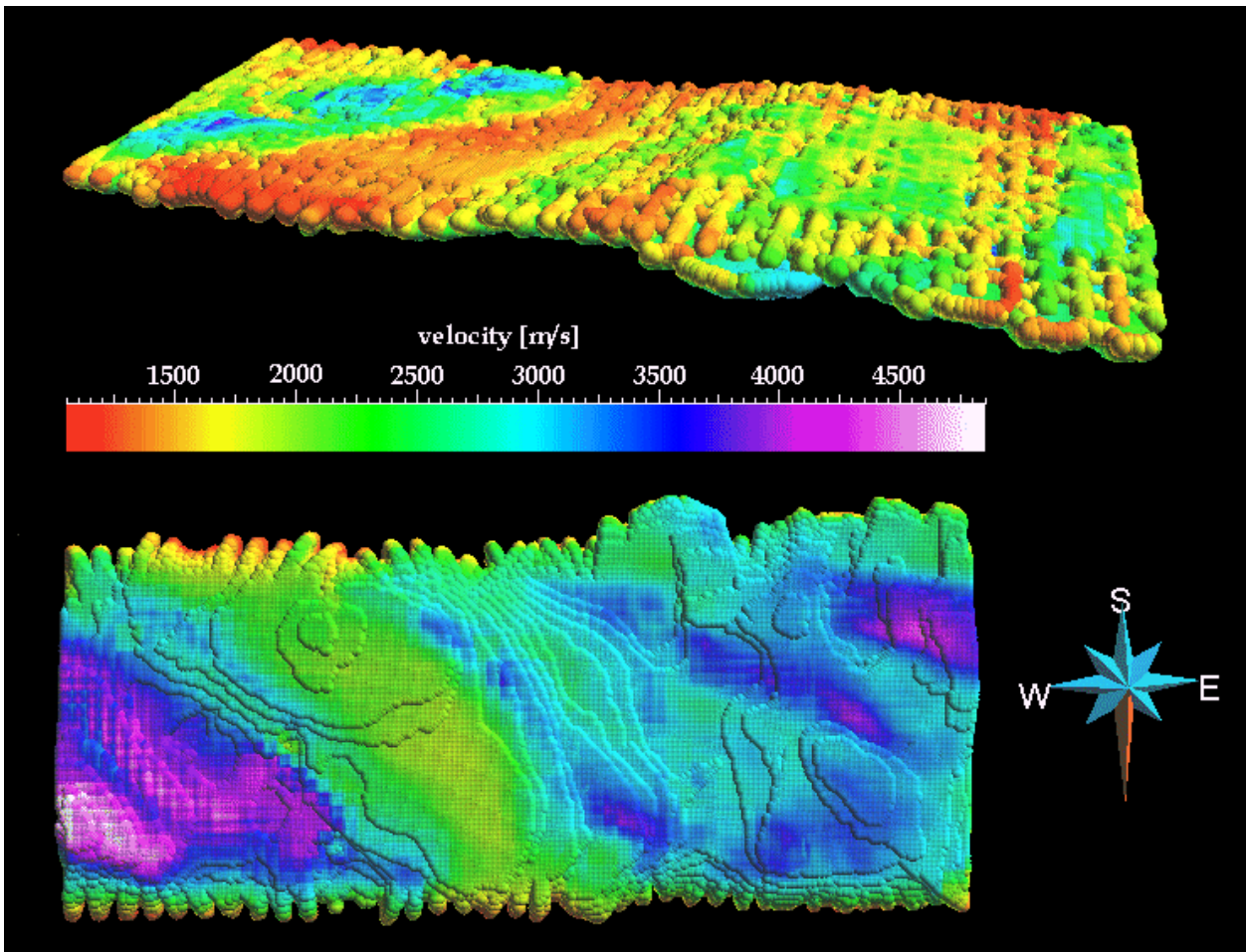
Figure 29 Visualisation of tomography; Top: 3D view from above, red dots along surface indicating extent of the Oichtental; Bottom: Swath viewed from below, showing low-velocity valley infill

The tomographic model appears much smoother than the 1D model, which is particularly recognisable when viewing the model from below. From there, it is not just possible to make out the course of the Oichtental more clearly, but what appears as contour lines is a measure of the penetration depth of the rays, giving a much smoother overall distribution than the erratic depth pattern from the 1D inversion. For Part 1 and Part 2 of the tomographic model, the deepest calculated velocity lay at 187.5m above mean sea level, Part 3 had a maximum penetration depth of 337.5m AMSL, while Part 4 only manage to calculate velocities to an absolute height of 387.5m, which can be explained through the generally higher surface elevations in Parts 3 and 4.

4.2.4 Validity of the Method

The advantage of a turning ray tomography over the 1D programme is that azimuthal velocity changes can be accounted for. This extra freedom, however, is compromised by the greater sensitivity to the initial model. The influence of pick errors

and the bias created with the starting model is far greater than during the application of the 1D method.

4.3 Interpolation of the Velocity Models and Computation of Statics

After visualising the models in GOCAD as a first quality check, the aim was to interpolate both data sets onto regular volume grids such as to obtain two as complete as possible 3D models, filling out any gaps where either algorithm was unable to calculate a velocity. At the same time, the models would have any unrealistic values removed and be cropped to the exact swath boundaries and topographic limits.

The 1D velocity data was read into MATLAB© as a four-column matrix, x, y, z and v, where x and y were the evenly spaced cell centre locations every 250m, and z the absolute heights at which velocities v had been computed. A much denser grid was defined, with a node spacing of 25m in the x and y direction and a 12.5m spacing in depth, as can be seen in the command lines below, where the minimum and maximum coordinates are defined by the values before and after the node spacing, respectively.

[x_grid] = (4571100 : 25 : 4580100)

[y_grid] = (5310700 : 25 : 5314950)

[z_grid] = (100 : 12.5 : 750)

The x range (4571100 to 4580100) corresponds to the test swath boundaries, while the y range (5310700 to 5314950) was that of the minimum to maximum receiver/source locations. The z range was decided on by looking at the topographic elevations and the maximum penetration depths found in both models, and choosing an appropriate limit above and below these to include all data points. It has to be noted that the 1D model reached greater depths than 100m above mean sea level at some grid nodes, yet the majority of the 1D model and all of the diving wave model was shallower, so increasing the entire cube volume to accommodate these one-offs would have led to excess computation time, which is likely to not be justified by the results. The available velocity values were linearly interpolated onto the densely spaced nodes and the new matrix (containing the columns x_grid, y_grid, z_grid, elevation and v_interpolated) was output as a .csv file. This underwent filtering to remove any n/a velocity values which arose wherever the algorithm was unable to extrapolate far enough, and to limit

the data so that only velocity values underneath the surface were included, as the gridding process assigned values to all nodes where interpolation or extrapolation was feasible, regardless of whether the node was above or below the topographic surface. The filtered file now had its x and y column sorted in ascending order, and the z column in descending order, and was read into Excel spreadsheets.

For the calculation of statics, a series of IF conditions and basic distance/velocity equations were employed; the vertical time from one node to the next was calculated using their spatial interval (12.5m) and the velocity value at the deeper of the two nodes. A cumulative time was calculated by summing all these vertical times for a specific [x,y] location, such as to obtain the static correction. For a sample of the spreadsheet, see Figure 30. Note that these cumulative statics are the total vertical time, down from the surface to the deepest available node at each grid point, and have no mutual reference level; they simply refer to the time down to the maximum depth to which the 1D model could be extrapolated.

Figure 30 Sample from the spreadsheet, showing equations used to calculate preliminary static times

A similar procedure was applied to the 3D tomography data; the four-columned file that was visualised in GOCAD was loaded into MATLAB and the data interpolated onto the same dense grid as the 1D data (25m node interval in x and y, 12.5m interval in depth). The gridded data was filtered to exclude n/a velocity values and those nodes

above ground level, then the columns were sorted in ascending order and imported into Excel for similar static calculations to the ones explained above.

At this point, a file for both the 1D and the 3D velocity field was available, containing surface coordinates and the static times down to the maximum resolved depth. The obvious need for a common reference level, down to which the vertical time should be computed, called for further steps. Judging by the absolute heights above mean sea level at which velocities were known, it became clear that both models often went deeper than the previously used reference datum of 300m. It therefore seemed a waste to cut the model off at 300m AMSL and neglect the additional information in the deep. Instead, it was decided to fill both models with velocity nodes down to 187.5m AMSL, which was the maximum penetration depth reached by the shallower of the two models (the tomography), and thus served as a comparative basis, regardless of the fact that the 1D model occasionally penetrated deeper. At those grid points which already had velocity functions down to the new reference datum, this required no further calculations. However, in places where the deepest available node was above 187.5m AMSL, the velocity value of the deepest node was taken and assigned to the whole space between the last node and the reference datum. In other words, given the cumulative statics calculated so far, in places where the velocity function did not go as deep as 187.5m, a further time had to be added which accounted for the filling of the space between the last node and the reference datum with a constant velocity (explained in Figure 31).
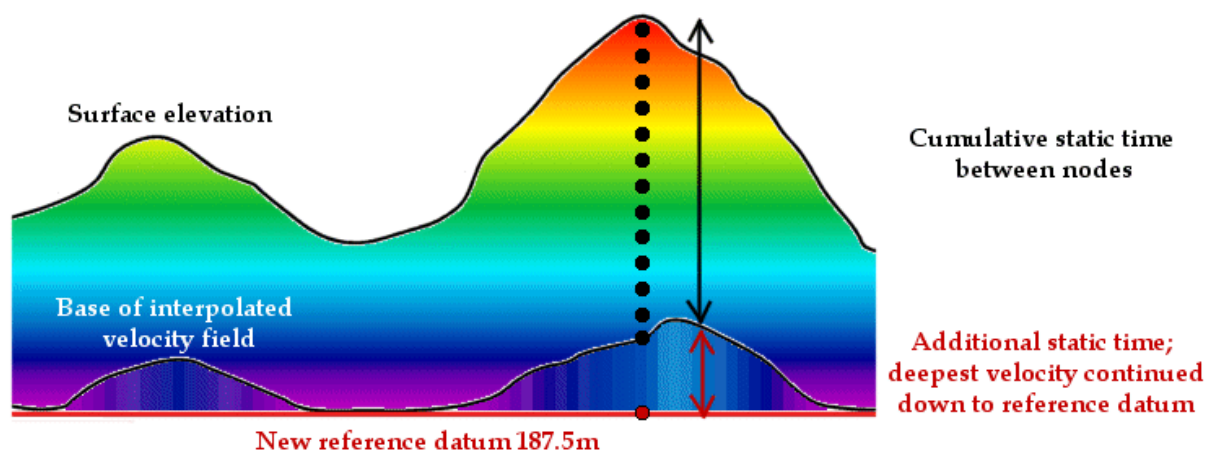
Figure 31 Maximum depth of tomographic velocity model was 187.5m AMSL; all grid points with their deepest interpolated node above this datum had their deepest velocity value assigned to the gap between new reference datum and last node

The new total static corrections, consisting of the cumulative statics between the vertical nodes and the time from the last node to the reference datum at a uniform velocity, were mapped in Figure 32 (Chapter 4.4) for both the 1D and the diving wave data. A discussion of the individual results, as well as a comparison between the two models can be found in the following chapter.

Since the original static computation by WesternGeco as part of the 2002 Nussdorf processing had a reference datum of 300m, it was decided to apply a similar datum to the above calculations for direct comparison. The two statics models, which currently had a reference datum of 187.5m, had their velocity model filled with the deepest available velocity value up to an elevation of 300m. In other words, the static corrections were now made up of the cumulative time through the interpolated model, plus – where necessary – the time from the deepest node to 187.5m at the deepest available velocity, minus the time from 187.5m back up to 300m, again with the deepest velocity; these static times are displayed in Figure 33.

4.4   Comparison of the 1D and 3D Method and Results
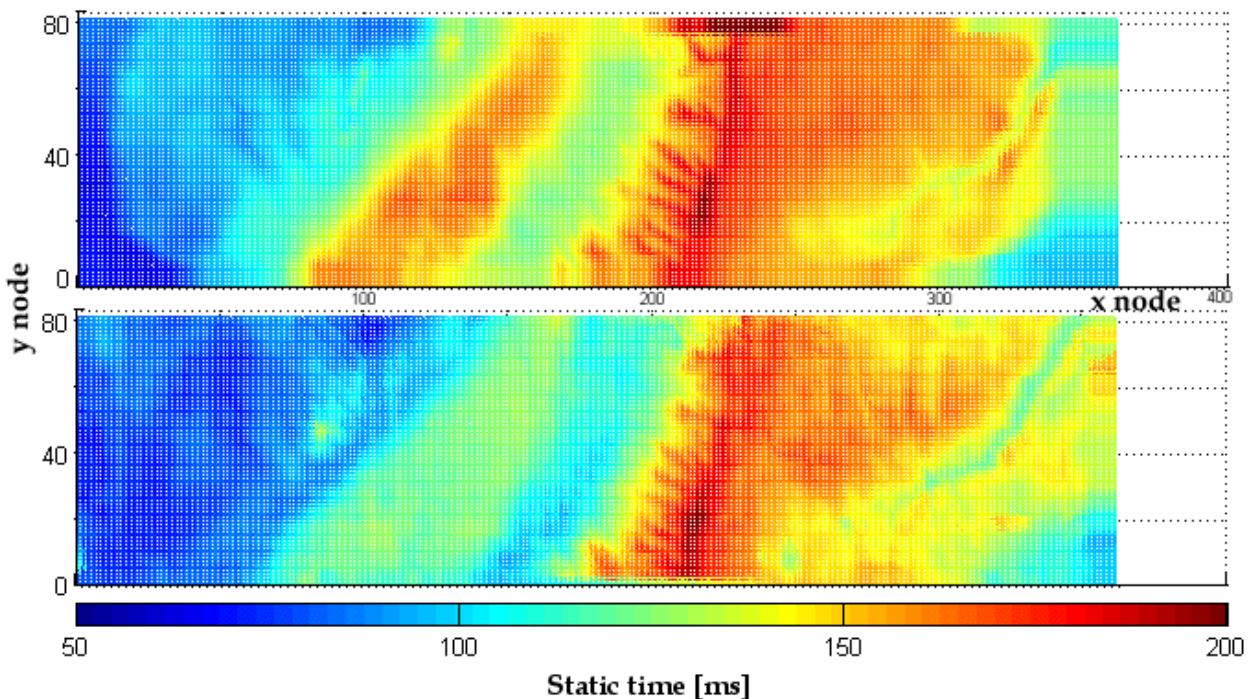
Figure 32 Static correction times to a datum of 187.5m; comparison between the 1D (top) and the diving wave model (bottom)
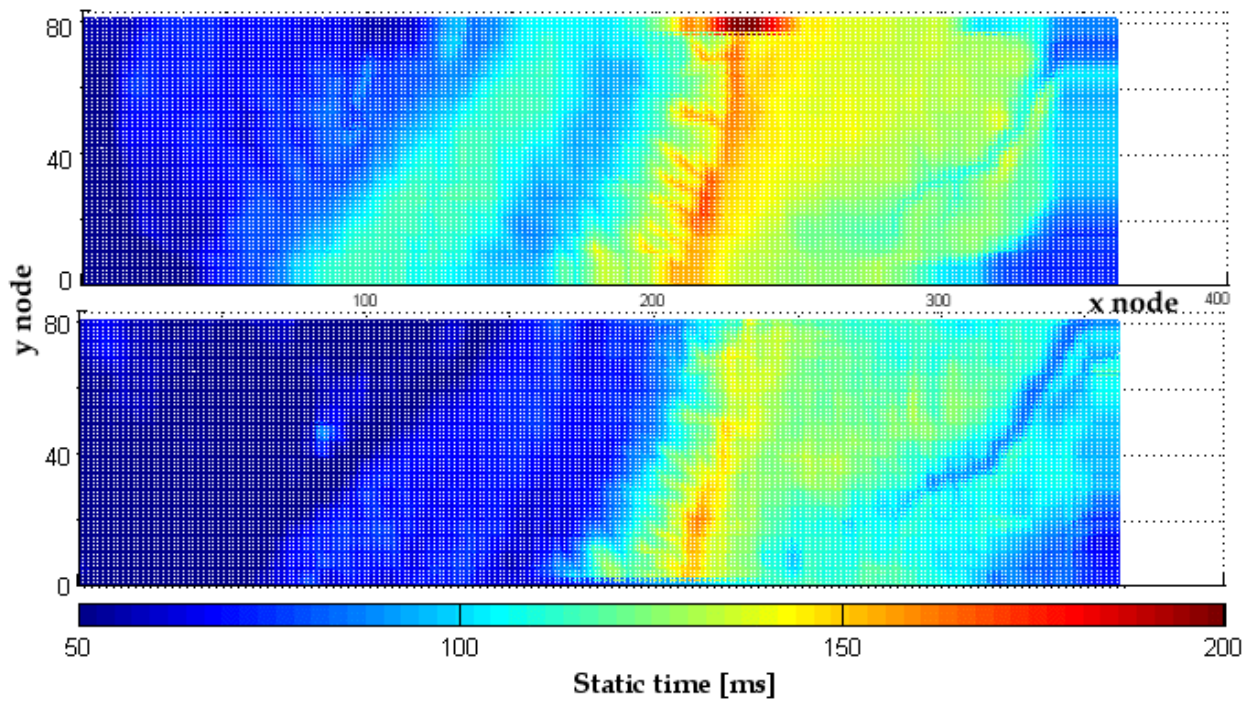
Figure 33 Static correction times to a datum of 300m; comparison between the 1D (top) and the diving wave model (bottom)

The figures above present the raw results of the thesis' investigation: the surface consistent static correction times of an 8.75km x 2km swath within the Nussdorf survey area, produced through a 1D inversion on the one hand, and a 3D diving wave tomography on the other. Both methods use a reference datum of 187.5m for a start, and then an extended model with a 300m datum for means of comparison to previous WesternGeco calculations. Note that in all cases, the static corrections are plotted as positive values in milliseconds, which means they need to be subtracted from the seismic times in order to remove the near-surface effects. The absolute range of values is approximately 60ms - 240ms for the 187.5m AMSL datum, and 35ms - 210ms for 300m AMSL. For display reasons, the colour bar legend in both Figure 32 and 33 was calibrated to encompass a range of 50ms - 200ms for all figures.

The diagrams show that the crux is the same for both tested methods; a low-velocity area which manifests itself as a large static correction is found in the region correlating to the location of the Oichtental, a north-east to south-west oriented channel in the western half of the test swath. In Figure 32, this region stands out more clearly in the 1D model than in the diving wave model, such that the static times are approximately 170ms for the former and merely around 130ms for the latter. On the

whole, the tomographic model appears to contain slightly more details and no erroneous values, such as the unrealistically high values on the northern edge of the 1D model, marked by the incongruous dark red region in both Figure 32 and 33. Such sharp anomalies can arise because the 1D method treats all cells separately and attributes them a velocity function independent of the function in the neighbouring cell. The tomography, however, not only treats all cells in the volume collectively by tracing rays through them in whatever direction the waves propagate, it also smoothes the velocities across a specified number of cells after each iteration, blurring any sharp contrasts to ensure a stable subsequent iteration. Despite such failures on part of the 1D method, which could easily be eliminated through post-interpolation smoothing, one cannot yet be sure that the static corrections from the tomographic method are more valid, seeing as there is a considerable time difference between the models and both of them show up almost identical structures. This can only be judged by looking at the stack quality once the corrections have been applied to the seismic.

The first noticeable difference between the static corrections in Figure 32 and 33 are the generally smaller times in the latter, which is to be expected, seeing as the sources and receivers only need to be projected down to 300m and not all the way to 187.5m above sea level. Again, both the top and bottom illustration in Figure 32 contain evidence of the low velocity valley infill, in the form of slightly greater static times than the surroundings. For the tomographic model, this distinction is rather faint though. Refilling the velocity model from 187.5m to 300m above sea level almost seems to eliminate the effect of the valley completely, which is unsurprising when considering that today's valley floor lies at an elevation of around 400m, so only 100m of calculated velocity information are used, and the rest simply filled up with a constant value. The detail which would be available when the reference level lies deeper is thus destroyed.

It is debatable whether the replacement velocities used at each grid point to reach a reference datum of 187.5m, and subsequently 300m, were fully valid. Since the process was automated to always use the deepest available velocity value, it is unsure if these values were actually adequate or unreasonably high and should thus have been replaced by a velocity calculated through the mean gradient at the depth in question. To illustrate this issue, Figure 34 shows plots of the maximum penetration depths after

interpolation for both the 1D and 3D method, while Figure 35 shows the interpolated replacement velocities at these depths.

The trend in penetration depths for both the Hole and 1D method in Fig. 34 seems roughly the same, with greater depths beneath the Haunsberg mountain range, then slightly shallower penetration in the Oichtental and again deeper penetration to the west of it. Note that the overall smoother appearance of the 1D plot is simply due to a smaller number of data points, which the algorithm was able to interpolate more smoothly, while the greater density of data points for the diving wave tomography yielded a patchier plot. The most remarkable thing is, however, when looking at the colour bars, it becomes clear that the values for the 1D inversion are almost twice that of the 3D tomography, giving a maximum penetration of 620m as opposed to simply 310m. This confirms the weaker penetration of the diving wave compared to the 1D method, as already indicated on the raw data plot in Figure 24.
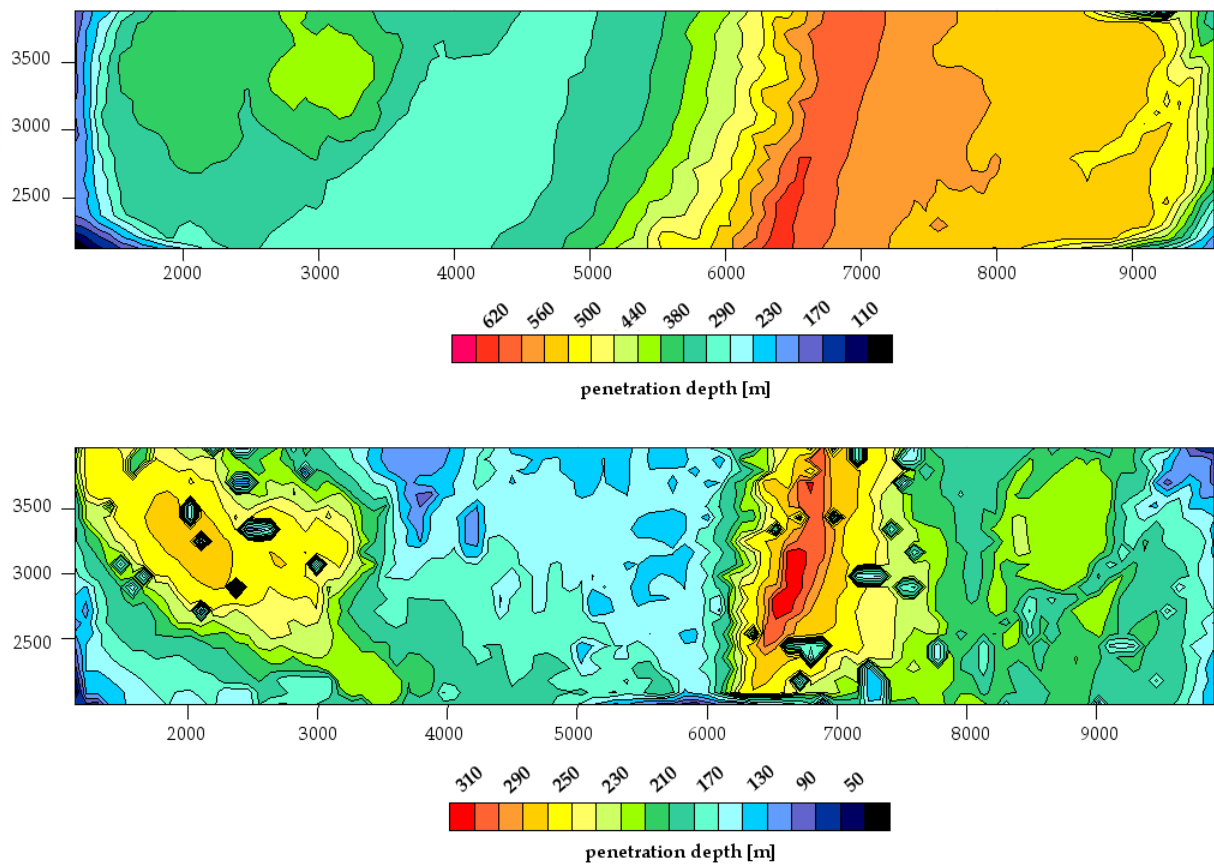
Figure 34 Maximum penetration depths after interpolation; Top: 1D Inversion, Bottom: Tomographic results
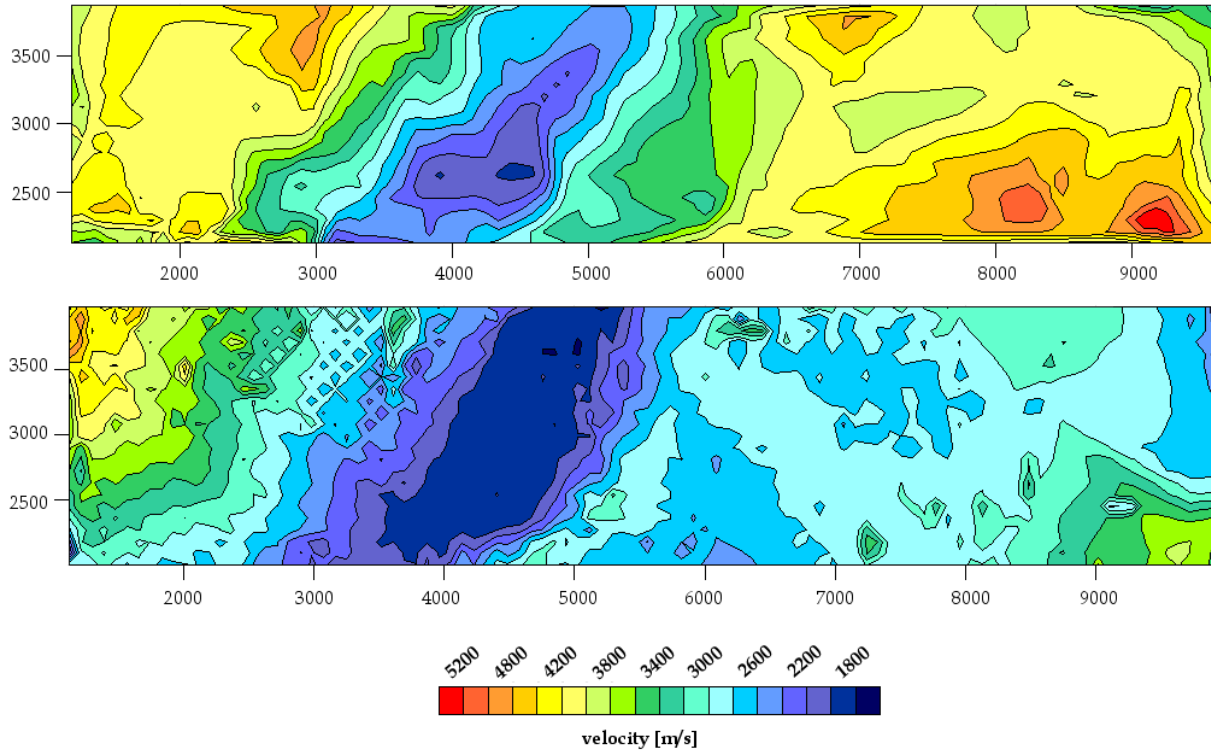
Figure 35 Replacement velocities used to extend the reference datum down to 187.5m where necessary, and then back to 300m; Top: 1D method, Bottom: Tomographic result

The interpolated replacement velocities in Fig. 35 used in both methods give an altogether valid impression, with values of around 1800-2200ms^{-1} in the infilled valley. This agrees with the average value for v_1 found by WesternGeco in their 2003 processing report, yet appears just slightly too high for what they thought the Oichtental should have (1500-1700 ms^{-1}). Only in a couple of occasional places – at the south-eastern edge of the swath – do values shoot up to an unrealistic 5200ms^{-1}, but this does not affect the result of the static correction in the interesting area of the Oichtental.

At the moment, the plots in Fig. 32 and 33 can only be quantitatively analysed in terms of detail and reasonability, but no qualitative statements can be made until the results are visualised in terms of inline and crossline stacks (see Chapter 5). So far, all four plots give a reasonable impression, barring the faulty results in the top row of the 1D inversion where times come across as implausibly large.

5 Applying the Static Corrections to the Seismic

A direct comparison between the static corrections by WesternGeco and the times calculated through the two investigated methods, demands a mutual reference datum. The 187.5m datum thus only served as a preliminary surface to include as much of the depth detail from the computed velocity fields as possible, yet the actual datum for comparing the new static times to the old WesternGeco ones was 300m. Seeing as 300m is the reference datum used when dealing with data in Austria (as opposed to 450m applicable in Bavaria), the comparison was carried out in Upper Austrian coordinates. Thus prior to applying the computed 1D and 3D static corrections, a simple coordinate transformation was necessary.

5.1 Processing Flow

The Nussdorf seismic with its relevant pre-processing (re-sampling, row sorting, binning to 25mx25m bins and surface consistent deconvolution) was read in and filtered to only contain those inlines and crosslines which fell into the test swath. These included inlines 5100-5600 and crosslines 1320-1440. Refraction statics were applied, using three different correction times: The first model incorporated WesternGeco's Gauss-Krueger 1 statics (GK1); the second model used the times derived from Hole's diving wave tomography; and the third, the static corrections from the 1D inversion. For the moment, no residual statics are applied.

NMO corrections were applied to all three models, using the final Dip-Moveout (DMO) velocities found during the TLN processing. The subsequent mute values were also taken from this previous processing. Following the amplitude scaling by automatic gain control (AGC), the three models underwent 3D stacking. The seismic finally underwent a band-pass filter (14-90Hz) and further amplitude scaling before being displayed. A summary of these processing steps is shown in Figure 36.
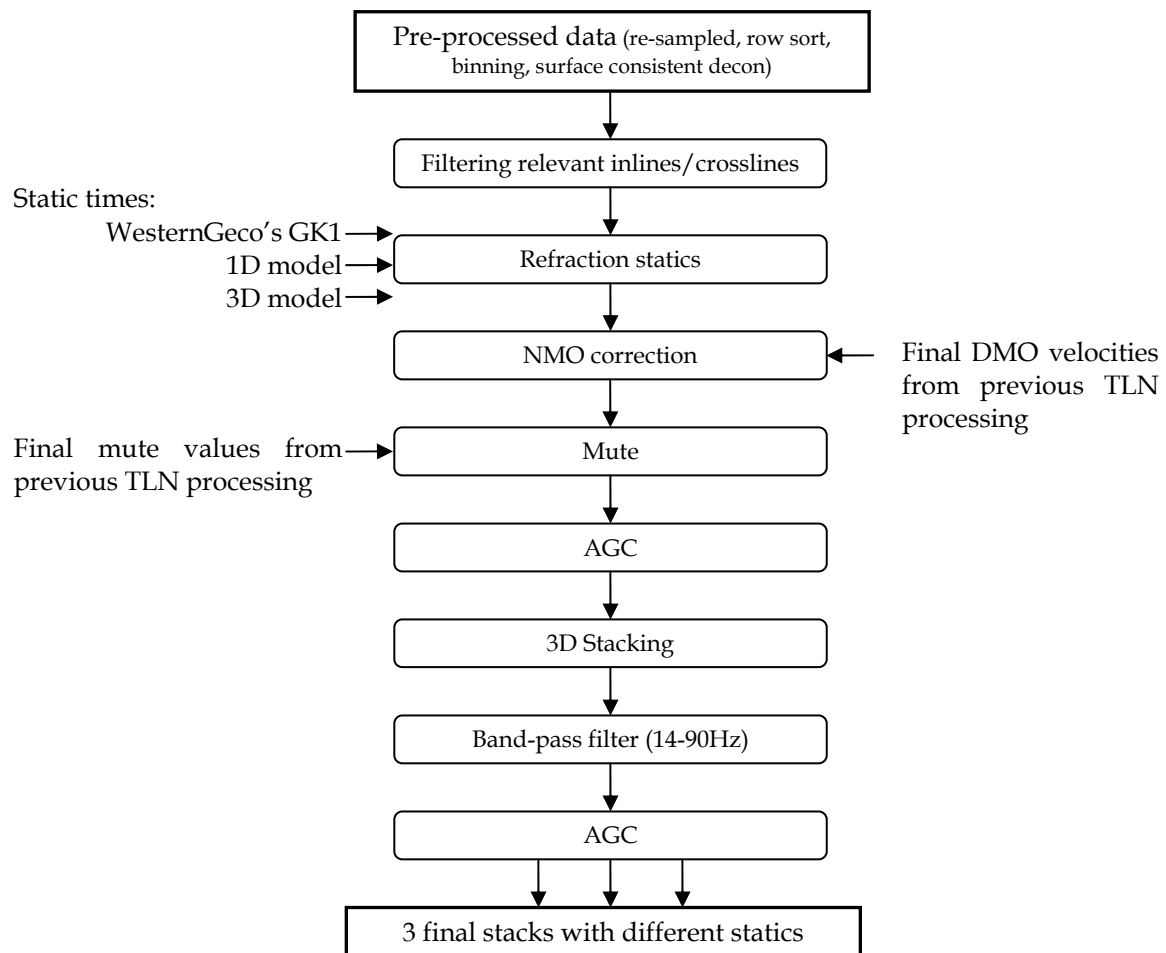
Figure 36 Processing sequence to create three comparable stacks with static corrections

5.2 WesternGeco Statics vs New 1D and 3D Statics

The three static models are collectively shown in Figure 37[25] (foldout). The first diagram (a) gives the original Gauss-Krueger 1 static times by WesternGeco, the second one (b) the 1D inversion statics, and the last one (c) the 3D tomography statics. The gross result is roughly the same for all three, though the most discernible contrast is how small the tomographically-derived static correction in the region of the Oichtental is compared to the other two. Statics in the valley average around -65ms to -75ms according to the Hole model, while the 1D and GK1 plots seem to suggest values around -110ms to -120ms, which is a considerable difference of almost 100%.

---

[25] QC Processing by Marc Merz, WesternGeco, Vienna 03.10.2008, using Omega software

QC PROCESSING WITH GK1 BASIC STATICS
WESTERNGECO DC VIENNA   M.MERZ 03.10.2008
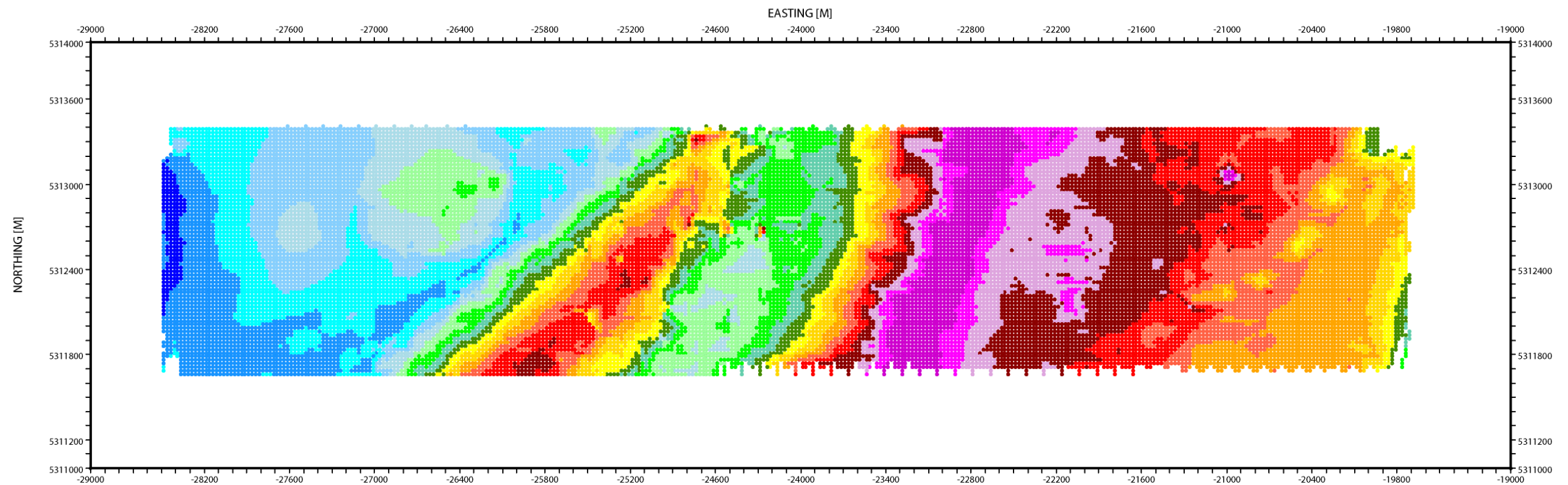
Fig. 37(a)

QC PROCESSING WITH SEISMON BASIC STATICS
TECHNICAL UNIVERSITY VIENNA   M.MERZ 03.10.2008

Fig. 37(b)

73

QC PROCESSING WITH DWTOMO BASIC STATICS

TECHNICAL UNIVERSITY VIENNA   DEPARTMENT PROF.DR.E.BRUECKL

M.MERZ 03.10.2008

Fig. 37(c)

Legend

DEFAULT_COLORS

Range	%	Value
(---, -144)	7 %	1924
[-144, -138)	6 %	1669
[-138, -132)	7 %	2070
[-132, -126)	7 %	2135
[-126, -120)	6 %	1760
[-120, -114)	6 %	1633
[-114, -108)	8 %	2363
[-108, -102)	6 %	1870
[-102, -96)	8 %	2207
[-96, -90)	6 %	1734
[-90, -84)	4 %	1042
[-84, -78)	5 %	1383
[-78, -72)	6 %	1749
[-72, -66)	9 %	2683
[-66, -60)	4 %	1098
[-60, -54)	3 %	817
[-54, -48)	1 %	268
[-48, -42)	1 %	240
[-42, ---)	2 %	597

OICHTENTAL 3D REPROCESSING 2008

WesternGeco

Figure 37 Plots comparing surface consistent static times: (a) WesternGeco's GK1 static corrections (b) static corrections from 1D velocity field and (c) static corrections from 3D Hole tomography

Location-wise, there is perfect agreement between the 1D and 3D model concerning the position and direction of the Oichtental. Likewise, they seem to agree with the GK1 model, although here the lateral extent of the valley seems to be more sharply defined, so that additional details such as a round blotch of slightly bigger static times in the west of the area (coordinates [-26500, 5312900]) can be made out.

Regarding the mountain range in the eastern half of the swath, all three methods agree on static corrections of about -130ms to -145ms. But again, the east-west extent of the mountains appears smaller for the diving wave model than for the other two, giving smaller static corrections as the elevation drops off to the east.

Analysing the three stacks themselves discloses no profound improvements. The central crossline transecting the area from east to west, xline 1380, was taken as a benchmark to compare the GK1 stack to the stack derived from the 1D model (Figure 38) and to the stack produced through tomographic results (Figure 39). In each of the double-page comparisons, the circled regions denote areas of better defined reflections. All four stacks start at 0ms, as seen from the reference datum i.e. none of the region above 300m above sea level is included.

There are clearly more regions in stack (a) by WesternGeco than in (b) derived from the 1D model, particularly towards the beginning and end of the crossline, where reflectors tend to be stronger or more continuous than in the middle. This central region roughly marks the position of the Oichtental, hence the goal would have been to achieve some more recognisable reflections underneath the valley, if the low-velocity region had been accurately and sufficiently removed to yield a more focused image. This does not seem to be the case for the 1D model, as its overall stack quality appears worse than that of the original GK1 stack.

The double-page spread for the GK1 and Hole stack in Figure 39, on the other hand, does reveal a few improvements, brought about by the diving wave tomography. Predominately on the western edge of the crossline, the stack of the 3D-model static corrections shows a greater high-frequency content.
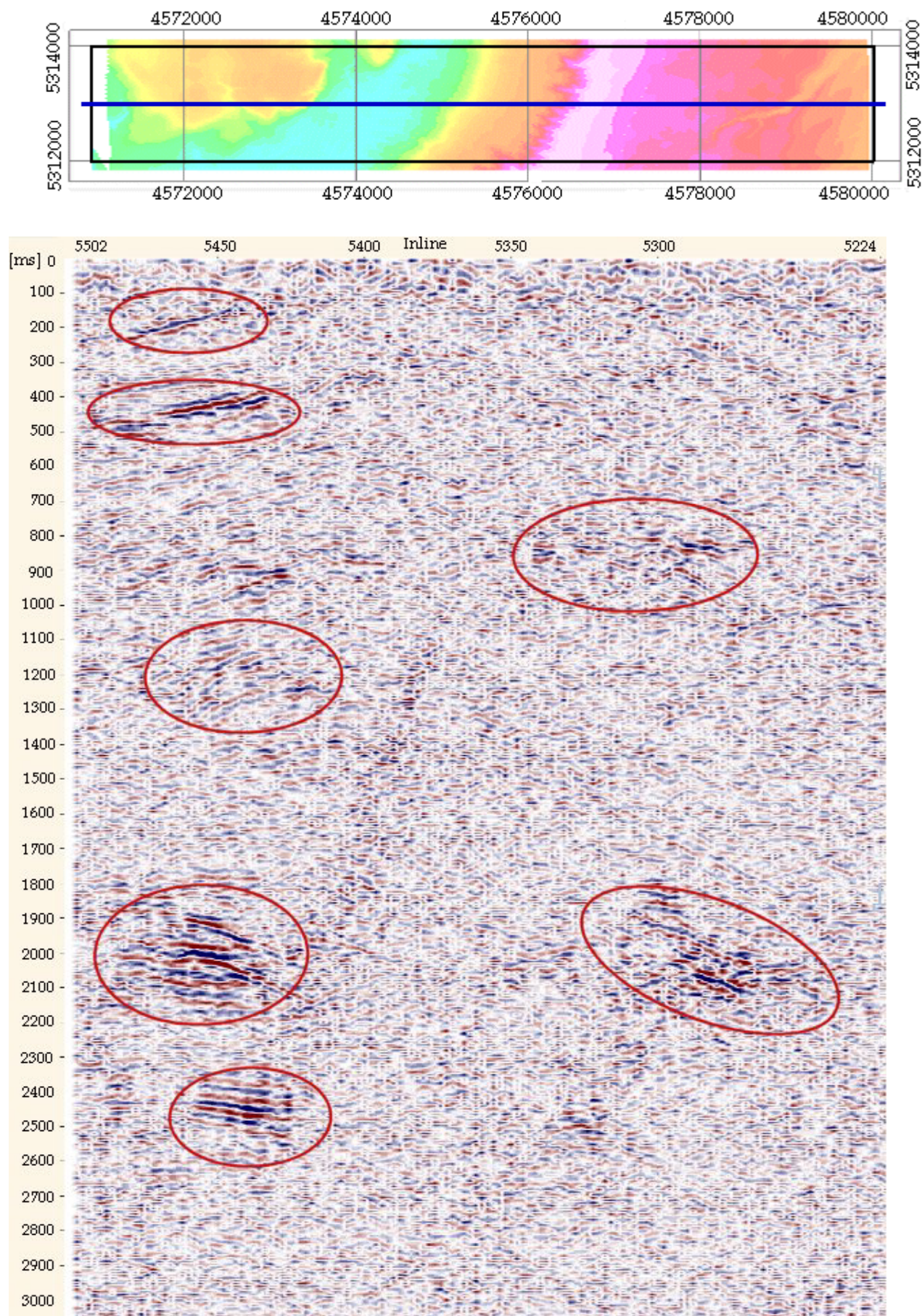
Fig. 38(a)
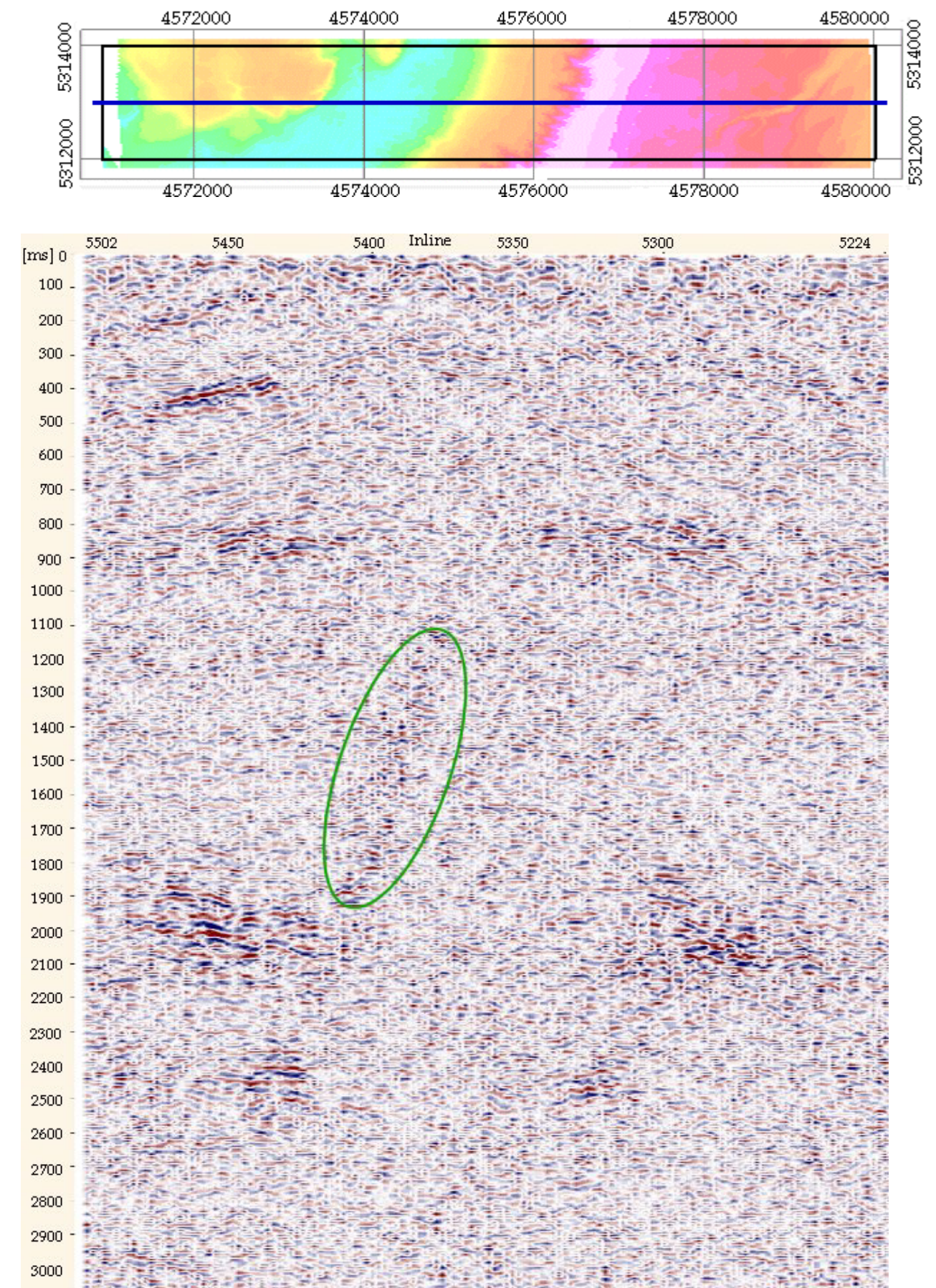
Fig. 38 (b)

Figure 38 Comparing (a) WesternGeco's GK1 stack to (b) stack produced after the 1D Inversion; circled areas contain clearer reflectors compared to the other stack; elevation map inserts at the top show relative position of these stacks within the test swath marked as a blue line
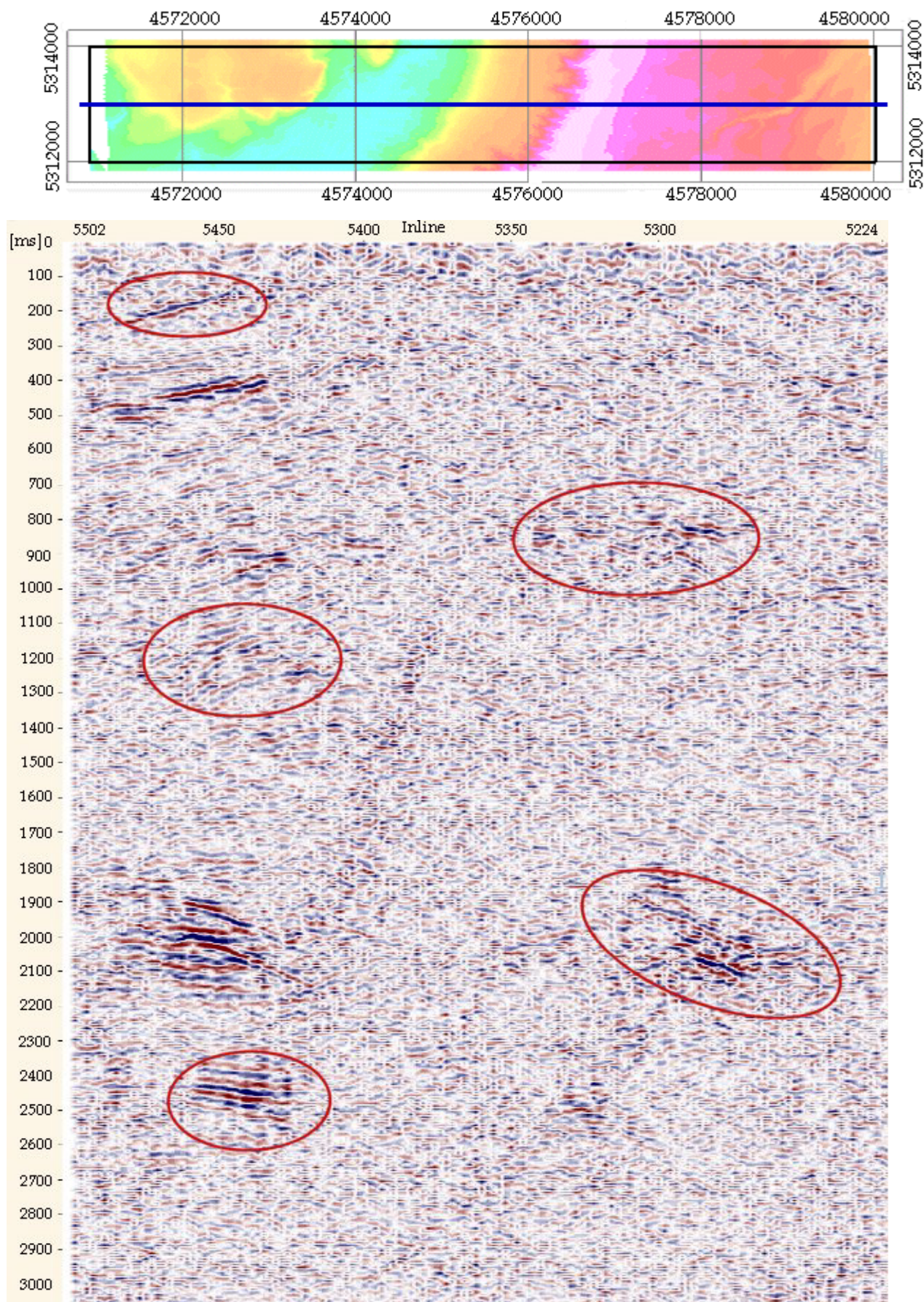
Fig. 39 (a)
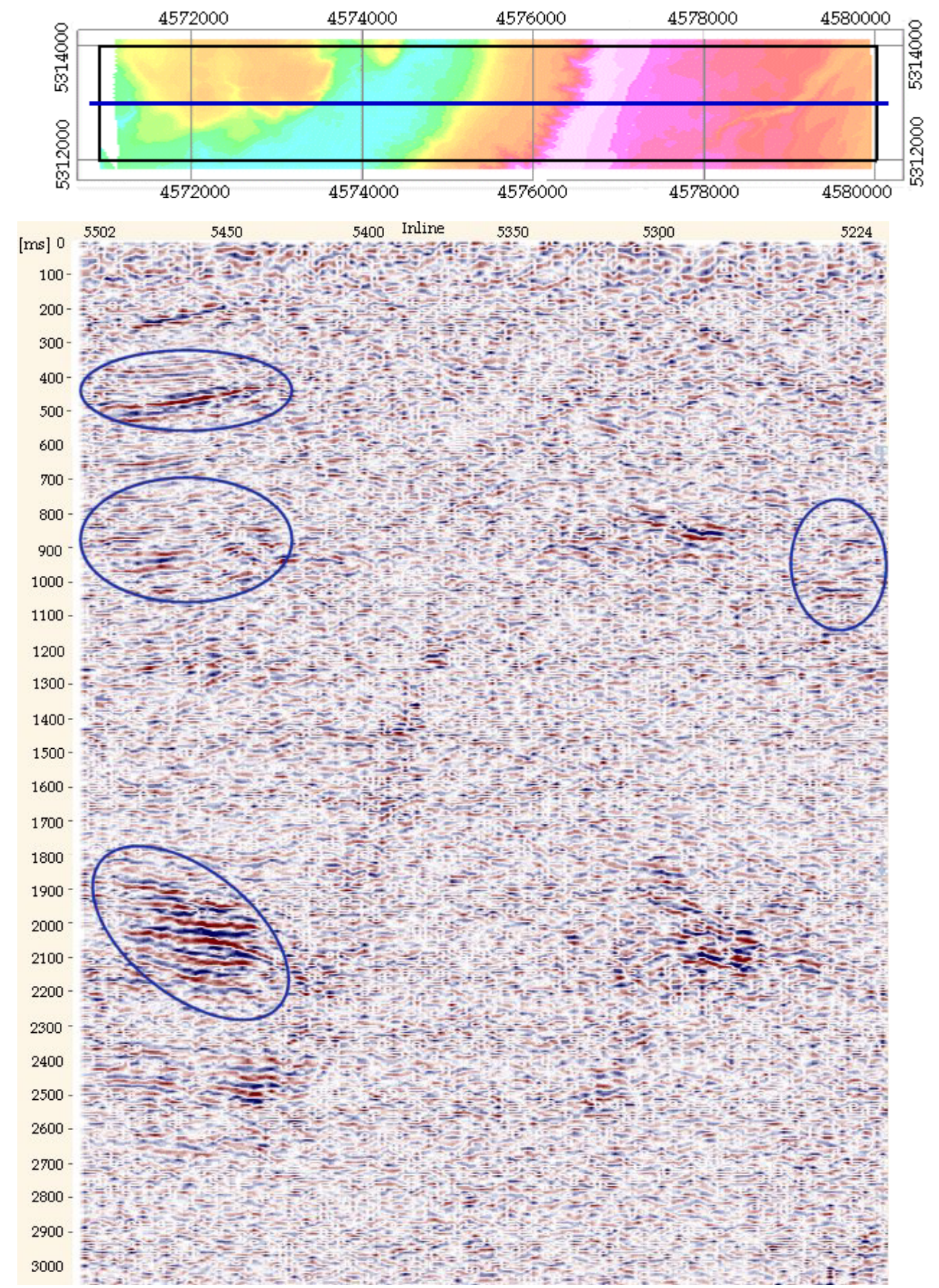
Fig. 39 (b)

Figure 39 Comparing (a) WesternGeco's GK1 stack to (b) stack produced after the 3D tomography; circled areas contain clearer reflectors compared to the other stack; elevation map inserts at the top show relative position of these stacks within the test swath marked as a blue line

The biggest enhancement by the diving wave model is the quality of the reflectors at 1800-2200ms travel time, likewise with a couple of shallower reflectors at 700-1000ms; reflections appear more coherent than in the GK1 stack. However, the main area of interest in the centre of the crossline where the Oichtental lies, shows no noteworthy changes. The aforementioned reflector at 1800-2200ms, which looks as if it continues on the western side of the crossline, disappears between inlines 5300 and 5400 – an effect which is attributable to the low-velocity valley infill in the shallow, that was inadequately removed by all three static models.

Information on which of the methods was the more accurate within the valley itself, in other words, whether the 1D inversion or Hole's tomography was able to delineate the base of the valley or reflectors within the infill, cannot be gained from these stacks.

6   Conclusion

6.1   Quality and Recommendations Regarding the Two Tested Methods

Looking back at the velocity models that were used to compute the new datum static corrections, there are a couple of very interesting points to note. In a direct comparison between the interpolated 1D model and the interpolated diving wave model, as in Figure 40, we can see that the 1D model on the left encompasses a much greater velocity range. Along the surface, there is a large red region, indicating velocities of 900ms^{-1} or below, particularly in and around the Oichtental. In the deep, on the other hand, the 1D model seems to have maximum values of up to 5200ms^{-1} in some places, which may be slightly too high to be plausible at that depth (300m below surface). The turning ray model covers a smaller range of values, never exceeding 4500ms^{-1} and hardly ever below 1500ms^{-1} in the shallow. Valuewise, the 3D approach may appear more realistic but fact is, that the 1D model had a much greater penetration depth and thus resolved the valley base much better.
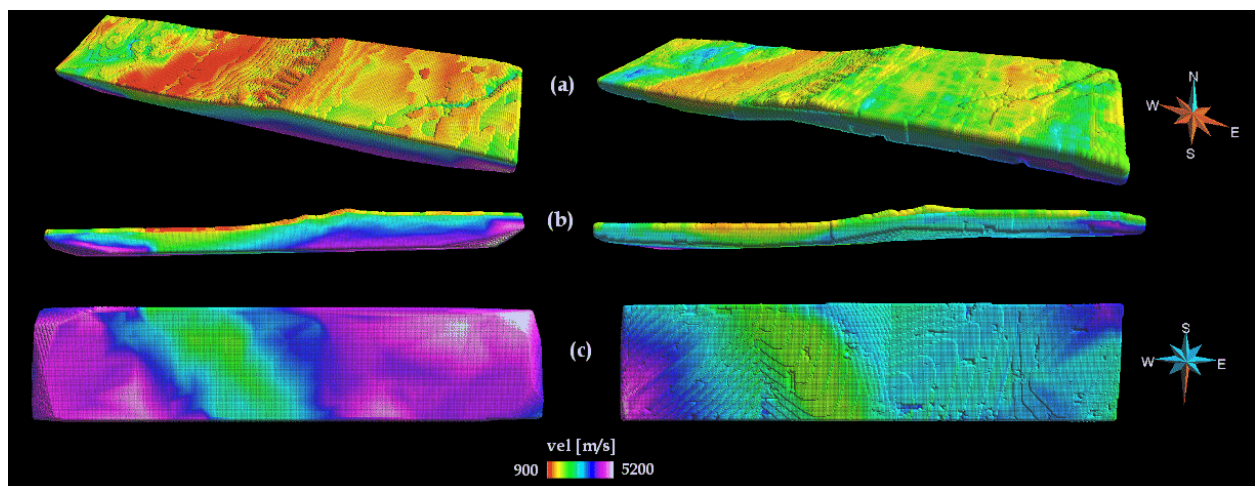
Figure 40 Interpolated velocity models from the 1D calculation (left) and the 3D diving wave approach (right) from three different points of view: (a) from an angle above (b) head-on view, where valley seems to be more distinct on the left and (c) from below

In the Nussdorf processing report 2002, WesternGeco suggested an Oichtental velocity of 1500 – 1700ms^{-1} and a thickness of 200-400m. The methods tested in this thesis, however, both seem to agree on a slightly higher velocity in the range of an

average 1700 – 2200ms^{-1} at mid-depth of the valley. In regard to thickness, neither of the above models seems to extend far enough to reach the absolute valley base. Both data sets were interpolated from the surface down to an elevation of 100m above sea level, yet this clearly does not suffice to fully delineate the valley, so the subsequently chosen reference data of 187.5m and 300m would pass on this inadequate resolution, meaning the statics are likely not to be optimal. The 1D method does a much better job at resolving the valley base, as can be seen when comparing the two head-on views in Figure 40b. There, the green area in the left diagram has a much more recognisable edge than the diving wave model on the right, and despite the left diagram appearing to be chopped off in depth, the diving wave model does not even seem to reach down to an elevation of 100m. Figure 41 shows the penetration depths of both methods, revealing a critical detail: The maximum penetration depth of the turning ray computation was only down to an elevation of 187.5m (Figure 41d), which meant that the interpolation to 100m was futile because the algorithm in MATLAB cannot extrapolate far. This was the reason for opting for a reference datum of 187.5m AMSL, so that the 1D and the 3D diving wave approach could be looked at on a comparative basis. The 1D model had highly variable penetration depths (Figure 41 a-c), but there were enough values to fully interpolate the cube to 100m and possibly even deeper, seeing as some of the deepest velocity function went down to almost sea level. It is noticeable that the majority of the velocity functions which extend further in depth lie within the Oichtental i.e. the low velocity region.

Another static model to try would perhaps see the 1D velocity data being used to interpolate a larger cube, going from the surface down to sea level, which might produce a complete delineation of the in-filled valley and then calculate the static corrections to a lower reference datum, according to a similar procedure as above. However, the appropriateness of the choice of reference datum needs to be kept in mind. The seismic target depth should still be considerably below the region included in the near-surface model, yet as much as possible of the delay effects produced by the low-velocity valley should be removed. Resolving a near-surface model down to sea level, calculating the weathering corrections down to 0m and then filling the model up with the deepest velocity values to obtain the elevation correction to 300m above sea level, for example, might be worth a trial.
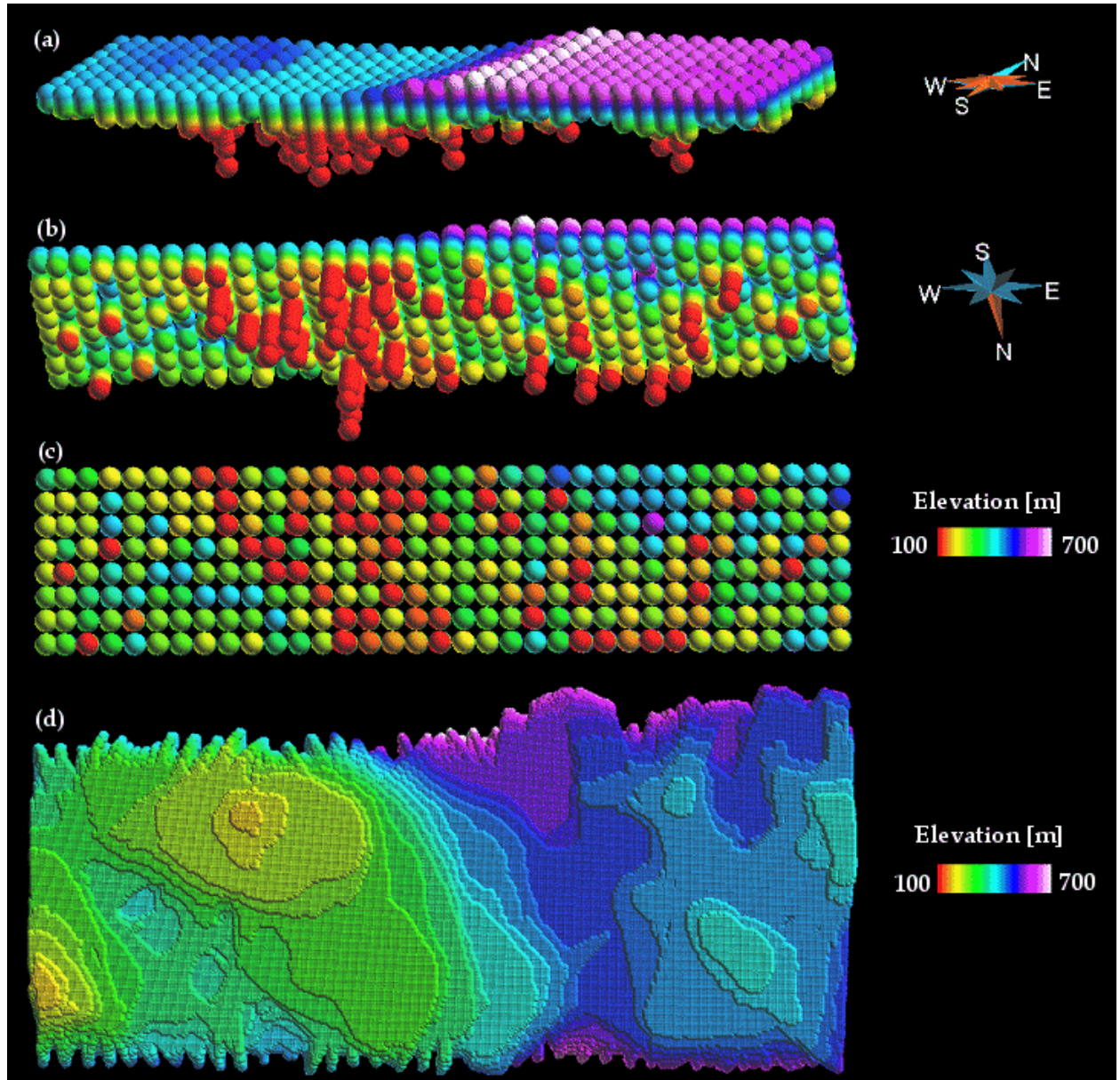
Figure 41 (a) – (c) depths of the 1D velocity functions, with red dots indicating penetration down to 100m above sea level or deeper, which is especially discernible in the Oichtental, whereas the lowest region in the Hole model (d), when viewing the model from below, is marked by orange shading (187.5m), also in the Oichtental valley

In terms of lateral resolution, the raw turning ray model doubtlessly beats the 1D model, yet after the interpolation, both models seem to be fairly detailed. A recommendation for future investigations using the 1D approach would be to reduce the cell size from 250m to 100m, which should still be usable, given the high fold of the seismic. Furthermore, the offset bins could thus be shrunk from 25m to 10m to increase the density of the computed velocity functions.

A validity test of the computed velocity models in the very shallow was made by checking the travel times measured during uphole shots against the travel times calculated from the average velocities in the two models. The first set of columns in the table of Figure 42 shows those uphole shots which fell into the investigated swath. Unfortunately, the source depths of the available check shots are not very deep, so the control is limited to the very near-surface layer (maximum 60m below surface). For this reason, the computed uphole times tend to be lower than the actually measured travel times.

When plotting the three travel time curves from this table against the x coordinates (Figure 43), it can be seen that the correlation on the whole tends to be very good – the travel times calculated from the 1D and 3D results systematically follow the trend set by the measured uphole times, if always at a slightly lower value. But at x coordinates ranging from 4572597 to about 4573810, the correlation appears to break down, with an average computed travel time of about 7ms but a measured uphole time of around twice that value (15ms). Coincidentally, this region – between the dark red lines – is where the Oichtental can be found.

Uphole Survey					1D Inversion results					3D diving wave tomography results				
Shot no.	X	Y	source depth [m]	Up-time [ms]	Nearest X node	Nearest Y node	Nearest depth node	Average velocity [m/s]	Up-time [ms]	Nearest X node	Nearest Y node	Nearest depth node	Average velocity [m/s]	Up-time [ms]
922	4571119	5313289	9	11	4571125	5313300	-	-	-	4571125	5313300	12.5	1810	7
920	4571615	5313368	18	15	4571525	5313375	14.5	1473	10	4571525	5313375	14.5	2058	7
919	4571851	5313454	12	12	4571850	5313450	13	1793	7	4571850	5313450	13	1704	8
918	4572090	5313524	18	20	4572100	5313525	17.5	2007	9	4572100	5313525	17.5	2028	9
4523	4572291	5313791	60	25	4572300	5313800	60	3914	15	4572300	5313800	60	2827	21
917	4572333	5313564	10	11	4572325	5313575	7	2110	3	4572325	5313575	7	2267	3
4524	4572351	5313295	48	27	4572350	5313300	47.5	3114	15	4572350	5313300	47	2975	16
4525	4572400	5313055	38	17	4572400	5313050	40.5	3064	13	4572400	5313050	41.5	3133	13
4526	4572433	5312794	39	17	4572425	5312800	40.5	2980	14	4572425	5312800	39.5	2702	15
4527	4572469	5312549	42	18	4572475	5312550	47	2718	17	4572475	5312550	44	2771	16
4528	4572497	5312344	44	22	4572500	5312350	42.5	2370	18	4572500	5312350	42	2481	17
4529	4572524	5312114	27	16	4572525	5312125	21.5	2193	10	4572525	5312125	21.5	2083	10
916	4572597	5313589	15	13	4572600	5313600	18.5	2395	8	4572600	5313600	18	2794	6
915	4572836	5313664	18	17	4572825	5313675	17.5	2313	8	4572825	5313675	17.5	2811	6
913	4573337	5313704	15	14	4573325	5313700	19.5	2736	7	4573325	5313700	19	2924	6
912	4573581	5313744	18	12	4573575	5313750	13.5	2347	6	4573575	5313750	26	3352	8
911	4573810	5313789	32	23	4573800	5313800	38.5	2115	18	4573800	5313800	26	2036	13
910	4574045	5313827	34	24	4574050	5313825	30.5	2161	14	4574050	5313825	30.5	2257	14
909	4574292	5313876	24	22	4574300	5313875	20.5	1184	17	4574300	5313875	20.5	2048	10
908	4574541	5313764	21	21	4574550	5313775	24	1886	13	4574550	5313775	24	1742	14
907	4574793	5313778	18	18	4574800	5313775	15.5	1256	12	4574800	5313775	15.5	1381	11
906	4575073	5313808	21	19	4575075	5313800	21.5	1238	17	4575075	5313800	21.5	1394	15
4193	4577921	5312260	14	8	4577925	5312250	11	2113	5	4577925	5312250	11	2157	5
4194	4577920	5312132	12	11	4577925	5312125	16.5	1858	9	4577925	5312125	16.5	1556	11
4192	4577982	5312491	21	14	4577975	5312500	15.5	1891	8	4577975	5312500	15.5	2429	6
4191	4578044	5312722	25	12	4578050	5312725	29	2078	14	4578050	5312725	29.5	2044	14
4190	4578173	5312951	19	14	4578175	5312950	14.5	2034	7	4578175	5312950	23.5	1918	12
4189	4578266	5313230	20	14	4578275	5313225	15.5	1918	8	4578275	5313225	14.5	1916	8
4187	4578334	5313712	20	14	4578325	5313700	20	1815	11	4578325	5313700	20	1812	11
4188	4578323	5313473	19	17	4578325	5313475	24.5	1825	13	4578325	5313475	24.5	1742	14

Figure 42 Table showing check shots available within the test swath (first set of columns), compared to travel times computed from 1D and 3D model
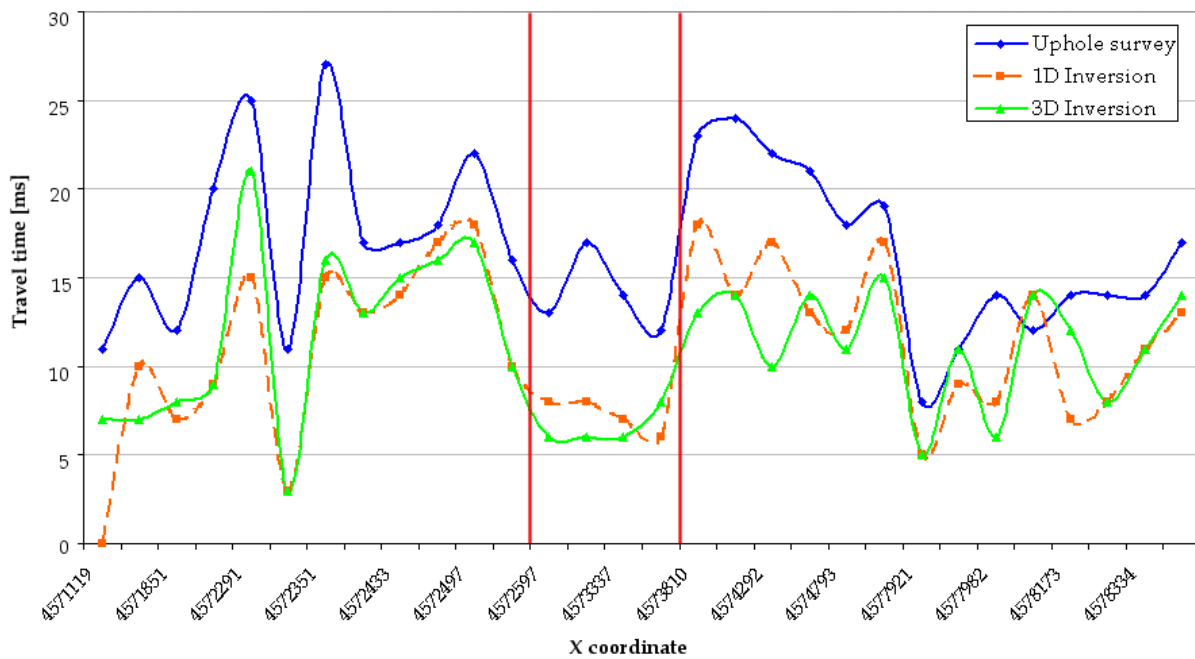
Figure 43 Three travel time curves to compare the uphole times against the two computed travel times, versus their x coordinate across the swath

6.2   Conclusive Summary

In brief, the result of this study has unfortunately not fulfilled the desired outcome of imaging the Oichtental correctly with respect to its low-velocity infill, which would ideally have led to an adequate removal of the weathering layers through static corrections, and subsequently improved stack quality beneath these Quaternary sediments.

There was a slightly surprising turn when considering the displays of the static corrections of the two investigated methods (Fig. 37) and the final stacks (Fig. 38 and 39). The correction times from the 1D inversion bore a fairly good resemblance to the WesternGeco GK1 times, while the diving wave tomography produced significantly smaller static corrections, and did not bring out the valley as conspicuously. In the end, however, the stack from the tomography turned out far better than the 1D model, and in places even better than the original stack by WesternGeco. Yet seeing as this only concerns area in the flat, low-lying plane to the west of the Oichtental, and occasionally in the east beyond the Haunsberg mountains, it is unclear how much better the Hole model performed over the 1D model in the actual location of the valley, because there all three stacks appear similarly blurry.

An important thing to note is that once residual statics were applied to the three data sets (Fig. 44), all stacks looked very similar, suggesting that a lot of incoherency can be eliminated with the help of residuals. The quality of the datum statics can, conclusively, be said to suffice if any remaining incoherencies are eliminated during the application of residual static corrections, as was the case herein for the two tested models.

Judging by the similarity of the three residual static stacks, the final output of the two new models seems to be equivalent to the WesternGeco model, despite the different intermediate outputs i.e. the static times themselves.
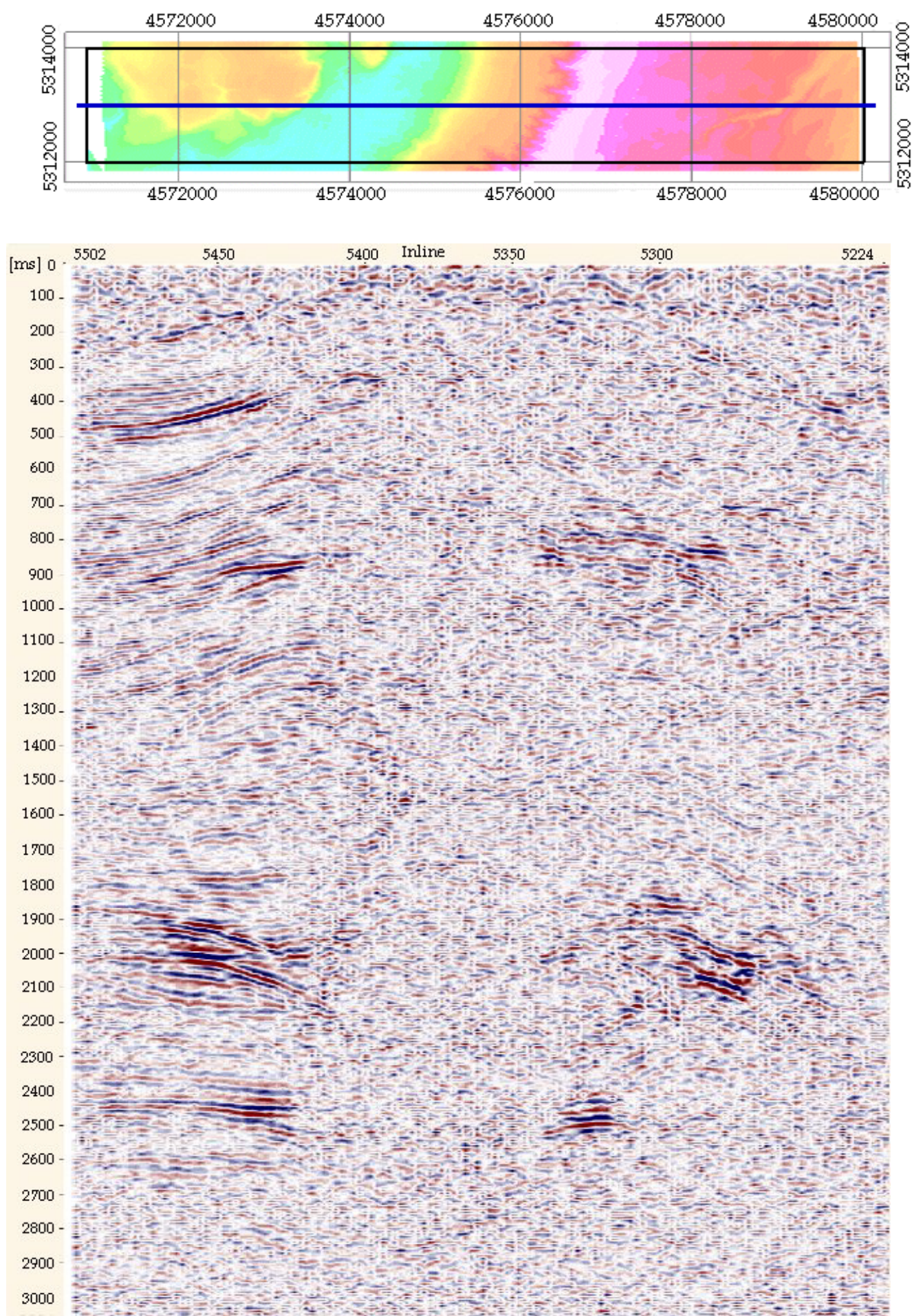
Fig. 44 (a)
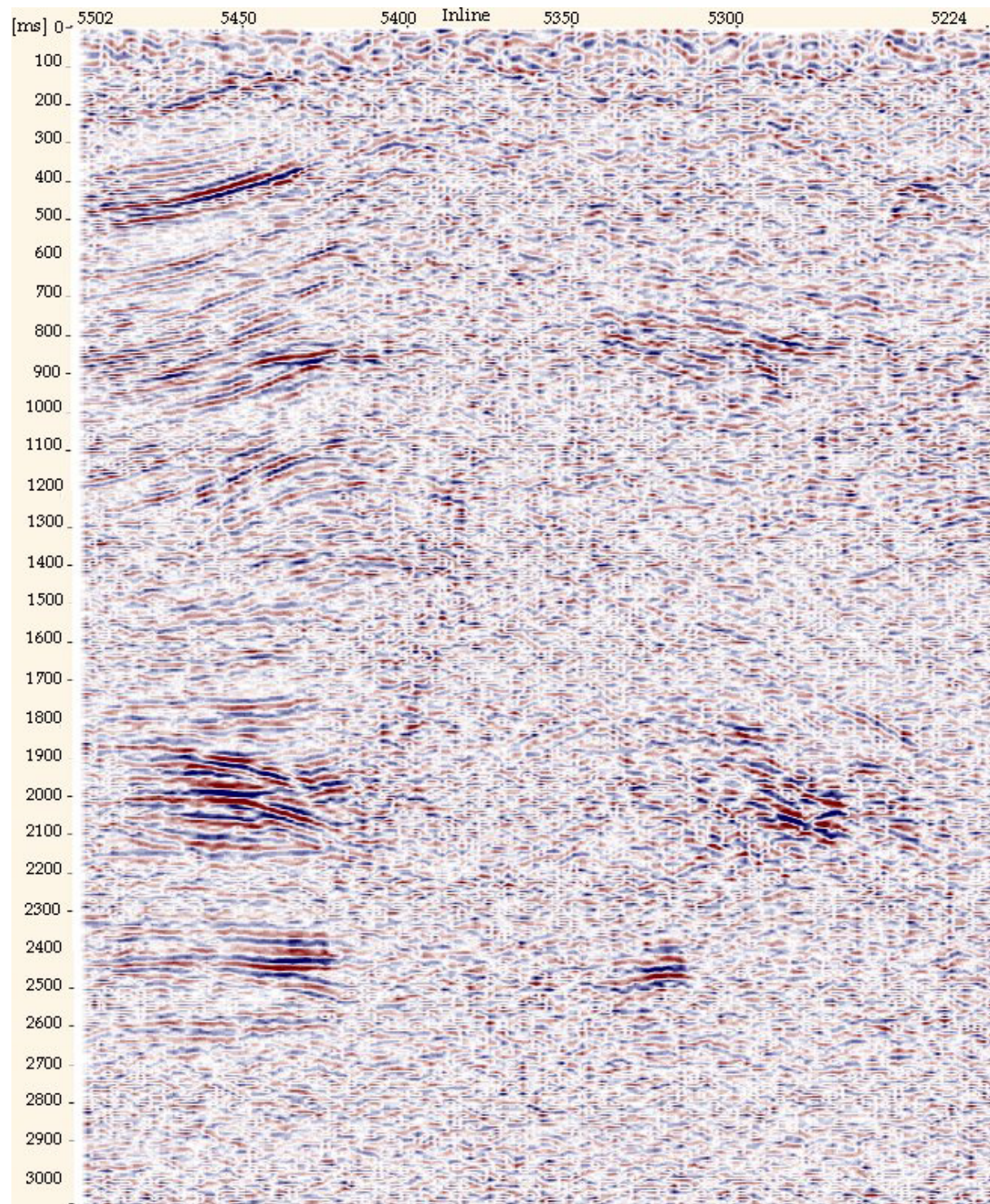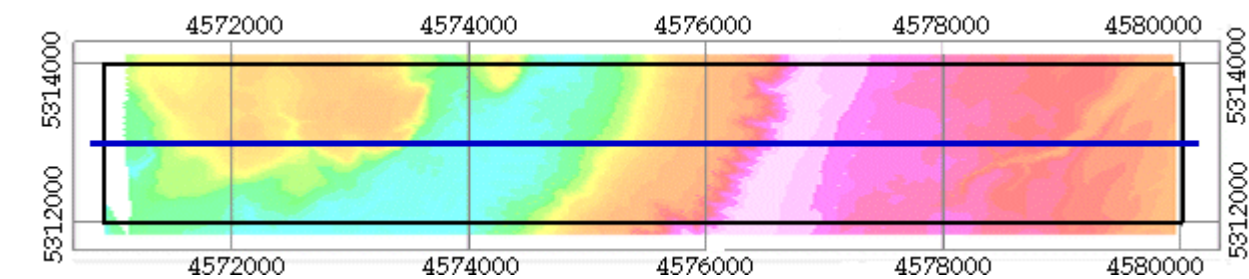
Fig. 44 (b)
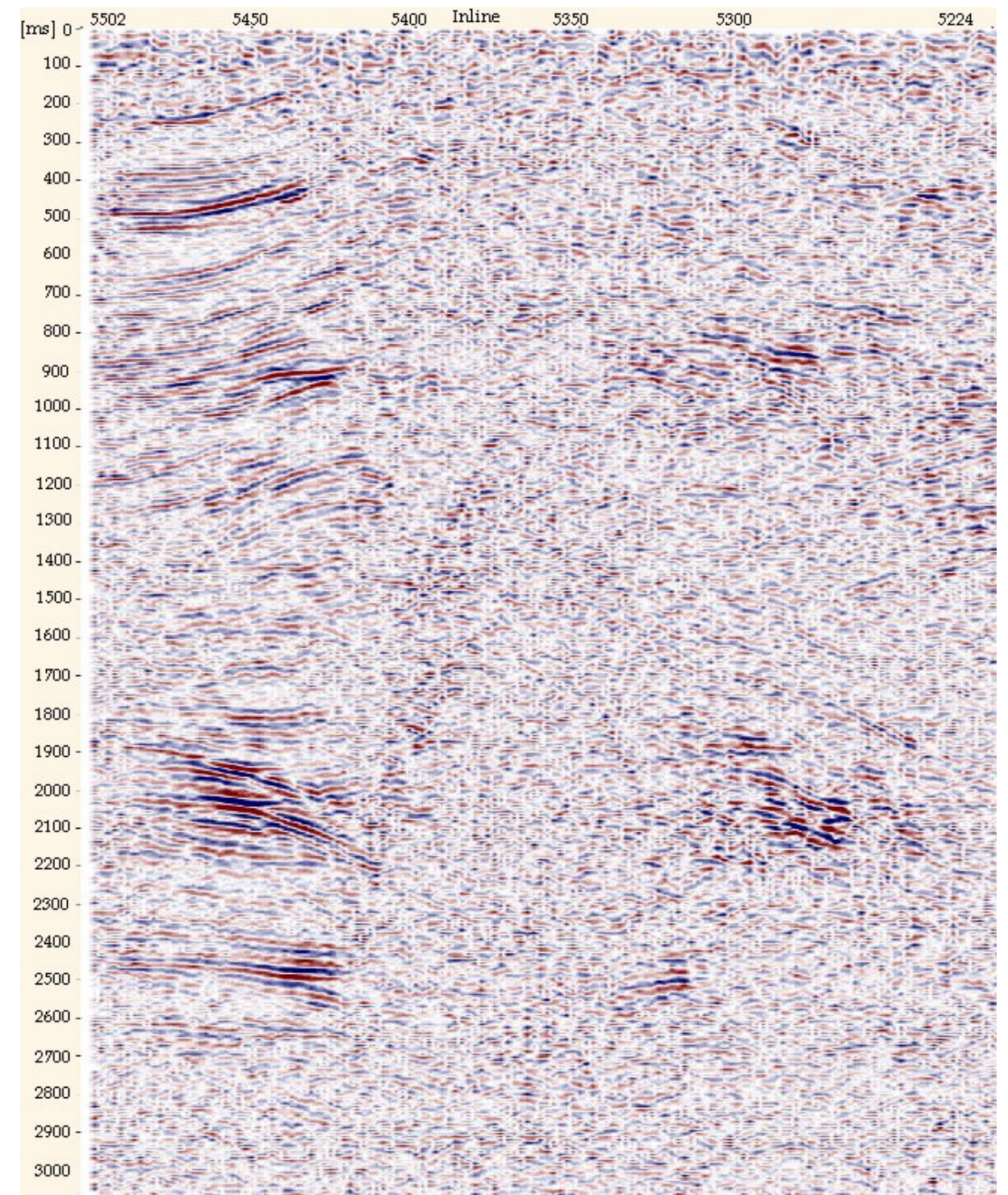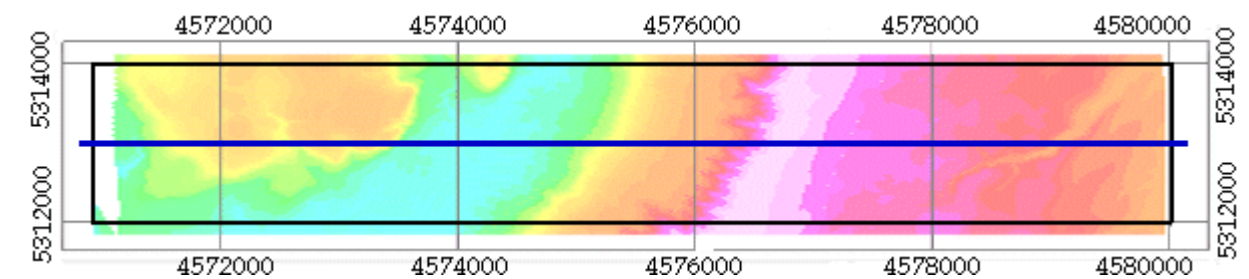
Fig. 44 (c)

Figure 44 Comparing the three final stacks once residual statics are applied (a) WesternGeco's GK1 model (b) 1D model stack and (c) 3D diving wave tomography stack; elevation map inserts at the top show relative position of these stacks within the test swath marked as a blue line

7 Acknowledgement

8 List of Figures

90

91

9 References

Brix, F., Schultz, O., 1993. Erdgas und Erdöl in Österreich, Enclosure 9

Behm, M., Brückl, E., Chwatal, W., Thybo, H., 2007. Application of stacking and inversion techniques to three-dimensional wide-angle reflection and refraction seismic data of the Eastern Alps, Geophys. J. Int.

Brückl, E., Brückl, J., Chwatal, W., Ullrich, Ch., 2007. Deep Alpine Valleys - examples of geophysical explorations in Austria

Cox, M.J.G., 1999. Static corrections for seismic reflection surveys

Gardner, L.W., 1939. An areal plan of mapping subsurface structure by refraction shooting: Geophysics, v.4, p. 247-259

Hagedoorn, J.G., 1959. The plus-minus method of interpreting seismic refraction sections: Geophysical Prospecting, 7, 159-182

Hole, J.A., 1992. Nonlinear high-resolution three-dimensional seismic travel time tomography. J. Geophys. Res., 97, 6553-6562

Karcher, J.C., 1987. The reflection seismograph: its invention and use in the discovery of oil and gas fields: The Leading Edge, 6, No. 11, 10-19.

Lowrie, W., 1997. Fundamentals of geophysics

Osypov, K., 2001. Refraction tomography: A practical overview of emerging technologies, CSEG Recorder

Palmer, D., 1980. The generalized reciprocal method of seismic refraction: SEG

Press, F., 1966. Seismic velocities, in Handbook of geophysical constants (ed. Sydney P. Clark)

Robein, E., 2003. Velocities, time-imaging and depth imaging in reflection seismics, 16

Sheriff, R.E., 1991. Encyclopedic dictionary of exploration geophysics

Slawinski, M.A., 2003. Seismic Waves and Rays in Elastic Media, Handbook of Geophysical Exploration (ed. Helbig, K., Treitel, S.)

Sleep, N.H., Fujita, K., 1997. Principles of Geophysics, 362

Thralls, H.M., Mossman, R.W., 1952. Relation of seismic corrections to surface geology, Geophysics 17, 218

Tipler, P.A., Mosca, G., 2003. Physics for scientists and engineers, 1010

URL: http://www.mathworks.com/access/helpdesk/help/techdoc/index.html

URL: http://www.npagroup.com/oilandmineral/offshore/oil_exploration/index.htm

Van Husen, D., 1987. Die Ostalpen in den Eiszeiten. Aus der geologischen Geschichte Österreichs. - Populärwiss. Veröff. Geol. B.-A.Wien, 24

Yilmaz, Ö., 1987. Seismic data processing, Society of Exploration Geophysicists

He who stays in the valley will never see over the hill.

Unkown

KAROLINE ALTEN

Jenullgasse 3/1
A-1140 Vienna
Austria

Tel.: 0043/ (0) 676 7931372
E-Mail: karolinealten@hotmail.com

Personal Data

Date of Birth:	15th June 1985, Graz/Austria
Nationality:	Austrian
Marital Status:	Unmarried

Education

October 2003 to spring 2009

Master's degree in Geophysics at the University of Vienna

October 1996 – June 2003

Northampton High School (UK), graduating with A-Levels in Physics, Chemistry, Biology and German, as well as AS-Level Mathematics, receiving Grade A in all of them

Work Experience

September 07 – November 07

Offshore internship with WesternGeco/Schlumberger in Ghana:

Offshore seismic data processing for 5 weeks onboard a WesternGeco vessel in the Gulf of Guinea.

November 06 – January 07

Internship at WesternGeco/Schlumberger in Gatwick, UK:

The project involved testing a diving wave tomography module for 3D marine data in order to improve the velocity model for depth imaging and resolve an underwater channel.

November 05 – October 06

Traineeship at RAG (Rohöl-Aufsuchungs AG), Vienna, department of Bavaria and New Ventures:

The work comprised the drawing of drilling programmes, geological profiles and maps, database creation and administration, and gathering of information from the IHS Energy Probe database.

September 2003 to date

English tuition for students of English as a foreign language:

Teaching groups of up to 14 people at WSI Language Institute in Vienna (www.wsi.or.at), as well as private tuition.

Translation of diverse projects and assignments, including websites, scientific papers, CVs and advertisements for various clients.

Summer 2003 to date

Logistical support during VibroSeis surveys in Austria, conducted by Univ. Prof. Dr. Peter Steinhauser: Investigation of body reverberations of buildings during construction work to extend train tracks in various parts of Austria e.g. Lainzer Tunnel

Summer term 2008

Tutor at the Technical University, Vienna, for geophysical field trips:
Seismic, GPR and EM measurements in a region of Lower Austria to investigate possible drainage sites for natural springs.

March 2008 – December 2008

Technical work at HERON Technik GmbH, Graz:
Website maintenance, graphic design work, proofreading of technical engineering reports, translation and administrative work.

Language Skills and Other Qualifications

- **English** – Mother tongue
  German – Mother tongue
  French – Basics
  Arabic – Beginner

- Training course at Wifi (February 2009) concerning Energy Certificates for Houses

- Good team work and cooperating with people, experience gained from teaching English to people of all skills and age groups

- Experience with a range of software besides standard MS Office tools, including ProMAX, Geosoft's Oasis Montaj, Omega and PGC Seismic Processing Workshop, as well as GEO Suite

Interests

Badminton, diving, long-distance travels, particularly countries in the Middle East (Oman, Syria, Jordan), Skiing, Literature, Dancing, Museums

References

Marc Merz
Senior Geophysicist

c/o Rohöl Aufsuchungs AG
Schwarzenbergplatz 16
A-1015 Vienna
Austria

Tel. +43 1 50 11 63 74
marc.merz@westerngeco.com